X-672-64-4

NASA TMX-55166

# IMP D&E FEASIBILITY STUDY

FACILITY FORM 602

| | |
|---|---|
| N65 19844 (ACCESSION NUMBER) | 1 (THRU) |
| 148 (PAGES) | (CODE) |
| TMX-55166 (NASA CR OR TMX OR AD NUMBER) | 31 (CATEGORY) |

JANUARY 1964

GPO PRICE $ ______

OTS PRICE(S) $ ______

Hard copy (HC) $4.00

Microfiche (MF) $1.00

NASA

GODDARD SPACE FLIGHT CENTER

GREENBELT, MARYLAND

(RQT-25696)

X-672-64-4

# IMP D & E FEASIBILITY STUDY

N65 19844

Prepared by
Paul G. Marcotte

GODDARD SPACE FLIGHT CENTER
Greenbelt, Maryland

IMP D & E FEASIBILITY STUDY

SUMMARY

1. The IMP D&E feasibility study has revealed that a 181-pound Interplanetary Monitoring Platform (IMP) spacecraft can be placed into a gravitationally anchored orbit about the moon by a thrust-augmented Delta (TAD) vehicle utilizing an X-258 third stage and a retrorocket (JPL apogee kick motor) for lunar injection.

2. In the improved nominal trajectory case, the success probabilities for achieving a stable lunar orbit are better than 90 percent; 58 of the 100 statistical cases employed would have a lunar orbit lifetime of 180 days or more.

3. Objectives of the satellite are to investigate interplanetary magnetic fields, solar plasma fluxes, solar and galactic cosmic rays, and cosmic dust distributions and lunar gravitational field variations in the vicinity of the moon.

4. Ten of the basic IMP D&E spacecraft components are identical to IMP-1 components; ten other IMP components require some modification before being used in the IMP D&E. The apogee kick motor, possible active thermal controllers, and some or all of the experiments would be new to IMP; however, the kick motor and probably most or all of the experiments selected would have prior successful flight experience on other satellites.

5. IMP D&E will be able to make scientific particle and field measurements on the front side and back side of the earth and moon in respect to the sun thirteen times a year, where standard IMP satellites will sample this region of the earth only once a year.

6. The IMP D&E should supply early knowledge of lunar environment and gravitational field variations in support of future scientific and manned lunar explorations. In fact, most of the possible IMP D&E orbits will be adequate to obtain some measure of the $J_3$ zonal harmonic coefficient of the moon's gravitational field, which would be of value in planning subsequent closer orbits. IMP D&E will have a fair change of determining tesseral harmonics which are of significant geophysical interest.

7. Being essentially lunar-anchored, IMP D&E will continue the basic IMP plasma and field measurements in a unique way.

8. The overall mission reliability is very high (better than 90 percent) because no midcourse corrections are required.

9. A short coast phase (10-15 minutes) or vehicle reorientation in pitch angle to 15 degrees, or a combination of both, is required to optimize the probabilities of success. This coast phase or pitch maneuver is well within the capability of the Delta second stage.

10. The reliability of the Delta for such a straight shot has been demonstrated repeatedly. The Delta has been successful in the last 20 out of 21 times; moreover, the Delta could have met the IMP D & E transfer orbit launch window in 17 out of 21 launches.

11. The lunar injection window allows up to 1 hour in the nominal case, and 2 hours in the improved nominal case, to fire the kick motor and achieve an acceptable and stable orbit.

12. The IMP D & E has fourfold redundancy in firing the kick motor.

13. Owing to the fact that better than 75 percent of the structure and instrumentation designs are completed, and much hardware is now available off the shelf, the total effort and funding should be minimized over that of an entirely new program. Moreover, limited effort could begin now on long-lead items and designs on a basis of noninterference with other established programs.

14. If approved and properly supported, the IMP D & E mission could be successfully carried out in a time period of 18 to 24 months after the experimenters were selected and funded.

CONTENTS

## ILLUSTRATIONS



## TABLES

# 1. INTRODUCTION

## 1.1 OBJECT

This report, prepared at the request of Dr. John W. Townsend, Jr., Assistant Director for Space Sciences and Satellite Applications, presents the results of a study to determine the feasibility and desirability of placing an IMP-type satellite in orbit about the moon. The basic assumptions were that a thrust augmented Delta (TAD) with an X-258 third stage would be the primary vehicle, a retro kick motor equal or similar to the JPL Syncom B apogee kick motor would be used for lunar injection, and the IMP-I spacecraft hardware and instrumentation would be used as much as possible.

## 1.2 PURPOSE

In view of the fact that little is known about the lunar environment in respect to energetic particles, cosmic rays, cosmic dust, and magnetic and gravitational fields, the mission of an IMP satellite anchored in interplanetary space by the moon's gravitational field was proposed and the feasibility study initiated. The results from this satellite should add significantly to man's scientific understanding of the earth's own satellite (the moon), and should also establish environmental and gravitational field knowledge in support of future scientific and manned lunar explorations. It will also continue in a unique manner the long-term measurements and monitoring of interplanetary conditions begun by IMP-1.

## 1.3 PARTICIPANTS

The IMP D & E feasibility study was conducted by the author with the assistance of the Project Resources Office (T&DS), Space Sciences Division, Spacecraft Systems and Projects Division, Spacecraft Technology Division, Theoretical Division, and Spacecraft Integration and Sounding Rocket Division. Major contributions to this study were made by:

| | |
|---|---|
| J. Kork | Appendix I, "Success Probabilities for the IMP D & E Mission" |
| R.K. Squires, R. Kolenkiewicz | Appendix II, "IMP D & E Orbital Study" |
| W.M. Kaula | Appendix III, "Calculation of Perturbations of Lunar Orbiters" |

| | |
|---|---|
| Dr. N. Ness | Appendix IV, "Anchored IMP Scientific Missions" |
| J. Webb | Appendix V, "Detailed Weight Distributions for IMP D & E," also mechanical layout and drawings |
| S. Ollendorf | Appendix VI, "IMP D & E Temperature Control" |
| L. Slifer, S. Mc Carron | Appendix VII, "IMP D & E Solar Paddles" |
| G.C. Kronmiller | Appendix VIII, "Transponder Power Required to Track IMP D & E at Lunar Distances" |
| W. Schindler | Appendix IX, "Planning Information on IMP D & E" |
| R. Rochelle | Telemetry received power calculations |

## 2. GENERAL

The Goddard Space Flight Center proposes to anchor an IMP satellite about the moon, to measure in detail the energetic particle population, magnetic fields, and cosmic dust in this orbit, and to explore the variations of the moon's gravitational field. The orbiting IMP will be anchored about the moon by the lunar gravity field and will be immersed in essentially interplanetary space. The spacecraft will be similar to the present IMP satellite and will weigh a total of 181 pounds.

The side and top views of the proposed IMP D & E are shown in Figures 1 and 2. The major differences in appearance from IMP-I are that the rubidium vapor magnetometer has been deleted, an apogee kick motor added, and the individual fluxgate sensors combined into one triaxial sensor package extending out from a paddle arm. In adding the apogee motor, a heat shield was included, and it was necessary to move the antenna to the outer edge of the spacecraft.

It is proposed that the IMP D&E be launched from Cape Canaveral during the calendar year 1966. The launch vehicle will be a thrust-augmented Delta with an X-258 third stage and a small apogee kick motor similar to the JPL kick motor used successfully in the Syncom B satellite.

A typical sequence of launch events is shown in Figure 3. The first eleven steps of injection into the transfer orbit are nominal Delta first, second, and third stage events. However, BTL cutoff is not certain, and the second stage cutoff may have to be determined by the output from an integrating accelerometer. The fluxgate sensor and companion booms, and solar paddles are released and locked into place in sequences 13 and 14. This reduces the spin from a nominal 100 rpm to approximately 25 rpm. Separation of the third stage occurs next (step 15) and the spin-stabilized satellite then coasts out to the lunar intercept area. From actual tracking data, a set of lunar orbit characteristics (Figures 4 and 5) is generated. These curves are examined and a time to fire is selected to meet the mission objectives. Approximately 2 hours before time to fire the apogee motor, the command to start an electronic apogee sequence timer is initiated. This redundant timer will initiate the firing of the motor and the separation of the motor from the spacecraft. If, according to telemetry data, the apogee motor has not fired within the prescribed time, a direct command to fire will be initiated. This signal will go through redundant command receivers, bypassing the timer function, and will fire the motor. This method provides four opportunities to fire and separate the apogee kick motor. The assumption here is that the retro kick motor is always fired before lunar intercept in the optimized trajectory case. The time to fire the apogee kick motor is not critical and allows up to 1 hour (Figure 4) in the nominal case and 2 hours (Figure 5) in the improved nominal case to achieve the desired range of lunar orbit characteristics.

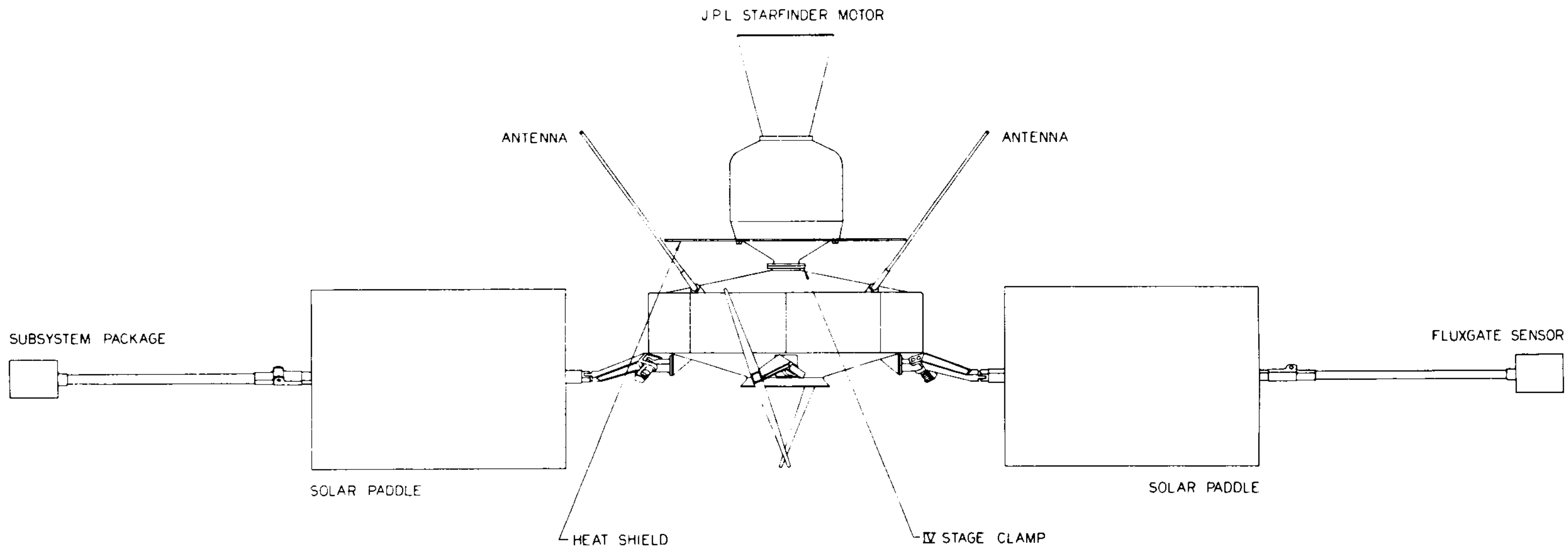


Prepared by
MECHANICAL SYSTEMS
BRANCH, GSFC

Figure 1--IMP D & E Spacecraft (Side View)

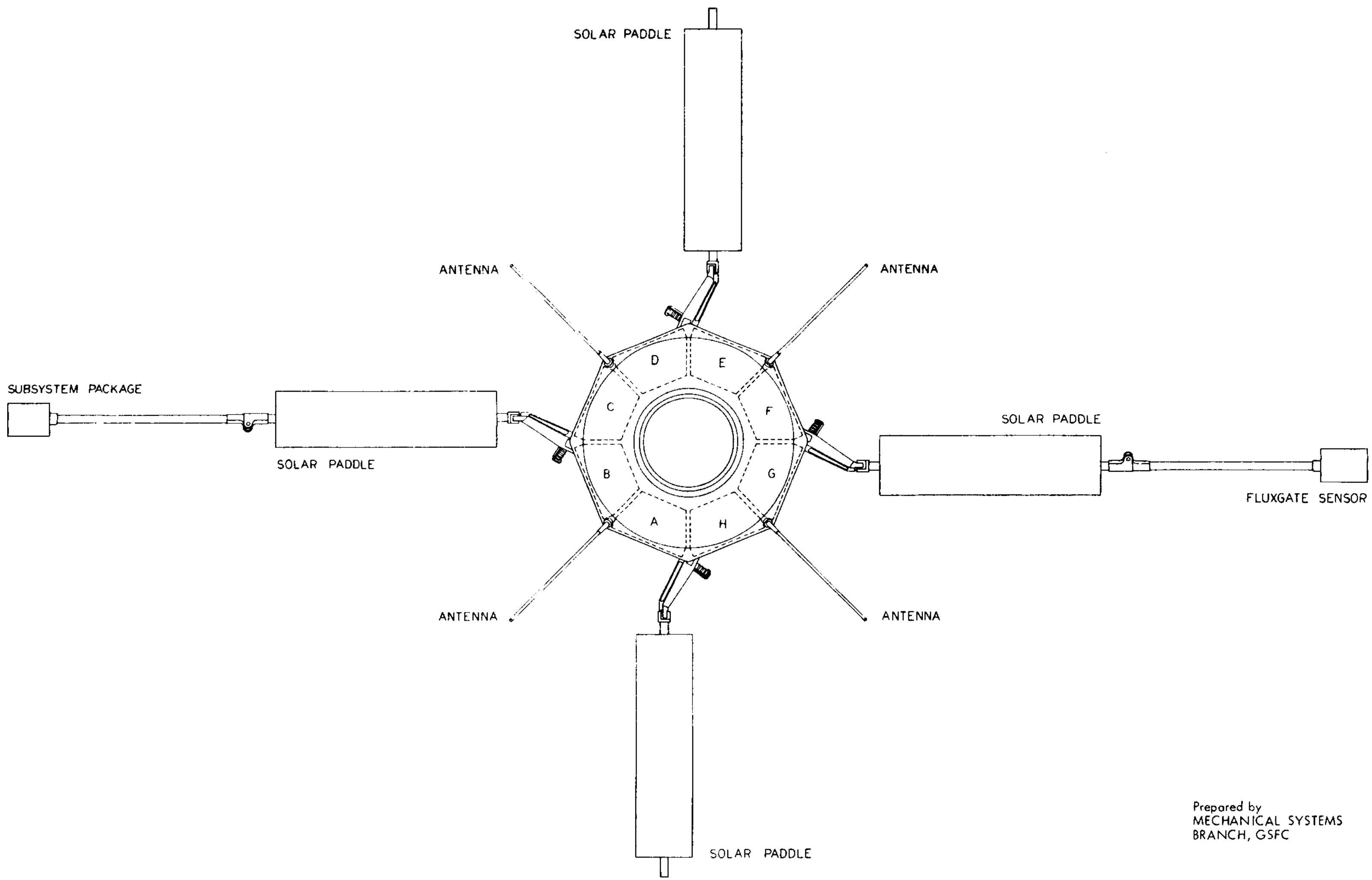


Figure 2--IMP D & E Spacecraft (Top View)

IMP D & E LAUNCH SEQUENCE

| SEQUENCE NO. | TIME/SEC | EVENT |
|---|---|---|
| 1 | 0 | STAGE I LIFTOFF |
| 2 | 146 | MAIN ENGINE CUTOFF |
| 3 | 150 | STAGE II IGNITION SIGNAL |
| 4 | 151 | STAGE I/II SEPARATION |
| 5 | 180 | JETTISON FAIRING |
| 6 | 317 | STAGE II CUTOFF |
| 7 | 330 | START COAST PHASE PITCH PROGRAM |
| 8 | 350 | END COAST PHASE PITCH PROGRAM |
| 9 | 355 | FIRE SPIN ROCKETS (SPIN UP) |
| 10 | 357 | JETTISON STAGE II - ACTIVATE RETRO SYSTEM |
| 11 | 371 | STAGE III IGNITION |
| 12 | 395 | STAGE III BURNOUT |
| 13 | 459.0 | FLUXGATE BOOM RELEASE (2) |
| 14 | 459.2 | SOLAR CELL PADDLE RELEASE (4) |
| 15 | 465 | SPACECRAFT/STAGE III SEPARATION - YO STAGE III |
| 16 | - | SPIN STABILIZED COAST |
| 17 | DBC | COMMAND TIMER |
| 18 | DBC + T | STAGE IV IGNITION |
| 19 | DBC + T + 20 | STAGE IV BURNOUT |
| 20 | DBC + T + 20 + 1200 | SEPARATE STAGE IV |
| 21 | - | IN ORBIT |
| 21 A | - | PROGRADE ORBIT - TRANSFER ORBIT VELOCITY BELOW NOMINAL |
| 21 B | - | RETROGRADE ORBIT - TRANSFER ORBIT VELOCITY ABOVE NOMINAL |

T = TIMER
DBC = DETERMINED BY COMPUTER

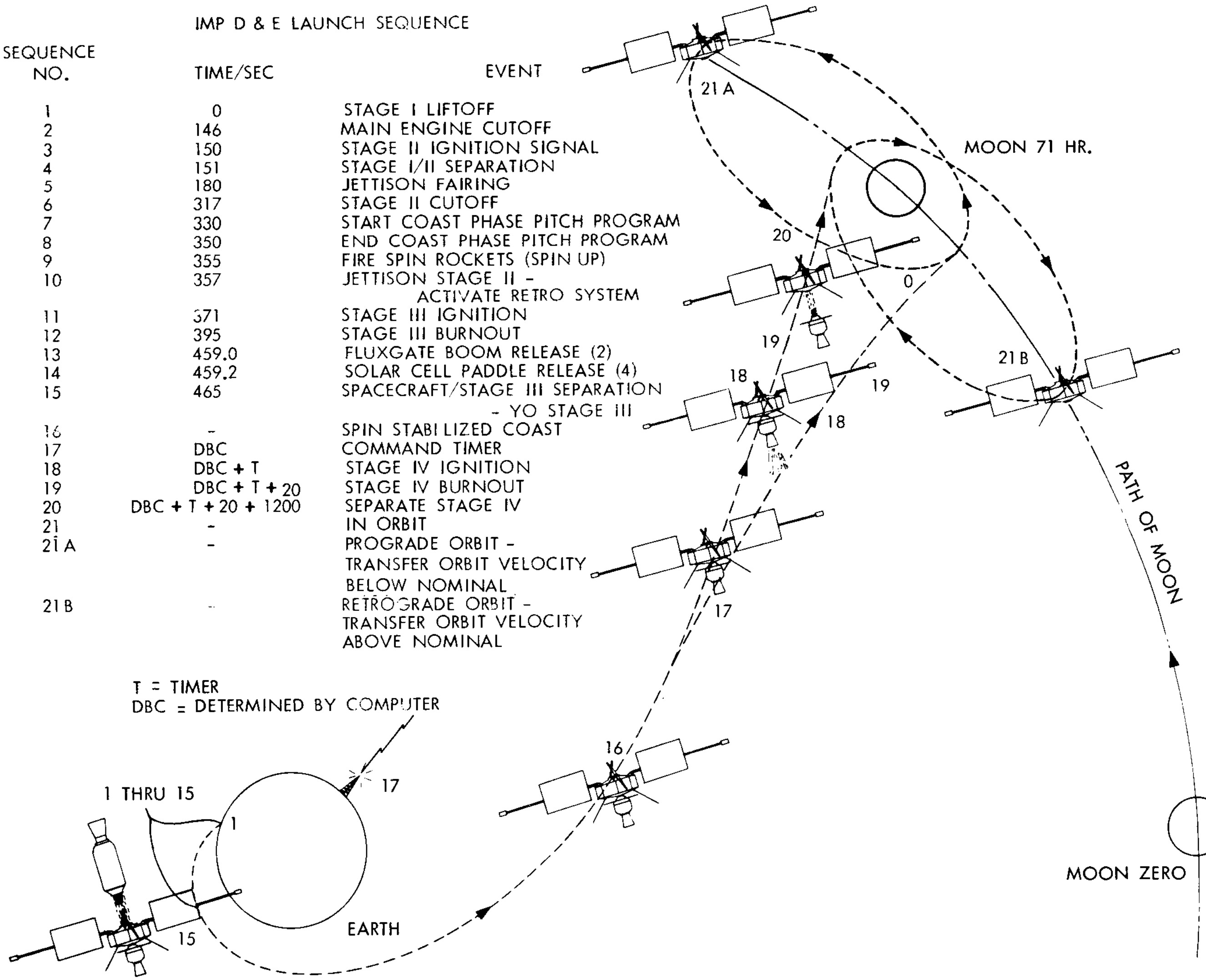


Figure 13 -- Earth-Moon Transfer Orbit

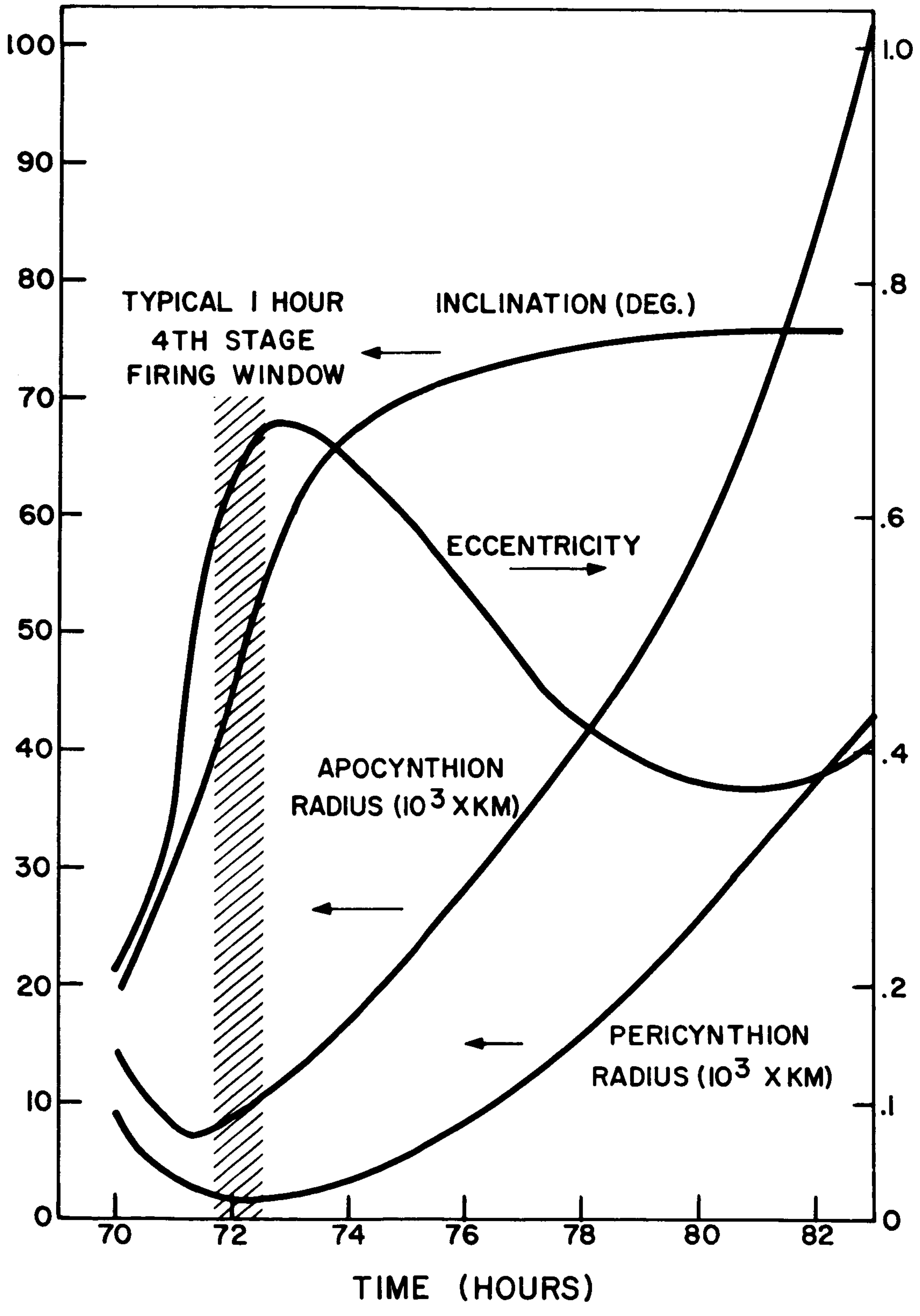


Figure 4 -- Nominal Anchored IMP Orbit Parameters (Delta Project Office Study)

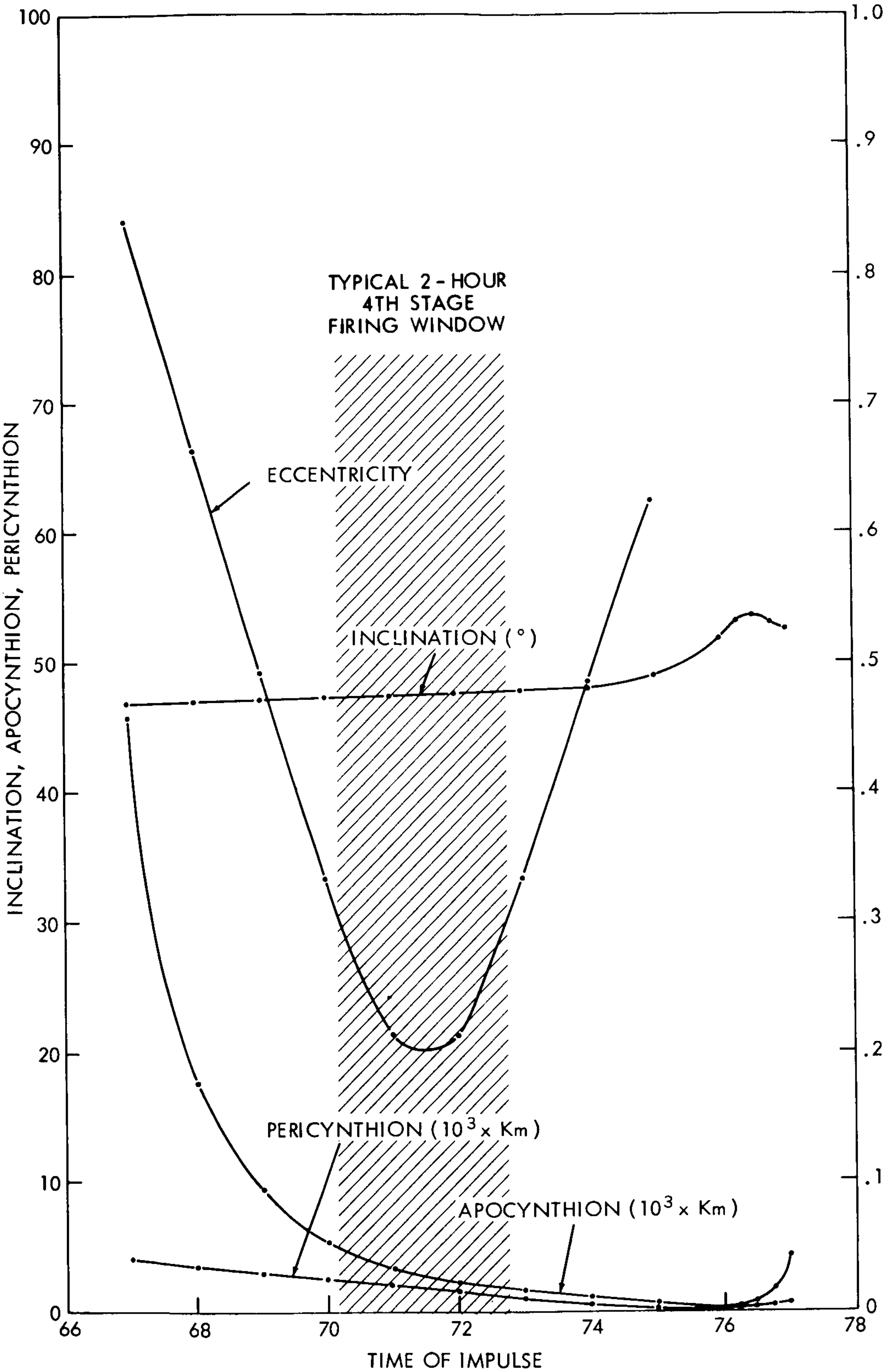


Figure 5 Improved Nominal Anchored IMP Orbit Parameters (Special Projects Branch Study)

The desirable range of lunar orbit parameters is as follows:

- Apocynthion -- 3000 km to 10,000 km (approx.)
- Pericynthion -- 500 km to 1,500 km (approx.)
- Inclination--highest possible up to 75 degrees
- Lifetime--6 months minimum

The optimum flight path appears to be one in which the spacecraft is aimed directly at the moon and is slowed down by the apogee motor so that it is captured by the moon's gravity field. Optimization attempts show no substantial difference in success probabilities between direct or retrograde lunar orbits. The details of the Delta Project Office trajectory study are included as Appendix I. Details of the Special Projects Branch orbital optimization efforts are shown in Appendix II.

The probabilities for achieving a particular orbit about the moon vary from 14 to 74 percent for the nominal orbit; higher probabilities have been achieved for higher flight-path angles. The probabilities for achieving any orbit vary from 70 to 99 percent in the improved nominal case. The overall mission reliability is very high, as there are no midcourse corrections required.

A small coast phase (10-15 minutes) or vehicle reorientation in pitch angle (up to 15 degrees) is required to optimize the success probabilities. This coast phase or pitch maneuver is well within the capability of the Delta second stage.

The reliability of the Delta vehicle for such a straight shot has been demonstrated repeatedly. (The last 20 out of 21 attempted Delta launches were complete successes.) The optimum launch time will be in either winter or summer for 3 successive days each month and the launch window for the transfer trajectory orbit for each day is 5 minutes long. However, this window may be enlarged to 20 minutes by BTL's ability to handset the second-stage parameters. The history of the Delta vehicle to achieve such a short launch window has, again, been repeatedly demonstrated. In fact, out of the 21 missions, 17 have gone on time or within 20 minutes of their scheduled launch time, on or within 3 successive days from the initial launch day (see Table 1).

A lunar orbit lifetime study (Appendix III) was made for the 100 Monte Carlo cases of the improved nominal trajectory case. This study revealed that 58 of the 100 orbits would have lasted 6 months or more.

## Table 1

## Delta Launch Vehicle Countdown Performance

| Launch and Spacecraft | Launch Date | "Hold Time"** | Reason for Hold | Previous Launch Attempts | Days Delay | Reason for "Scrub" |
|---|---|---|---|---|---|---|
| 1. Passive Communications*** | May 13, 1960 | 5 minutes | High Altitude Winds | | | |
| 2. Echo I | Aug. 12, 1960 | 22 minutes | Vehicle Problem | 1 | 1 | Vehicle problem |
| | | | | 2 | 2 | Vehicle problem |
| | | | | | | Range-vehicle problems |
| 3. TIROS II | Nov. 23, 1960 | On time | None | None | | |
| 4. Explorer X | Mar. 25, 1961 | On time | None | None | | |
| 5. TIROS III | July 12, 1961 | On time | None | None | | |
| 6. Explorer XII | Aug. 15, 1961 | 11 minutes | Range problem | None | | |
| 7. TIROS IV | Feb. 8, 1962 | 40 minutes | Vehicle problem | 2 | 2 | Ground support equipment problem |
| | | | | | | Vehicle problem |
| 8. OSO I | Mar. 7, 1962 | 5 minutes | Range problem | 1 | 1 | Vehicle problem |
| 9. Ariel I | Apr. 26, 1962 | 50 minutes | Ground support equipment problem | 1 | 16 | Vehicle problem |
| 10. TIROS V | Jun. 19, 1962 | 140 minutes | Vehicle problem | None | | |
| 11. Telstar I | July 10, 1962 | On time | None | None | | |
| 12. TIROS VI | Sep. 18, 1962 | 10 minutes | Ground support equipment problem | None | | |
| 13. Explorer XIV | Oct. 2, 1962 | 13 minutes | Vehicle problem | None | | |
| 14. Explorer XV | Oct. 27, 1962 | On time | None | None | | |
| 15. Relay I | Dec. 13, 1962 | On time | None | None | | |
| 16. Syncom | Feb. 14, 1963 | 35 minutes | Ground support equipment problem | None | | |
| 17. Explorer XVII | Apr. 2, 1963 | On time | None | None | | |
| 18. Telstar II | May 7, 1963 | On time | None | None | | |
| 19. TIROS G | June 19, 1963 | On time | None | 1 | 1 | Vehicle problem |
| 20. Syncom B | July 26, 1963 | On time | None | 1 | 1 | Vehicle problem |
| 21. IMP I | Nov. 26, 1963 | On time | None | 1 | 14 | Vehicle problem |

* Terminal Countdown: T-35 minutes to launch

** Includes recycle time, if any

*** Unsuccessful, vehicle malfunction

Ten of the basic IMP D & E spacecraft components are identical to IMP-I components; ten other IMP-I components require some modification prior to use in IMP D & E. The only actually new items (different from IMP-I) would be the apogee kick motor and possible active thermal controllers. The kick motor was used successfully on Syncom B. The proposed temperature controllers are similar to those used on the Atlas-Able 4 program. However, this program did not produce a successful satellite, and as a result no flight data are available on this design. Some development and testing would be needed to incorporate active temperature control for IMP D & E. However, passive thermal control is adequate to meet the basic spacecraft mission if the initial lifetime spin axis-sun angle is maintained between 30 and 150 degrees, and only pericynthion-type shadows are encountered. Consideration is being given to placing this type of active temperature controller (rotating vane) as an experiment on S-3c and/ or an early IMP to flight-prove the design.

## 3. OBJECTIVES

The primary goal of the IMP D & E will be to investigate interplanetary magnetic fields, solar plasma fluxes, solar and galatic cosmic rays, and interplanetary dust distributions in the vicinity of the moon. A principal problem in cosmic electrodynamics is the interaction of a moving magnetized plasma and a solid object. This phenomenon can be definitively studied with IMP D & E satellites whereby the interaction of the solar wind and the moon can be studied without the complicating effects of a planetary magnetic field. High-energy particle detectors and ionization chambers are included in the proposed instrumentation, as well as a cosmic dust detector and a triaxial fluxgate magnetometer. Information on the lunar ionosphere may also be obtained by analysis of the telemetry data (e.g., entrance and exit times of the satellite behind the moon).

Performing simultaneous measurements in space with magnetometers and plasma and particle detectors on the IMP D & E and other spacecraft will provide invaluable data on the propagation of solar transient disturbances in interplanetary space. In addition, the anchoring of a satellite in the lunar gravitational field will allow the magnetohydrodynamic wake of the earth in the interplanetary medium to be studied at lunar distances thirteen times a year, instead of once a year as is the case of the standard IMP's.
A second major objective of the IMP D & E will be a detailed analysis of its orbital dynamics. This will provide critical information on the lunar gravitational field and will permit investigation of the mass distribution in the moon.

IMP D & E will also assist in the determination of the earth-moon mass ratio and the figure of the moon. Accurate knowledge of the lunar gravitational field is important in determining the bulk properties of the lunar body and the development of more specific models of the lunar interior. Finally, detailed knowledge of the lunar gravitational field will be of importance in future lunar missions requiring accurate trajectory orbit manuevers. A more extensive treatment of the scientific justification for this mission is given in Appendix IV.

## 4. SPACECRAFT AND SUBSYSTEMS

### 4.1 ASSUMPTIONS

The basic assumption for the IMP D & E spacecraft was that the IMP-I structure and instrumentation be utilized as much as possible. In reviewing the proposed IMP D & E spacecraft, the following items were changes to the basic IMP-I satellite:

- For the experiments, the rubidium vapor magnetometer, Chicago telescope, orthogonal Geiger counter, and Ames proton analyzer have been deleted. A full triaxial flux gate magnetometer is proposed in place of the Rb magnetometer. The proposed solar wind experiment will have two sensors 180 degrees apart from one another, in place of the single one now used on IMP-1. A cosmic-dust experiment, and one or two cosmic-ray experiments (E vs dE/dX, or an ion chamber, or both) are proposed to complete a typical experiment lineup.

- The optical aspect system will be identical to that used on IMP-I. The power system will be identical except that IMP D & E will have 3-mil glass instead of 12-mil glass on the solar paddles, owing to lack of trapped radiation about the moon.

- There will be a small modification to the prime converter to furnish more power to the transmitter, since the transmitter will now require 6 watts output for the IMP D & E instead of 4 watts output for the IMP-I. The wiring harness will be modified for the new layout and the slightly changed experiments.

- The telemetry data system will be basically the same except for internal modifications in the reformatting of the information. The same building block modules will be used throughout the encoder. The programming will be provided in three basic cards which will include the undervoltage detector, fluxgate calibration, killer-timers, and the apogee sequence timer functions.

- The performance parameter card is essentially the same except for two added functions: the apogee-motor firing signal and the signal indicating separation from the apogee motor.

- The transmitter and range-rate package will be identical with the exception of 2 watts additional output from the transmitter and the addition of a redundant command receiver.

- The antenna is a modified turnstile which will be placed at the outer edge of the spacecraft instead of around the central boom as is the case in IMP-I.

The only actually new items are the JPL apogee kick motor and possibly active thermal controllers. The JPL kick motor was successfully flown on the Syncom B satellite, and is made by the Jet Propulsion Laboratory in California. Active temperature controllers will require development and testing, if used. There is not a great deal of change between the IMP-1 and the IMP D & E, and what change there is should be accomplished with a minimum of complications. (See Table 2 for component comparison listing.

## 4.2 STRUCTURE

The IMP D & E structure is essentially identical to the IMP-1 structure, except that it will be smaller in height, will have aluminum honeycomb and sheet-metal covers, and will have small conical areas on the top and bottom of the spacecraft which can support active thermal-control rotating blades. The prime converter chimney stack will now come out of the bottom of the spacecraft instead of the top.

Table 3 gives a summary of the weight distribution for IMP D & E. The total spacecraft weight, minus the motor systems, is 110 pounds. The apogee kick motor weighs 70.9 pounds. The detailed weight distribution is included as Appendix V. Table 4 shows the weight saving on IMP D & E compared to that of the IMP-I spacecraft. Figure 6 shows the proposed placement of the experiments and instruments within the IMP-type structure. Figure 7 is a side view of the spacecraft facets. In utilizing the IMP-I basic spacecraft design and essentially the same instrumentation, much of the design, fabrication, and layout have already been accomplished.

### 4.2.1 Stabilization

Inertial stabilization of the satellite spin axis will be accomplished by gyroscopic spin of the satellite. The satellite will be despun from a nominal 100 rpm to 25 rpm by means of deploying the booms and paddles. No yo-yo despin system will be used. Calculations indicate that spin variations should not exceed ±5 rpm from the nominal.

## 4.3 THERMAL CONTROL

The critical parts within the spacecraft in regards to low temperature operation appear to be the cosmic ray experiment (Facet A) which may be permanently damaged by temperatures below -15°C and the encoder (Facet E) which goes out of calibration below 0°C; however, the encoder does function at lower temperatures. During the lunar transfer with a sun angle looking down on top of the spacecraft, the battery and the facets run at a low temperature somewhere between -10 to -20°C. This is due to the fact that the heat shield for the kick motor shades the top part of the spacecraft (see Figure 1). With a transparent heat shield, these temperatures can be raised to approximately + 3°C and +24°C, utilizing passive thermal control. During orbit about the moon, with spin axis-sun angle restricted to variations from 30 to 150 degrees, the

TABLE 2

IMP - I - IMP D & E COMPONENT COMPARISON LIST

| IMP-1 | IMP D & E | Change |
|---|---|---|
| Experiments | | |
| Cosmic ray | Approximately same | |
| Cosmic ray | Approximately same | |
| Magnetic field | Triaxial fluxgate | No $R_b$ magnetometer |
| Solar wind | Approximately same | Two sensors instead of one |
| Not onboard | Cosmic dust | New experiment |
| Optical Aspect System | Same | |
| Power System | | |
| Solar paddles (4) | Approximately same | 3-mil glass instead of 12 mil |
| Prime converter | Approximately same | More output power for transmitter |
| Battery | Same | |
| Solar array regulator | Same | |
| Encoder converter | Same | |
| Multiconverter | Same | |
| Internal electrical | Approximately same | Modify harness to suit new layout and circuitry |
| Telemetry Data System | | |
| Encoder and DDP | Approximately same | New format - simpler design, many sub-modules and components on shelf and checked out |
| Programmer No. 1 and undervoltage detector | Approximately same | Regrouped |
| Programmer No. 2, fluxgate cal. and killer-timer | Approximately same | Regrouped |
| Programmer No. 4 and apogee sequence timer | Approximately same | Regrouped and new function |
| Parameters card | Approximately same | Add motor firing and separation signal |

Table 2 (cont'd.)

| IMP - I | IMP D & E | Change |
|---|---|---|
| Telemetry Communications and Range and Range-Rate System | | |
| Transmitter | Approximately same | 6-watt output instead of 4 watts |
| R&RR 1 | Same | |
| R&RR 2 | Same | |
| R&RR 3 | Same | |
| Command receiver | Same as R&RR receiver | Added for redundancy |
| Antenna system | Approximately same | Moved to outer edge of spacecraft |
| Structure | Approximately same | Smaller height, aluminum covers, prime converter stack-out bottom |
| Apogee Kick Motor | New | JPL motor fire and proved out on Syncom |

TABLE 3

SUMMARY WEIGHT DISTRIBUTION FOR IMP D & E

| ITEM | | TOTALS |
|---|---|---|
| Experiments | | |
| Cosmic ray | 6.7 | |
| Cosmic ray | 2.0 | |
| Magnetic field | 5.5 | |
| Solar wind | 7.0 | |
| Cosmic dust | 4.5 | |
| | 25.7 | 22.2 (allowable) |
| Optical Aspect System | | 1.8 |
| Power System | | |
| 1. Solar Conversion | 35.8 | |
| 2. Internal Electrical | 4.9 | 40.7 |
| Telemetry Data System | | 7.9 |
| Telemetry Communication System | | 7.2 |
| Spacecraft Structure | | 30.2 |
| Total (Spacecraft minus apogee motor) | | 110.0 |
| Apogee Motor | | 70.9 |
| Total (Spacecraft plus apogee motor) | | 180.9 |

TABLE 4

WEIGHT SAVING ON IMP D & E COMPARED TO IMP-1

| | Pounds Saved | Change |
|---|---|---|
| Fluxgate sensors | 3.0 | Reduced |
| Fluxgate signal processor | 1.0 | Reduced |
| Chicago telescope and electronics | 7.6 | Deleted |
| Geiger counter experiment | 3.0 | Deleted |
| Plasma probe and electronics | 1.6 | Reduced |
| Solar paddles | 3.0 | Reduced |
| Digital Data Processor Mod B | 1.0 | Deleted |
| Programmer No. 3 | .9 | Deleted |
| Aspect sensor guide | .2 | Reduced |
| Paddle arms | .5 | Reduced |
| Bias sphere | .5 | Deleted |
| Despin assembly | .2 | Deleted |
| Support tube | .5 | Reduced |
| Rb magnetometer assembly | 5.7 | Deleted |
| Ames experiment | 1.5 | Deleted |
| Platform and top cover | 2.0 | Reduced |
| | 32.2 | |

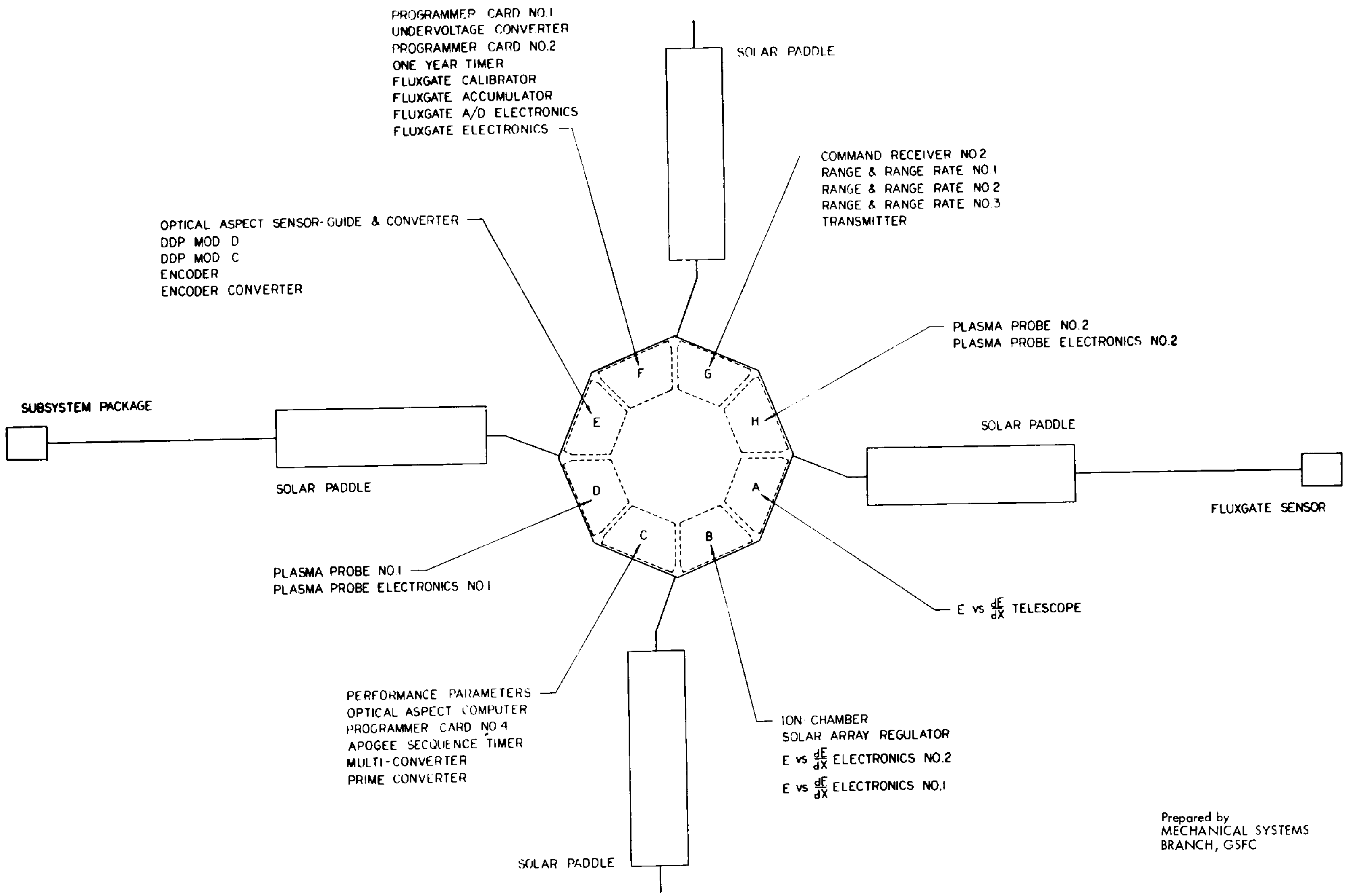


Figure 6--IMP D & E Module and Facet Locations

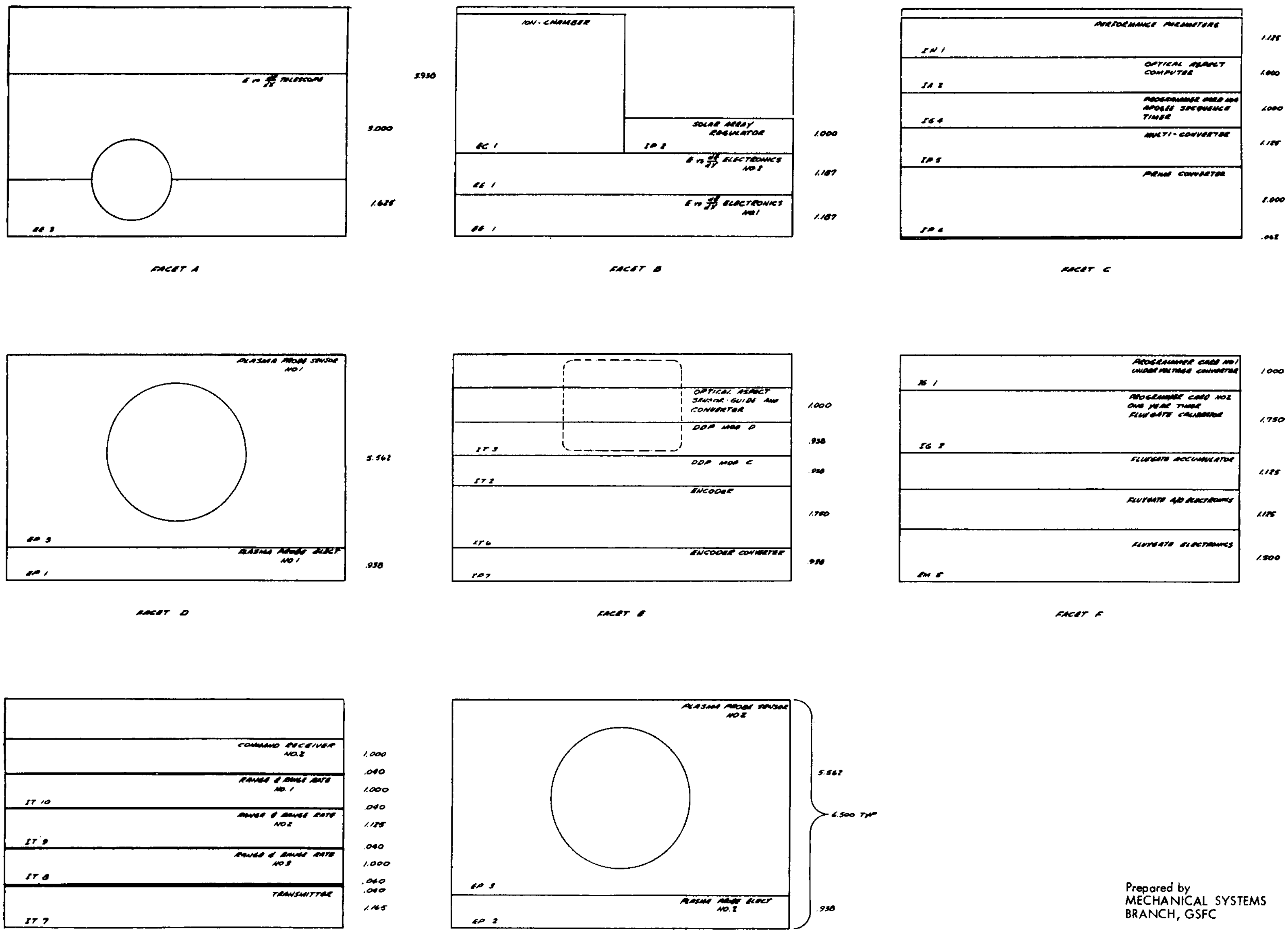


Prepared by
MECHANICAL SYSTEMS
BRANCH, GSFC

Figure 7--IMP D & E Module Frame Locations

satellite temperatures can be held to reasonable values of -5 to +50°C using passive thermal control, if there are only perigee-type shadows of about 1 hour. For shadows longer than 1 hour, a severe cooling problem occurs if the spacecraft has only passive thermal control. The temperatures within the facets and the battery can drop to -30 to -40°C during long shadows. Passive thermal control will be used for the IMP D & E spacecraft to fulfil the basic 6-month mission lifetime requirements. Active thermal controllers will be used if the design proves satisfactory.

Active thermal control by means of shutters and rotating elements has been investigated (see Appendix VI). These temperatures can be controlled so that they are within a practical range (for example -10°C minimum for the critical parts). Inclusion of active temperature control of course necessitates a small weight penalty; however, active temperature control can be included within the framework of the weight available. With a reduction in the size af the solar paddles and use of a titanium case for the kick motor, a higher basic spacecraft weight can be allowed.

### 4.3.1 Spacecraft Temperature Control

An evaluation was made of various active control systems for the IMP D & E spacecraft. Three cases were studied.

- Case I — Shutters on sides, rotating blades top and bottom
- Case Ia – Shutters on sides, passive coatings on top and bottom
- Case II – Rotating blades on top and bottom, passive coating on sides

Table 5 shows the summary of the evaluation of the three systems over the full range of spin axis-sun angles (0 to 180 degrees) for the nominal orbit, listing the advantages and disadvantages of each system.

For the purpose of choosing an adequate temperature control system, a ground rule has been adopted which limits the spin axis-sun angle to the 30- to 150-degree range. The criteria for such a system should be its ability to maintain temperature limits during the transfer phase and extended shadow orbits using the simplest, most reliable means.

#### 4.3.1.1 Case I

Examination of Table 5 shows that Case I, using a total active system, maintains the minimum temperatures best, is lightweight (in that no heat shield is required), but is most complex. As shown in Table 5, minimum temperatures in the facets fall to -18°C if the spacecraft were to enter the shadow at 0-degree or 180-degree sun angles. This would not be the case, however, if the sun-angle restriction were imposed. The minimum temperature in the critical facets could be maintained above -15°C. Case Ia is only a slightly less complex system, but results in lower mean spacecraft temperature during shade periods.

Table 5

Evaluation of Active Temperature Control Systems for the IMP D & E (Over the Full Range of Spin Axis-Sun Angles (0° to 180°) for the Nominal Orbit $R_p = 2500$ km, $R_A = 7500$ km)

| Case | Temperature Control | Complexity | Weight | Apogee Rocket Heat Shield | Transfer Phase | Remarks |
|---|---|---|---|---|---|---|
| I<br>Sides: shutters<br>Top: rotating blades<br>Bottom: rotating blades<br>$\epsilon$ veh (eff) = .21 | (a) Good control over variation in sun angles (+10° to 50°C)<br>(b) Fair fail safe qualities (-5° to 75°C)<br>(c) Highest mean spacecraft temperatures during shade orbits:<br>(1) pericynthion shade +14°C<br>(2) apocynthion shade -1°C<br>(d) Best minimum temperature control for apocynthion shadow periods (minimum temperature -18°C) | Most complex to mechanize<br>(1) shutters and blades require an actuator at each louvre (~25) and blade<br>(2) each actuator must be calibrated<br>(3) stops must be provided to prevent blade controllers from overshooting | 2.0 lbs.<br>5 facets<br>15% coverage top and bottom | None required (neglecting blowback) | No problem without heat shield | Best control; responds best during pericynthion and apocynthion shades |
| I(a)<br>Sides: shutters<br>Top: passive coatings<br>Bottom: passive coatings<br>$\epsilon$ veh (eff) = .24 | (a) Good control over variation in sun angles (+10° to 50°C)<br>(b) Good fail safe qualities (-5° to 65°C)<br>(c) Does not maintain as high mean spacecraft temperatures during shade orbits:<br>(1) pericynthion shade +12°C<br>(2) apocynthion shade -5°C<br>(d) Fair minimum temperature for apocynthion shadow periods (minimum temperature -23°C) | Complexity reduced over Case I in that blade controllers are removed | 1.5 lbs.<br>5 facets only | a) Same as Case I | Same as Case I | Good control except will result in lower mean spacecraft temperatures for apocynthion shades than Case I above |
| II<br>Sides: passive coatings<br>Top: rotating blades<br>Bottom: rotating blades<br>$\epsilon$ veh (eff) = .21 | (a) Fair control over variation in sun angles (0° to 50°C)<br>(b) Poor fail safe qualities (-20° to +70°C)<br>(c) Lowest mean spacecraft temperatures during shade orbits:<br>(1) pericynthion shade +8°C<br>(2) apocynthion shade -17°C<br>(d) Poor minimum temperature control for apocynthion shadow periods (minimum temperature -32°C) | Least complex as no shutters required | 1.9 lbs. (including heat shield)<br>40% coverage top and bottom | Required – may result in 10°C rise in component temperature during rocket firing | Heaters at critical components required or use of transparent shield | Simplest system; however, restricted to pericynthion shade orbits |

4.3.1.2 Case II

Case II is a much simpler and more reliable approach than Case I, the main consequences being lower mean orbital temperatures during extended shadows at low sun angles, the need for a heat shield, and a relatively wide swing in temperatures in the event of a failure.

As in Case I, the minimum facet temperature can be raised to proper levels during extended shade periods for all orbital altitudes by restricting the spin axis-sun angle to 30 to 150 degrees. This also closes the band on the temperature swing during a failure mode (+5°C to +70°C). The heat-shield requirement will not be a weight penalty since the rotating-blade temperature control system is lighter than the shutter system. Thus, taken on a total-weight basis, the two systems approach each other. The restricted spin axis-sun angle also removes the need for heaters during the transfer phase, as spacecraft temperatures do not exceed the lower limits.

In summary, the most worthwhile system for the restricted spin axis-sun angle mission involves the use of rotating elements mounted to the spacecraft top and bottom surfaces. However, if this system were chosen, and the sun-angle restriction removed, the life of the spacecraft would be limited to either 100 percent sunlight or pericynthion shadow orbits. To circumvent this problem to include all shadow orbits for the nominal mission, a total active control system similar to Case I would have to be applied.

4.3.2 Rocket Thermal Control

In order to prevent severe cooling of the propellant during transfer to the moon, super-insulation will have to be applied to the case. Additionally, a thermal cover of superinsulation may have to be provided over the nozzle to keep it at near propellant-case temperatures at the time of arrival at the moon. There are no data available from the manufacturers at present which places a lower limit on the material (carbon cloth and phenolic) or maximum allowable gradients in the nozzle. Tests on the material may prove that a coating of evaporated aluminum on both outside and inside surfaces of the nozzle will suffice.

## 4.4 EXPERIMENTS

Four basic experiments are proposed for this mission: magnetic field experiment, solar wind experiment, cosmic ray experiment (E vs dE/dX and/or a Neher-type ion chamber) and a cosmic dust experiment. Depending upon a finalized weight figure, possibly all five experiments will be used. A full description of the experiments is given below and the sensor look angles are shown in Figure 8.

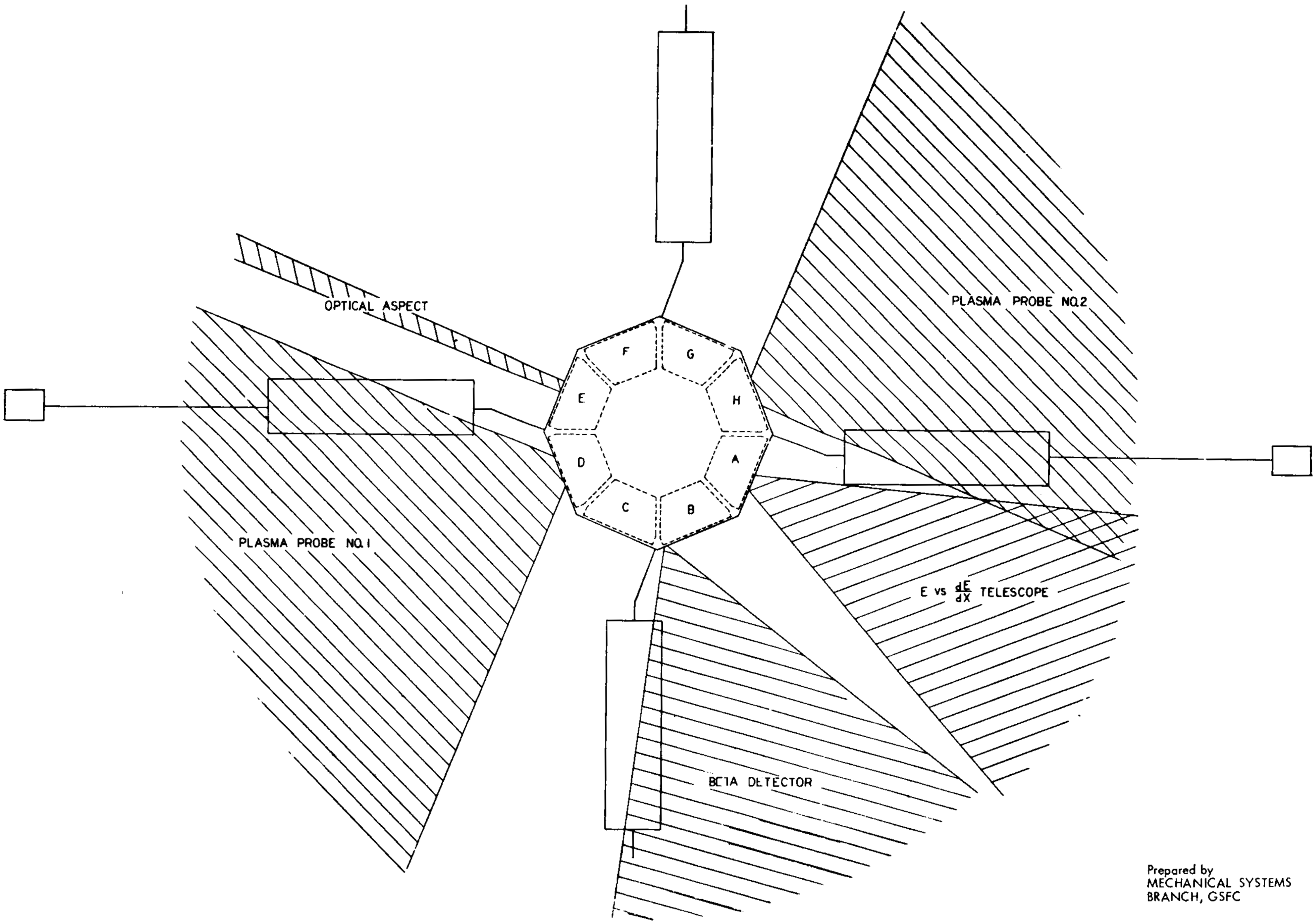


Prepared by
MECHANICAL SYSTEMS
BRANCH, GSFC

Figure 8 -- IMP D & E View Angles

#### 4.4.1 Magnetic Field Experiment

A triaxial set of fluxgate sensors is used to measure the three orthogonal components of the vector magnetic field. Each sensor measures the component of the magnetic field along its axis by detecting a second harmonic content in the secondary of the sensor transformer. The dynamic range of the unit is ±64 gammas on each component with a sensitivity of ±0.5 gamma.

#### 4.4.2 Solar Wind Experiment

Two Faraday cup detectors will measure the integrated flux of low-energy positive particles. The field of view of the two sensors is chosen to include all fluxes coming from directions within 30 to 150 degrees of the spacecraft spin axis. A set of grids in the sensor rejects electrons and low-energy ions while modulating the velocity of the flux to various levels. The detection of the modulated flux is achieved with an electrometer circuit for fluxes from $10^6$ to $5 \times 10^{10}$ particles/cm$^2$/sec at energies from 10 ev to 10 kev.

#### 4.4.3 Cosmic Ray Experiment (E vs dE/dX)

A thin dE/dX crystal is placed in coincidence with a thick total-energy scintillator. This experiment furnishes precision separation of protons, electrons, alpha particles, and heavy primaries, and is sensitive down to very small flux values. This provides a means of determining energy and charge spectra. Proton and alpha-energy sensitivity covers the regions 10 to 100 Mev per nucleon. It also provides mass separation of singly charged particles.

#### 4.4.4 Cosmic Ray Experiment (Neher-Type Ion Chamber)

This instrument measures total ionization produced per unit of time in a unit volume of standard-density air. It is simple to operate, maintains a constant calibration for extended periods of time, and is intended to serve as a basic radiation monitor.

#### 4.4.5 Cosmic Dust Experiment

The cosmic dust experiment will measure the momentum, kinetic energy, speed and approximate radiants of individual dust particles detected by the sensors over a long period of time. The cosmic dust sensor is a coincidence unit and comprises an acoustical sensor, an ionization sensor, and condenser sensor. The pulse-height analysis of the sensor signals will reveal the kinetic energy and momentum. Elapsed time measurements between sensor elements will reveal the velocity, and approximate directions will be determined from the aperture look angles.

## 4.5 INSTRUMENTATION

### 4.5.1 Optical Aspect System

The optical aspect system, a sun- and an earth-aspect sensing system, will be identical to that flown on IMP-I.

### 4.5.2 Power System

The primary power system consists of solar paddles, battery, and a solar array regulator with following converters to convert the prime system voltage to individual voltages used within the spacecraft. Solar paddles will be essentially those used on the IMP-I except for 3-mil glass shielding, since there is much less radiation expected about the moon than about the earth, and the mission lifetime of 6 months requires less shielding.

A summary of the power estimated for the spacecraft is shown in Table 6, and the power output curves for a three-paddle and four-paddle configuration are shown in Figure 9. As seen from these curves, three IMP-I paddles are marginal and four are more than adequate to perform the mission as estimated. The details of the three-paddle power calculation are given in Appendix VII. The final solar array chosen can be optimized in paddle spar angle and pitch angle so that four paddles smaller than the IMP-I paddles could be used with a resultant weight saving.

The solar-array regulator regulates the power output from the paddles and limits the charging voltage to the battery. The prime converter, multiconverter, encoder converter, and the optical aspect converter are essentially the same as those used in IMP-I except that more power output will be required from the prime converter to supply the transmitter for this particular mission and the individual converter voltages may have to be adjusted for the new experiments. The battery will be identical to that on the IMP-I satellite and the internal electrical harness wiring will be modified to adapt to the new spacecraft experiments and layout.

### 4.5.3 Telemetry Data System

The existing and well-proven pulsed frequency modulation (PFM) telemetry system will be employed. It is uniquely designed for scientific satellites to process both analog and digital data inputs from the various sensors. The system has been optimized in power, weight, and volume to encode this information onto the telemetry link. The system uses essentially a voltage-controlled oscillator (VCO) for handling the analog inputs, and a digital oscillator to handle digital data inputs. The digitization of the analog data is accomplished on the ground during data processing. The bit rate is 9 bits per second for the digital experiments, and 22 or 44 bits per second for the analog experiments depending on whether burst-blank or continuous transmission is used for that particular experiment.

TABLE 6

IMP D & E POWER SUMMARY

| | Peak Power watts | Average Power (watts) |
|---|---|---|
| Cosmic ray experiment | | 1.7 |
| Cosmic ray experiment | | 0.2 |
| Magnetic field experiment | | 0.8 |
| Solar wind experiment | 3.6 | 1.0 |
| Cosmic dust experiment | | 0.4 |
| Optical aspect system | | 0.3 |
| Transmitter and range and range-rate system (6-watt radiated power) | | 17.5 |
| Command receiver No. 2 | | 0.1 |
| Encoder, DDP and converter | | 0.7 |
| Apogee sequence timer | | 0.6 |
| Parameter card | | 0.05 |
| Undervoltage detector system | | 0.20 |
| Solar array regulator | | 0.24 |
| Battery | | 1.00 |
| Multiconverter | 3.7 | 3.3 |
| Prime converter | 14.8 | 11.8 |
| Total Average Power: | | 39.89 |
| Additional Peak Power: | | +6.0 |
| Total Peak Power: | | 45.89 |

The telemetry encoder and digital data processor (DDP) will be modified to fit the new experiment lineup, and a typical telemetry format is shown in Figure 10. The encoder and DDP will use identical submodules to those in IMP-I arranged in a different order to suit the IMP D&E needs. Three basic programmer cards will be used in the satellite. The undervoltage detector, the fluxgate calibrator, and the apogee sequence timer function will be combined within the IMP-I programmer cards 1, 2 and 4. The same IMP-I performance parameter card will be used except that the functions concerning the firing and separating of the apogee motor will be added.

4.5.3.1 Telemetry Received Signal Power

Transmitter output power will be 6 watts. The sideband power for a ±57-degree phase-modulated signal is twice the carrier power, or 4 watts.

$$P_t = +36.0 \text{ dbm}$$

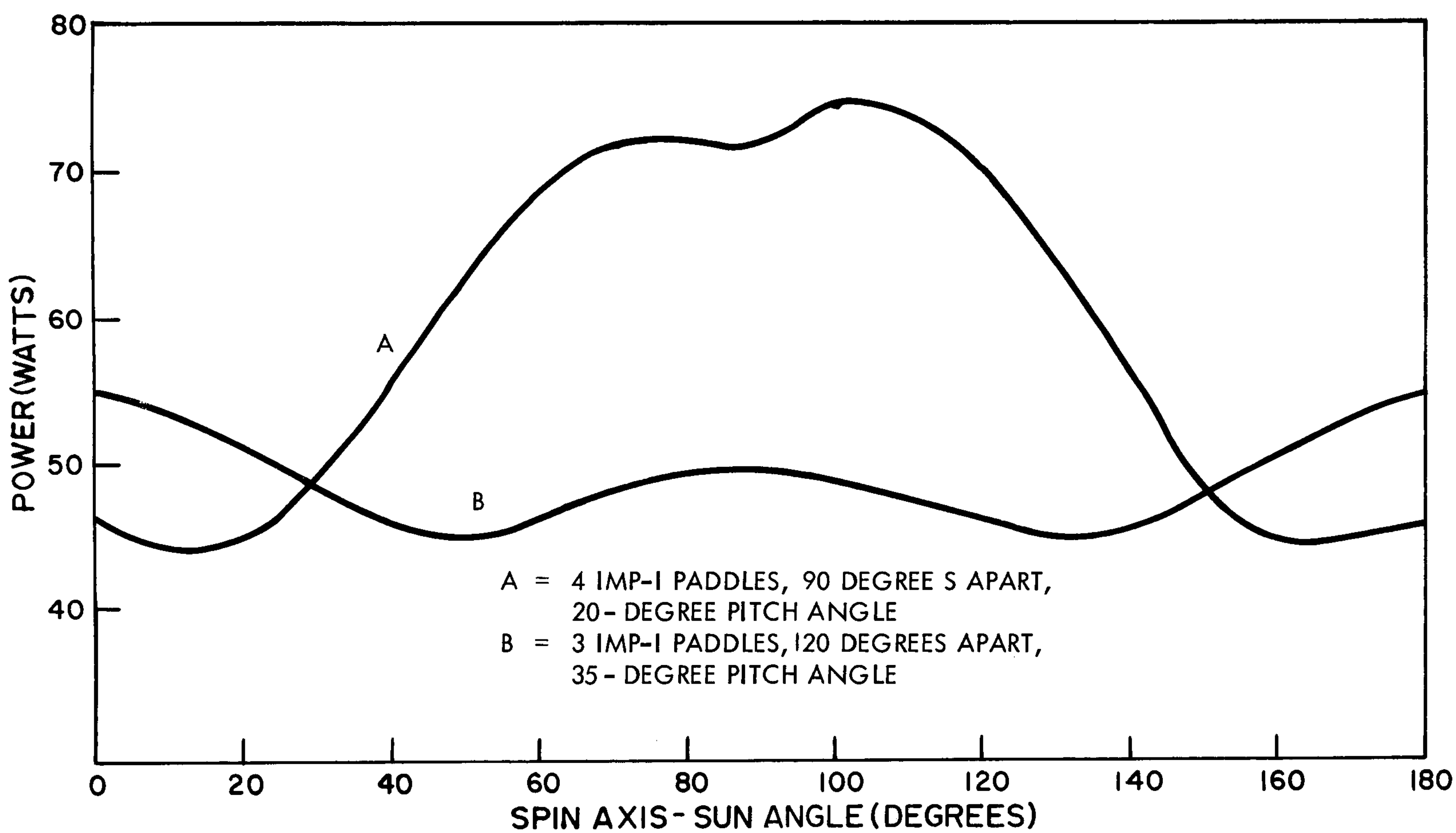


Figure 9--Approximate Initial Average Solar Array Power vs Spin Axis-Sun Angle

| FRAME \ CHANNEL | 0 | 1 | 2 | 3 | 4 | 5 | 6 | 7 | 8 | 9 | 10 | 11 | 12 | 13 | 14 | 15 | MODE |
|---|---|---|---|---|---|---|---|---|---|---|---|---|---|---|---|---|---|
| 0 | | PERFORMANCE PARAMETERS | | | | | | | | | | | | | | | A |
| 1 | | MAGNETOMETER | | | | | | | | | | $CR_1$ | | | | | D |
| 2 | | PLASMA | | | | | | | | | | | | | | | A |
| 3 | | MAGNETOMETER | | | | | | | | | | $CR_2$ | | | | | D |
| 4 | | IONIZATION CHAMBER$_{3,3}$ | | | | | | | | | | $CLOCK_4$ | | | | | D |
| 5 | | MAGNETOMETER | | | | | | | | | | $CR_1$ | | | | | D |
| 6 | | PLASMA | | | | | | | | | | | | | | | A |
| 7 | | MAGNETOMETER | | | | | | | | | | $CR_2$ | | | | | D |
| 8 | | OPTICAL ASPECT | | | | | | | | | | | | | MAG. ID | | D |
| 9 | | MAGNETOMETER | | | | | | | | | | $CR_1$ | | | | | D |
| 10 | | PLASMA | | | | | | | | | | | | | | | A |
| 11 | | MAGNETOMETER | | | | | | | | | | $CR_2$ | | | | | D |
| 12 | | IONIZATION CHAMBER$_{3,3}$ | | | | | | | | | | $CLOCK_4$ | | | | | D |
| 13 | | MAGNETOMETER | | | | | | | | | | $CR_1$ | | | | | D |
| 14 | | PLASMA | | | | | | | | | | | | | | | A |
| 15 | | MAGNETOMETER | | | | | | | | | | $CR_2$ | | | | | D |

( 1- 4 ARE 15 BIT ACCUMULATORS IN DDP )

Figure 10--IMP D & E PFM Telemetry Format

Transmitting-antenna gain includes the dipole gain, wiring-harness loss, and circular polarization loss.

$$G_t = -4 \text{ db}$$

Receiving-antenna gain is based on the assumption that the 21-db gain array of crossed-yagi antennas (NASA 16) will be used.

$$G_r = +21 \text{ db}$$

Attenuation due to the 250,000 nautical-mile maximum path loss is:

$$\left(\frac{\lambda}{4\pi r}\right)^2 = \frac{300}{136 \times 4\pi \times 2.5 \times 10^5 \times 1853}$$

$$= \left(3.80 \times 10^{-10}\right)^2 = 14.4 \times 10^{-20}$$

$$= 1.44 \times 10^{-19}$$

$$= 1.6 \quad -190 \text{ db}$$

$$= -188.4 \text{ db}$$

Substitution of the above factors in the received power equation yields:

$$W_r = P_t G_t G_r \left(\frac{\lambda}{4\pi r}\right)^2$$

$$= +36.0 -4 +21 -188.4 = -135.4 \text{ dbm}$$

$$= 2.9 \times 10^{-17} \text{ watts}$$

4.5.3.2 Safety Margin

Sky-noise temperature at 136 Mc in the plane of the ecliptic has an average value of about 600°K; however, there is a hot spot of about 2000°K looking toward the center of the galaxy.

The receiver-noise figure is 3 db. This corresponds to a receiver-noise temperature of 290°K.

The noise temperature due to the earth seen by the antenna side lobes and atmospheric noise is 55°K.

The noise temperature then becomes:

$$T_n = 600° + 290° + 55° = 945°K$$

A set of 128 contiguous filters will be used in the detection process during data reduction to enhance the output signal-to-noise ratio. The bandwidth of each filter is $\frac{100}{16}$ or 6.25 cps.

The performance of the telemetry system can best be judged by knowing the probability of a word error as a function of a parameter that is independent of the detection process. This parameter, $\beta$, is the received energy per bit divided by the noise-power-density $P_n$.

$$\beta = \frac{Wr \times T}{P_n \times n}$$

where $Wr$ = received power

$T$ = time length of word

$P_n$ = noise power density

$n$ = degree of coding

The power spectral density of the noise at the input to the receiver is given by $P_n = k\,T_n$

where $k = 1.38 \times 10^{-23}$ watt seconds per degree

$$P_n = 1.38 \times 10^{-23} \times 9\ 45°K$$

$$= 13.0 \times 10^{-21} \text{ watt seconds}$$

The parameter $\beta$ becomes:

$$\beta = \frac{2.9 \times 10^{-17} \times 0.16}{13.0 \times 10^{-21} \times 7} = 50.8 \text{ or } + 17.1 \text{ db}$$

In Figure 11 a vertical line is drawn corresponding to a value of $\beta$ of 50.8 or 17.1 db. At an error probability of one error in one thousand words, the safety margin that exists for a perfect comb filter is 12 db.

4.5.4 Telemetry Communications and Range and Range-Rate System

The spacecraft transmitter functions as a PFM-PM telemetry transmitter and also as a range and range-rate (R&RR) transponder. In lunar orbit and during the ranging transmission, no telemetry data will be sent, and likewise during telemetry transmission no ranging data will be transmitted. The optimum time sequence of the R&RR versus the telemetry-data transmission will be determined at a later date. The spacecraft transmitter will be identical to the IMP-I transmitter, except that the output power will be boosted from 4 watts to 6 watts. This is required for both telemetry and R&RR functions. (See Appendix VIII for a detailed R&RR power calculation.) The R&RR system will be identical to IMP-I, except that an additional command receiver will be added for redundancy. The antenna will be a modified turnstile and will be located on the outer periphery of the spacecraft.

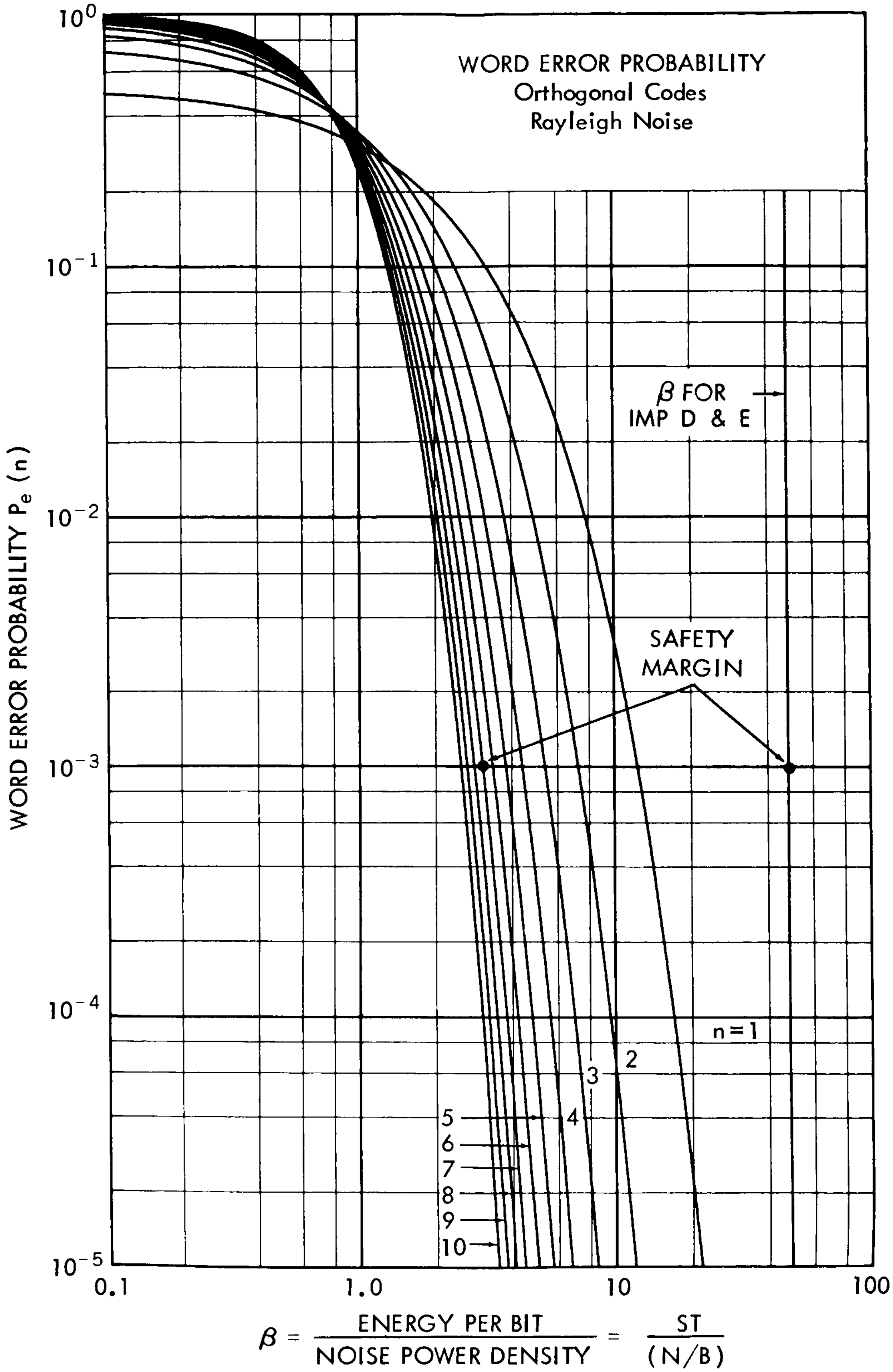


Figure 11--Word-Error Probability Curves for Rayleigh Noise

# 5. LAUNCH

## 5.1 ORBIT AND TRAJECTORY CONSIDERATIONS

A nominal typical flight plan for this mission was prepared by the Delta Project Office and a similar plan was worked out by the Douglas Aircraft Company. The two compared favorably, although the Douglas Company was more conservative in their approach. However, probability results agree satisfactorily when compared on a common basis (see Appendix I). Spacecraft weight and vehicle feasibility for this mission is reconfirmed by the Delta project office in Appendix IX. The Special Projects Branch ran studies which confirmed the above work and improved the success probabilities by improving the transfer trajectory.

A nominal orbit and the probabilities of achieving a lunar orbit from the nominal orbit were computed (Appendixes I and II). The fourth-stage motor was fired at 1-hour intervals for the nominal case. For the nominal orbit, the probabilities for achieving a particular orbit varied from 14 to 74 percent; however, higher probabilities have been achieved for higher flight-path angles. Probabilities for achieving any orbit about the moon vary from 70 to 99 percent in the improved nominal case. The overall mission reliability is very high as there are no mid-course corrections required. A small coast phase (10—15 minutes) or vehicle reorientation in pitch angle (up to 15 degrees) is required to optimize the success probabilities for the transfer trajectory. This coast phase or pitch maneuver is well within the capability of the Delta second stage. The reliability of the Delta vehicle for such a straight shot has been demonstrated repeatedly.

The basic flight plan, shown in Figure 3, is as follows:

(a) From the latest performance figures of the TAD and the X-258, and the spacecraft final weight, an optimum nominal transfer trajectory will be generated.

(b) The vehicle will be launched into this optimum nominal trajectory.

(c) The spacecraft/fourth-stage combination is boosted into the transfer trajectory by the X-258 and, after separation, coasts out to the lunar intercept area while spin-stabilized at 25 rpm.

(d) Depending upon the performance of all stages and the pointing accuracy obtained, the transfer trajectory will follow the optimum nominal transfer trajectory within certain deviations.

(e) The spacecraft will be tracked by range and range-rate and other tracking systems; a set of orbital parameters and lifetime contours will be generated and improved almost continuously during the approximately 70-hour transfer trajectory flight time.

(f) From the latest lunar parameter and lifetime data, the project manager and project scientist will select the optimum time to fire the fourth stage.

(g) The command to initiate the apogee sequence timer will be given two hours before optimum kick-motor fire time.

(h) Functioning of the timer during the 2-hour interval will be confirmed by telemetry. If confirmation of kick-motor firing is not received within appropriate tolerances, a direct command to fire the motor will be initiated.

(i) This direct command bypasses the timer function and fires the motor igniter as a direct output from one of the command receiver channels. This system allows a fourfold opportunity to fire the motor.

The launch window for the transfer trajectory, it should be pointed out, occurs for only 3 succeeding days a month, and then for only 5 minutes a day during these 3 days. The launch window can be enlarged up to 20 minutes a day by BTL's ability to handset the trajectory parameters. However, to achieve a desirable range of spin-axis sun angles (between 30 and 150 degrees for purposes of power, experiment look angle, and temperatures), launch must be made in either December or June to achieve the first 4 months of orbital life within these spin-axis requirements. Launching the following month would result in only the initial 3 months within the desired spin-axis sun angle.

The launch window for lunar injection is not critical, and excellent orbits can be obtained during a 1-hour period in the nominal case or a 2-hour period in the improved nominal case.

## 5.2 ORBIT LIFETIME CONSIDERATIONS

A Runge-Kutta integration of the Lagrangian planetary equation was carried out for the 100 orbits of the improved nominal transfer trajectory (Appendix III). For these orbits, the important part of the disturbing function is the earth effect, which is long-periodic with respect to both the lunar satellite and the earth-moon orbit. The results, shown in Figure 12, may be summarized as follows: Out of 100 orbits considered, 92 orbits survived 40 days; 75, 80 days; 67, 120 days; 61, 160 days; 56, 200 days; 48, 300 days; and 43, 400 days.

## 5.3 LAUNCH VEHICLE

The launch vehicle for the Lunar IMP will be a thrust-augmented Delta utilizing an X-258 third stage and a JPL kick motor for the fourth stage. The launch configuration is shown in Figure 13. Prime contractor for this three-stage launch vehicle is the Douglas Aircraft Company.

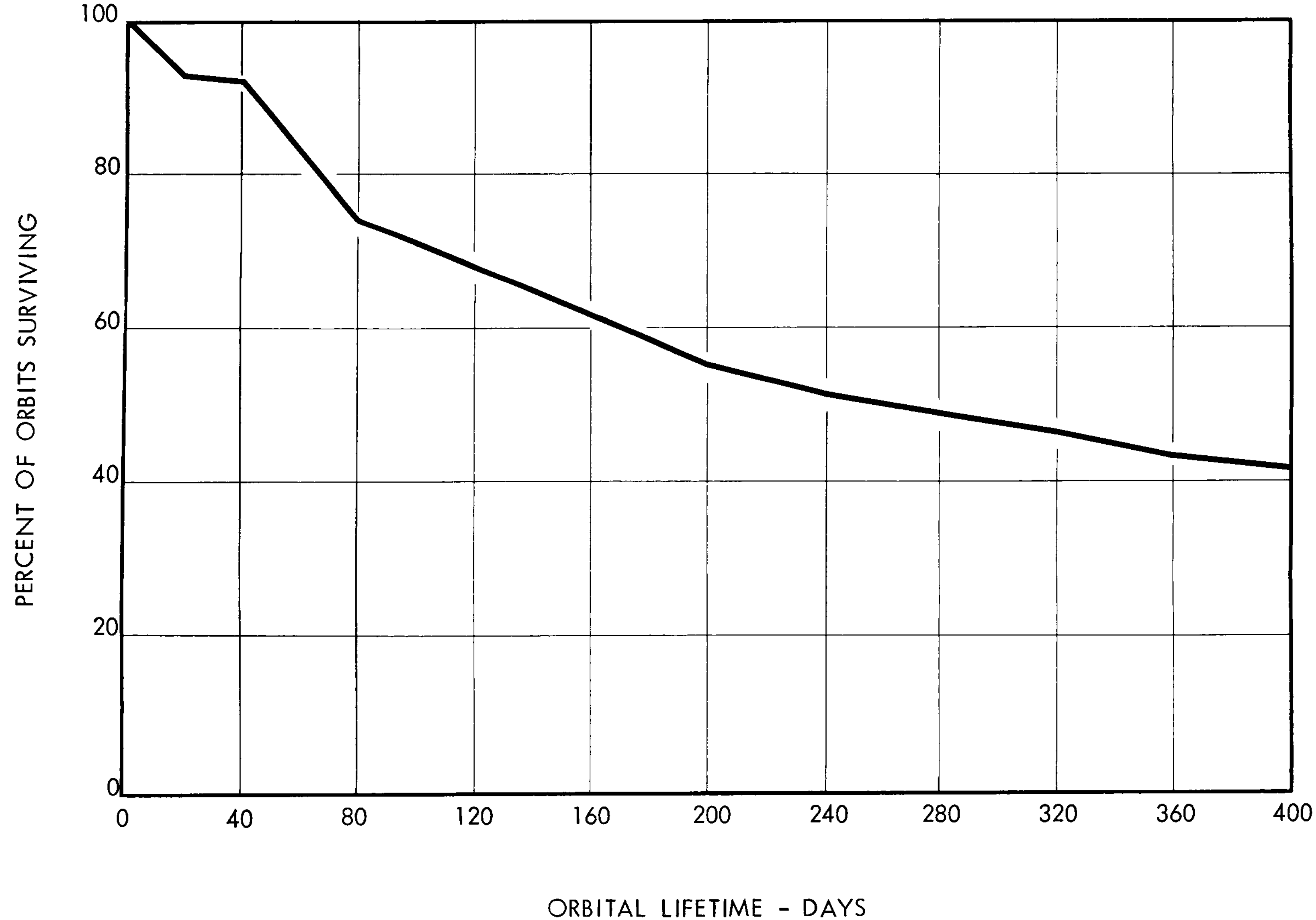


Figure 12 - - Results of a Lifetime Study for a 100-Run Monte Carlo Analysis of the Improved Nominal Lunar Transfer Trajectory

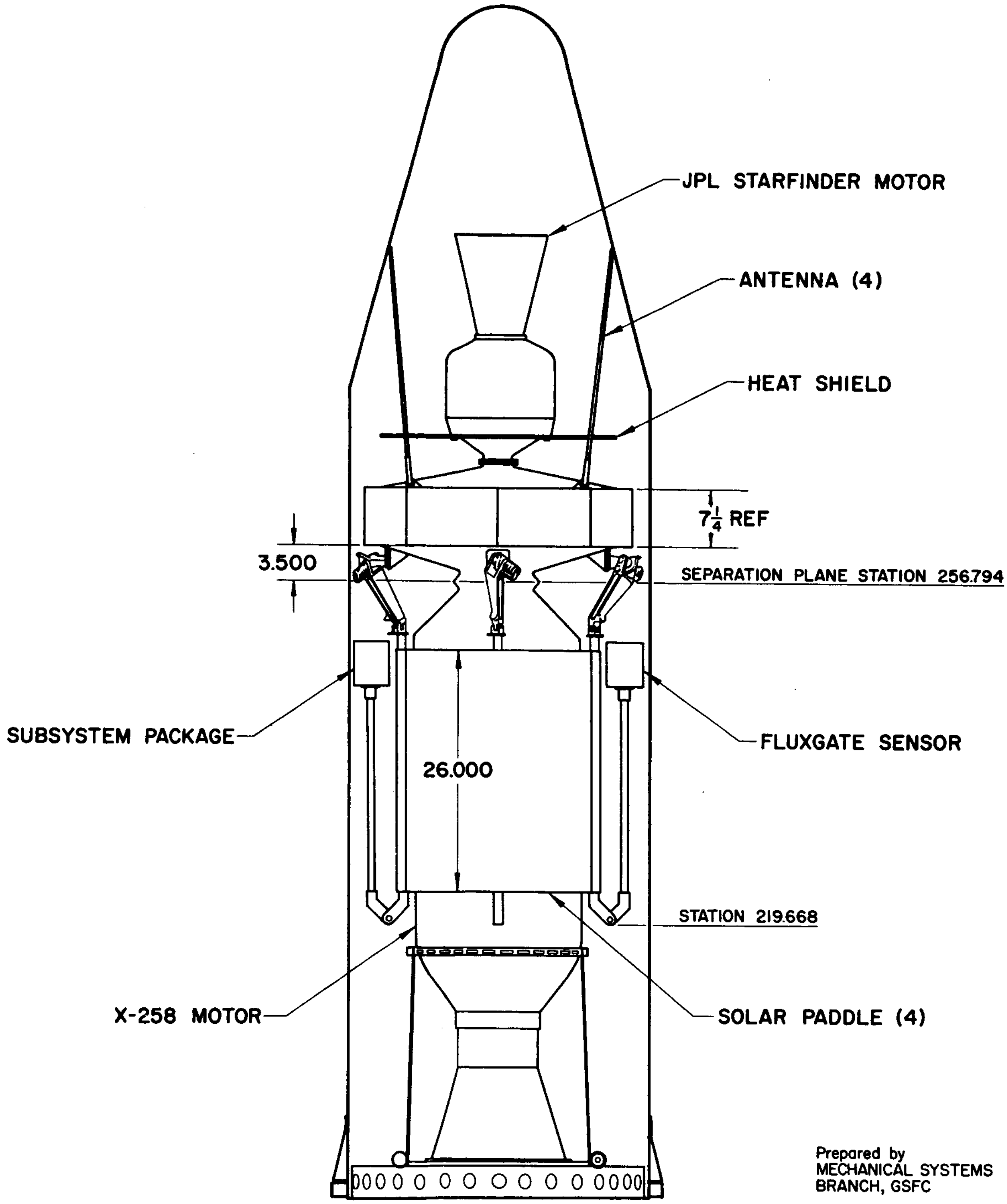


Figure 13 - - IMP D&E Nosecone (Side View)

# 6. GROUND SYSTEMS

## 6.1 LAUNCH SUPPORT EQUIPMENT

The Atlantic Missile Range and the launch vehicle contractor, Douglas Aircraft Company, will supply suitable personnel to handle the following tasks:

- Assemble the Delta launch vehicle

- Assume responsibility for checkout of the vehicle's transmitters and range safety beacon

- Prelaunch checkout and launching the vehicle

GSFC will be responsible for delivery of the completed IMP D & E satellite to the Atlantic Missile Range, and for an operational checkout of the satellite after installation of the launch vehicle. The final test of the satellite before launching will be made at a time break in the count-down.

## 6.2 SPACECRAFT GROUND TEST EQUIPMENT

The equipment of the IMP D & E test stand is divided into five major categories:

- Transducer simulators - and simulated sources, such as radioactive and light sources to energize transducers of some spacecraft experiments. (Current inputs and count inputs are used as simulators for other experiments.)

- Spacecraft control and monitoring equipment – such as blockhouse control unit, external power supplies, and high-accuracy voltmeters

- Signal receiving and storage – included here are equipment for receiving, displaying, and demodulating the phase-modulated carrier, and for RF frequency and power measurements, as well as WWV time signals, and tape recorders

- PFM decoding to extract channel, frame, and master-frame synchronization signals, and generate gates to select any desired channel for examination and printout

- Experiment logic decoding – collects PFM-to-digital decoder outputs, restores original format, and converts to equivalent decimal form (Programmers are used to identify the experiments being transmitted, select proper conversion format, and provide inputs to printout equipment.)

## 6.3 TRACKING OPERATIONS

The IMP D & E satellite will utilize a range and range-rate transponder. The Orbiting Geophysical Observatories (S-49/50) ground stations will be employed for range and range-rate tracking.

At launch, early tracking data will be collected by Ascension Island and Johannesburg. Azusa and other Atlantic Missile Range radar information will be available to GSFC for incorporation into a computer program. The vector information from the AMR radar track on range and velocity of the booster stages will provide inputs for computing the initial injection-point velocities of the spacecraft to a nominal orbit, after which data from the range and range-rate and Minitrack stations will be added into the computer problem to correct the orbit calculations. As the tracking stations receive additional data, the accuracy of the calculated parameters of the orbit will be continuously improved.

## 6.4 TELEMETRY OPERATIONS

Three receiving stations (Woomera, Australia; Johannesburg, South Africa; and Santiago, Chile) are properly equipped and spaced in longitude to record the telemetry signal for most of the time. These telemetry-receiving antennas have 21-db gain, and may be circularly polarized. Other stations may be utilized as required in accordance with their capability using the following receiving antennas: 40-foot dish, 21-db gain; 85-foot dish, 27-db gain; 16-yagi linearly polarized 21-db gain. Present plans are to record telemetry continuously for 6 months and periodically thereafter as required by the project scientist. The minimum expected life of the spacecraft is 6 months.

## 7. INFORMATION-PROCESSING SYSTEM

### 7.1 GENERAL

The information-processing system designed to treat the IMP D & E satellite data is identical to the IMP-I information processing system.

### 7.2 OBJECTIVES

The objective of the IMP D & E information-processing system is to provide the scientist with precise data from his experiment in as short a time as possible in the most useful format. Inherent in the system is the utilization of high-speed electronic data-processing machinery (EDPM) and high-performance analog-to-digital conversion equipment. The principal operation is one of conversion of telemetry-tape signals, representing either encoded digital data or continuous signal data, to a universal digital representation. This information is recorded on magnetic tape in a form suitable for handling by EDPM. The operations of checking, editing, putting into format, and scattering of an individual experimenter's data is an internal operation in a medium-scale computer.

The basic output of the system will be in two forms: computer magnetic tape in IBM high- or low-density bit modes with formats (binary coded decimal) suitable for computer analysis, using an algebraic compiler language such as FORTRAN; and accompanying paper printouts of the tape information in a format bearing a one-to-one correspondence with the tape recorded format. If necessary, additional or complementary output media will be provided upon special request from the experimenter and approval by the project staff.

### 7.3 SCIENTIFIC EXPERIMENTAL DATA

Each experimenter will receive his experimental information with accurate time reference. There will be no scaling of the information in order to return the processed analog data to its original form (i.e., a voltage from 0 to +5), but a calibration and scaling procedure (mathematical formula and error analysis) will be provided.

No merging of scientific data with trajectory information will occur directly in the IMP D & E information-processing system (IPS). The justification for not merging this information by the system is that the trajectory data normally undergoes a series of modifications and refinements before finalization. Hence, the scientific data will be ready for distribution to the experimenters before the trajectory and orientation information is available. In the initial stages of data analysis, it is not necessary for the experimenter to know precisely where the spacecraft is located or oriented. Interpretation and correlation of scientific data among the experimenters can proceed at a rapid rate even when an accurate time reference alone is provided.

## 7.4 SPACECRAFT ORIENTATION AND TRAJECTORY DATA

Each experimenter will receive a master trajectory tape and printout of the orientation and trajectory location of the spacecraft as a function of time (UT). This information (and the corresponding units) will include:

(1) Universal time (month-day-hour-minute)

(2) Geodetic coordinates of subsatellite point (latitude, longitude – degrees)

(3) Geocentric distance of satellite (earth radii)

(4) Elevation of satellite (kilometers)

(5) Geomagnetic coordinates of subsatellite point (latitude, longitude – degrees)

(6) Celestial inertial coordinates of satellite location (earth radii)

(7) Location of sun in payload coordinates (polar angle relative to spin axis of satellite and azimuth direction relative to the optical aspect sensor – degrees)

(8) Center of moon in celestial coordinates (earth-centered and in earth radii)

(9) Spacecraft subsatellite position in lunar coordinates (latitude, longitude-degrees)

(10) Distance of spacecraft (km) from center of moon

These items are to be provided at suitable time intervals. Interpolation formulas or computer subroutines will be provided to allow an increase in the effective sampling rate of this information.

The function of the master trajectory tape and printout is to provide the experimenter with the essential spacecraft information required to reach definite conclusions and interpretations regarding the significance of his scientific data. Intercorrelation of experimenter's data will be the responsibility of the individual experimenters. At no time will the distribution of information permit one experimenter to receive information pertaining to another experiment directly from the IMP IPS.

## 7.5 INFORMATION-PROCESSING SYSTEM

The IMP D&E telemetry system utilizes a hybrid time-multiplexed pulse-frequency modulation (PFM) encoding technique whose salient features are described in Reference 1. The details of applying the PFM technique to the IMP D&E have been adequately presented in the IMP interface document of Reference 2. The essential fact is that the IMP D&E telemetry system, through time-multiplexing, combines a variety of experimental-data bit rates and modes (i.e., digital, analog or continuous signal) in a maximally efficient and convenient manner. Although the system inherently operates with a burst-blank time envelope, provision is made for continuous information transmission from certain experiments as required. Detection and identification of this information in its various modes, digitization, and final transfer into EDPM format for analysis are the goals of the processing system. Four major functions are performed by the system:

- Telemetry tape digitization
- Master data tape production
- Experimenters data tape production
- Master trajectory tape production

References: 1. Rochelle, R. W., Pulse Frequency Modulation, NASA-GSFC Technical Note D-1421 (1962)

2. White, H. D., IMP PFM Encoder, NASA-GSFC IMP Project (1962)

OPTIONAL FORM NO. 10
5010-104

UNITED STATES GOVERNMENT

# *Memorandum*

APPENDIX I

TO : William R. Schindler
Delta Project Manager

DATE: June 24, 1963

FROM : Jyri Kork

SUBJECT: Success Probabilities for the IMP D & E Mission

REFERENCE: Memorandum dtd May 14, 1963 W.R. Schindler to Dr. N.F. Ness

This is a short presentation of the results of a Monte Carlo study establishing the success probabilities for the IMP D & E mission. The basic outline of the trajectory analysis taken by the Delta group was established in reference 1.

A nominal lunar trajectory was generated for a December 1964 launch date. A thrust augmented Delta with an X-258 third stage and a payload weight of 180 lbs. was used, employing the following initial conditions: $V_i$ = 35985.0 fps, $h_i$ = 100 n. mil, $\gamma_i$ = 1.2° and $A_i$ = 85° (AMR launch). The nominal flight time was about 72 hours. No vehicle re-orientations or midcourse corrections were considered, the satellite axis being fixed in inertial space by spin stabilization.

A 100 run Monte Carlo analysis was generated around this nominal trajectory, using the Republic n-body program at Goddard and a normal probability distribution.

The following $1\sigma$ deviations in the launch conditions were used:

| | | |
|---|---|---|
| Velocity: | $\Delta V$ | = ±41 fps |
| Flight path angle: | $\Delta\gamma$ | = ±0.5° |
| Azimuth: | $\Delta A$ | = ±0.22° |

For each individual run the fourth stage (JPL spherical motor) was "fired" at every full hour of flight time, resulting in a tabular printout of corresponding lunar orbit osculating elements (pericynthion - apocynthion radii, eccentricities, inclinations, etc.). The fourth stage lunar orbit injection window was found to be 2 - 4 hours in general, running in certain cases even up to 15 hours.

It was assumed that during the lunar transfer phase sufficient tracking data can be accumulated and optimum firing time for each individual flight may be utilized (within ±1/2 hour).

Probabilities for establishing lunar orbits with a Delta vehicle were found to be the following:

| REQUIREMENTS | PROBABILITY |
| --- | --- |
| $h_p < 1000$ km; $40° < i < 80°$ | 14% - 16% |
| $h_p < 1000$ km; $20° < i < 80°$ | 23% - 25% |
| $h_p < 3000$ km; $40° < i < 80°$ | 33% - 42% |
| $h_p < 3000$ km; $20° < i < 80°$ | 46% - 57% |
| $h_p < 3000$ km; $10° < i < 80°$ | 58% - 74% |
| All orbits (any $h_p$, any $i$) | 70% - 90% |

The lower limits of the probability spreads are obtained by selecting only "stable" lunar orbits (i.e. apocynthion radii less than the Hill's surface for escape in a restricted 3-body problem). The upper limits include all circumlunar orbits that do not escape or hit the moon.

It should be pointed out, at this point, that the overall mission reliability is very high, as there are no parking orbits, no missile reorientations or midcourse corrections required. The reliability of the Delta vehicle for such a "straight shot" has been demonstrated repeatedly. The launch window at AMR can be enlarged up to 20 minutes (on three days each month) by BTL's ability to hand-set the trajectory parameters.

A similar Monte Carlo analysis was conducted by the Douglas Aircraft Company, using 2000 sample runs. The probability for obtaining lunar orbits in the DAC study was 57% - 63% (corresponding to our 70% - 90%). Actually, DAC study is extremely conservative and based on somewhat more restricted ground rules. If our results are reduced to DAC ground rules, a perfect correlation between the trends of the probability distributions has been shown to exist.

Jyri Kork

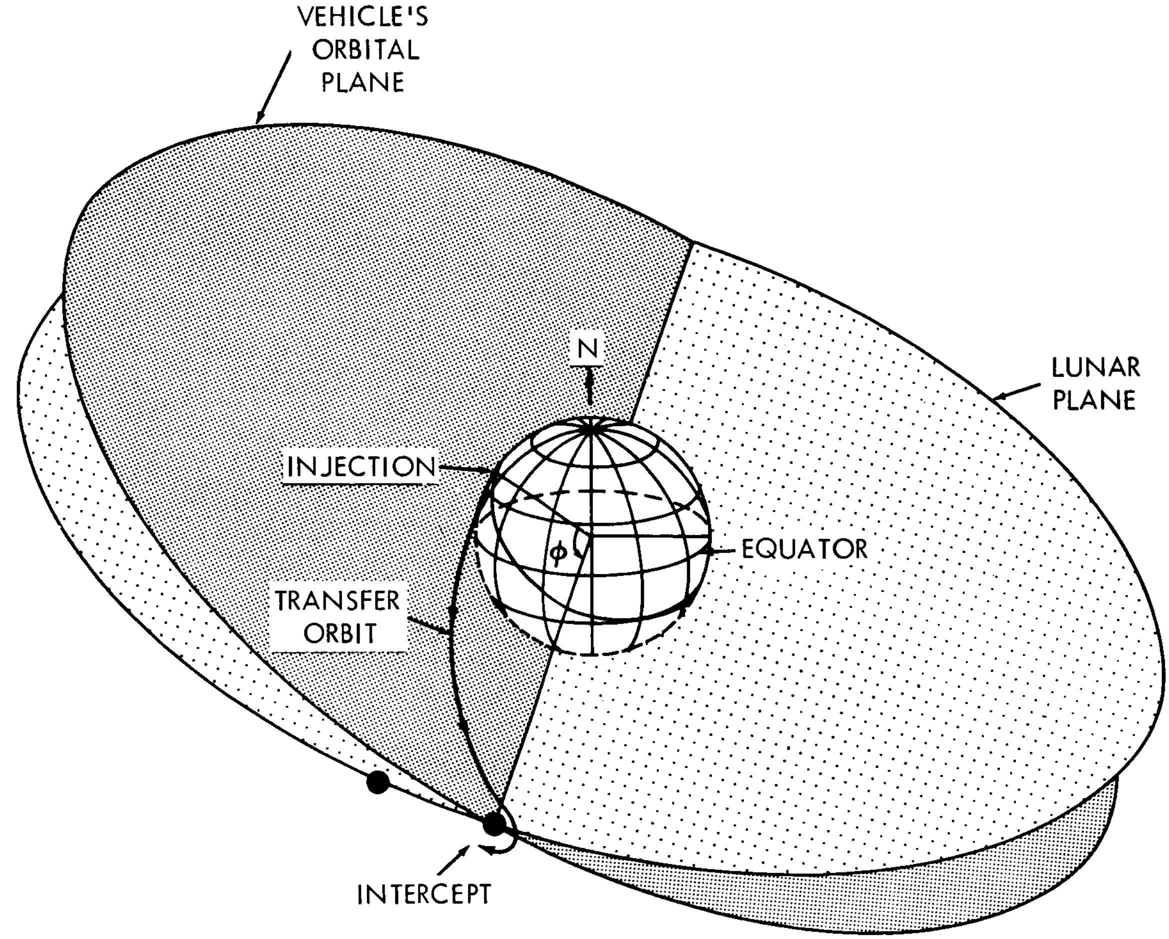
VEHICLE'S
ORBITAL
PLANE
N
LUNAR
PLANE
INJECTION
$\phi$
EQUATOR
TRANSFER
ORBIT
INTERCEPT

# NOMINAL TRAJECTORY PARAMETERS

## ASCENT & TRANSFER

| | |
|---|---|
| Burnout Velocity, $V_b$ | 35,985.0 fps |
| Altitude, $h_b$ | 100 n. mi. |
| Flight Path Angle, $\gamma_b$ | +1.2° |
| Latitude, $L_b$ | +19.2° |
| Longitude, $\lambda_b$ | -23.9° |
| Launch Azimuth, $A_L$ | 85° |
| Injection Date, $t_b$ | Dec. 5, 1964 |

## LUNAR ORBIT

| | |
|---|---|
| Fourth Stage $\Delta V_4$ | = 3684 fps |
| Pericynthion Radius | = 2500 km |
| Apocynthion Radius | = 7500 km |
| Inclination | = 142° (Retro-grade orbit) |
| Eccentricity | = 0.55 |

$\Delta V_4$ Fired at 71.5 hours

## 1 σ INJECTION ERRORS

| | |
|---|---|
| Velocity, $\Delta V$ | 41 fps |
| Azimuth, $\Delta A$ | 0.22° |
| Flight Path Angle, $\Delta\gamma$ | 0.5° |

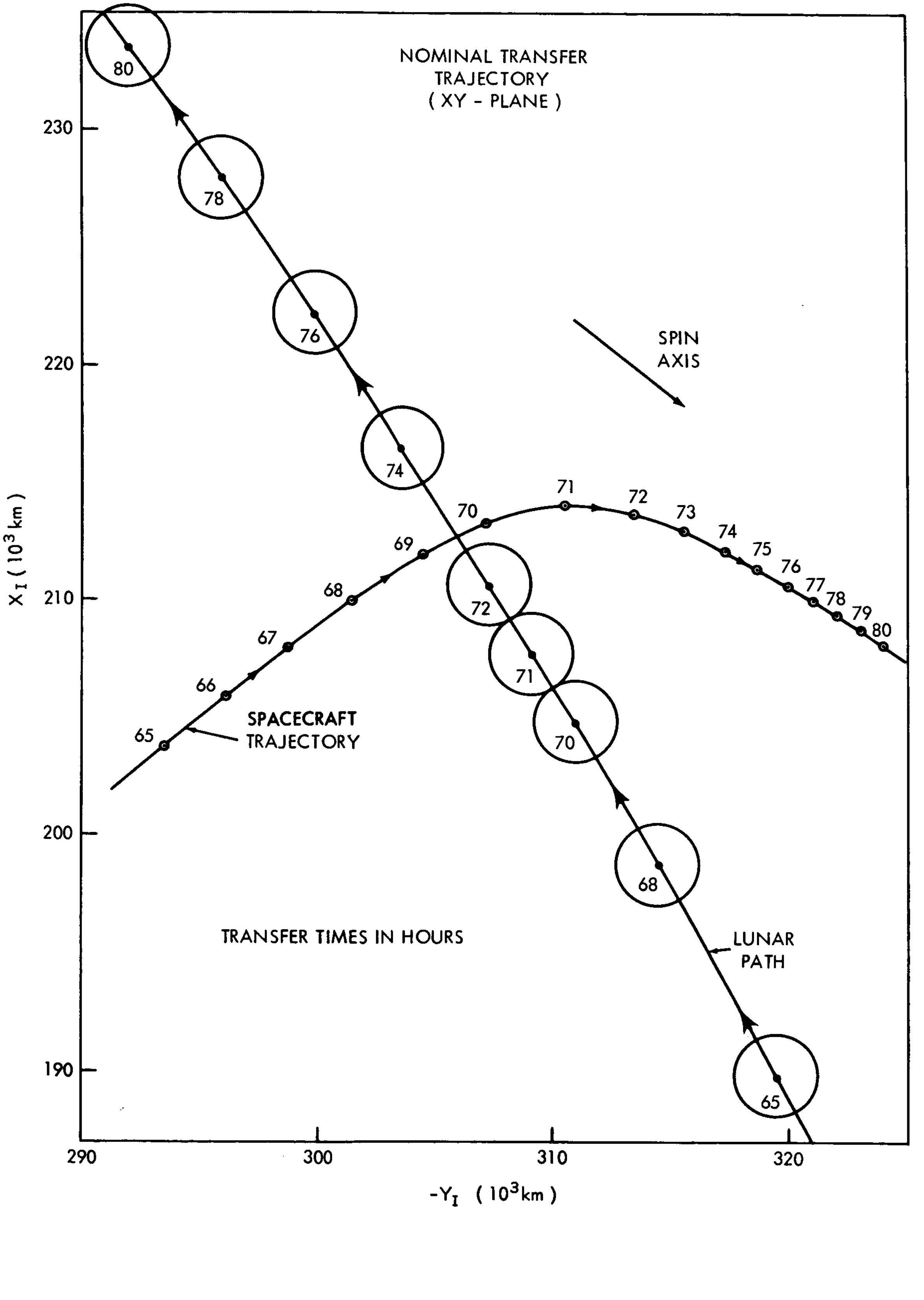
NOMINAL TRANSFER
TRAJECTORY
( XY - PLANE )
SPIN
AXIS
SPACECRAFT
TRAJECTORY
LUNAR
PATH
TRANSFER TIMES IN HOURS
$X_I$ ( $10^3$ km )
$-Y_I$ ( $10^3$ km )
230
220
210
200
190
290
300
310
320
65
66
67
68
69
70
71
72
73
74
75
76
77
78
79
80

## SUCCESS PROBABILITIES FOR THE IMP D & E MISSION

| ORBIT REQUIREMENTS | PROBABILITY |
|---|---|
| $h_p < 1000$ km; $40° < i < 80°$ | 14%-16% |
| $h_p < 1000$ km; $20° < i < 80°$ | 23%-25% |
| $h_p < 3000$ km; $40° < i < 80°$ | 33%-42% |
| $h_p < 3000$ km; $20° < i < 80°$ | 46%-57% |
| $h_p < 3000$ km; $10° < i < 80°$ | 58%-74% |
| All Orbits (any $h_p$, any $i$ ) | 70%-90%* |

*DAC results: 57%-63%
(Conservative approach)

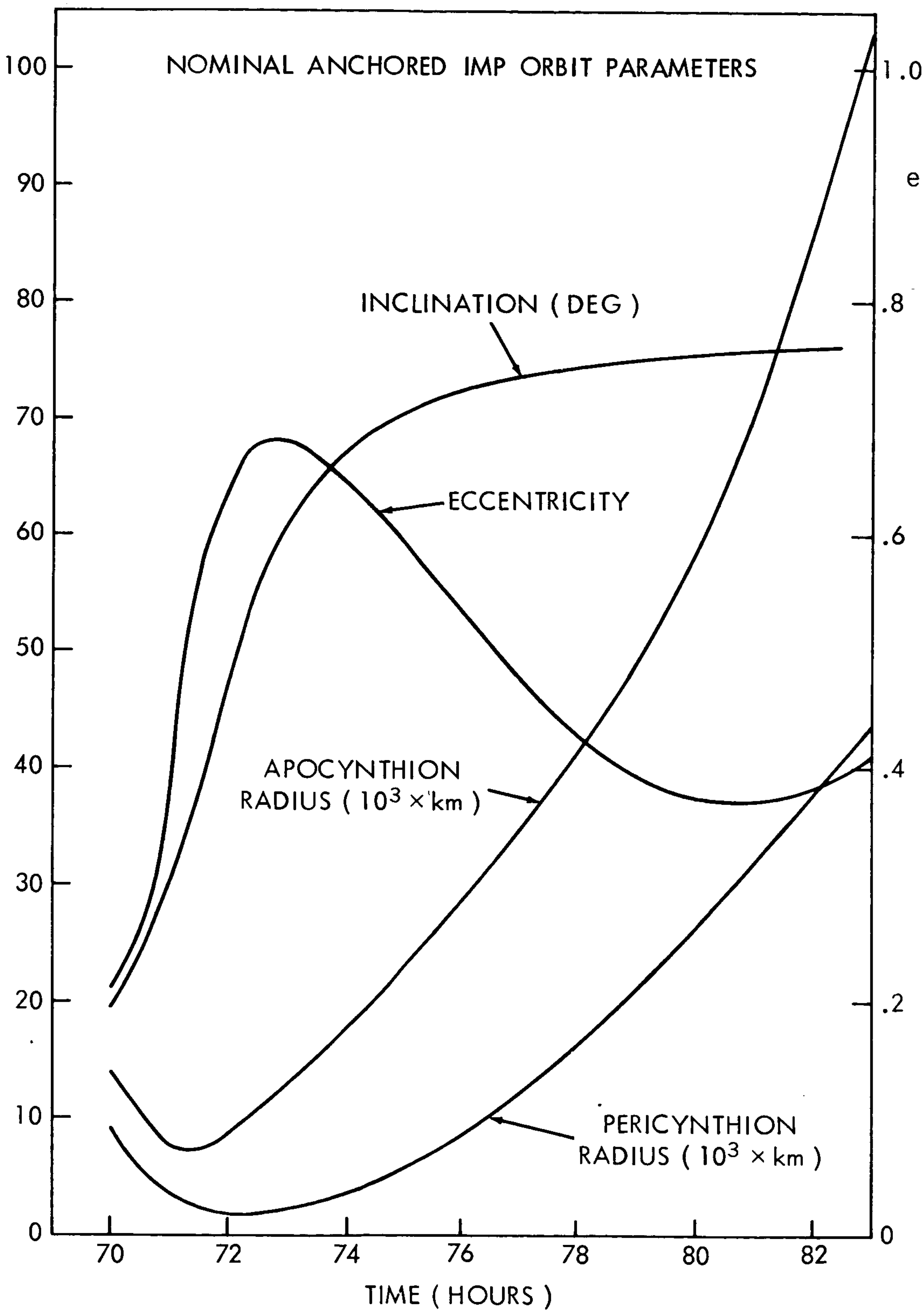

NOMINAL ANCHORED IMP ORBIT PARAMETERS
100
90
80
70
60
50
40
30
20
10
0
1.0
e
.8
.6
.4
.2
0
INCLINATION ( DEG )
ECCENTRICITY
APOCYNTHION RADIUS ( $10^3 \times$ km )
PERICYNTHION RADIUS ( $10^3 \times$ km )
70
72
74
76
78
80
82
TIME ( HOURS )

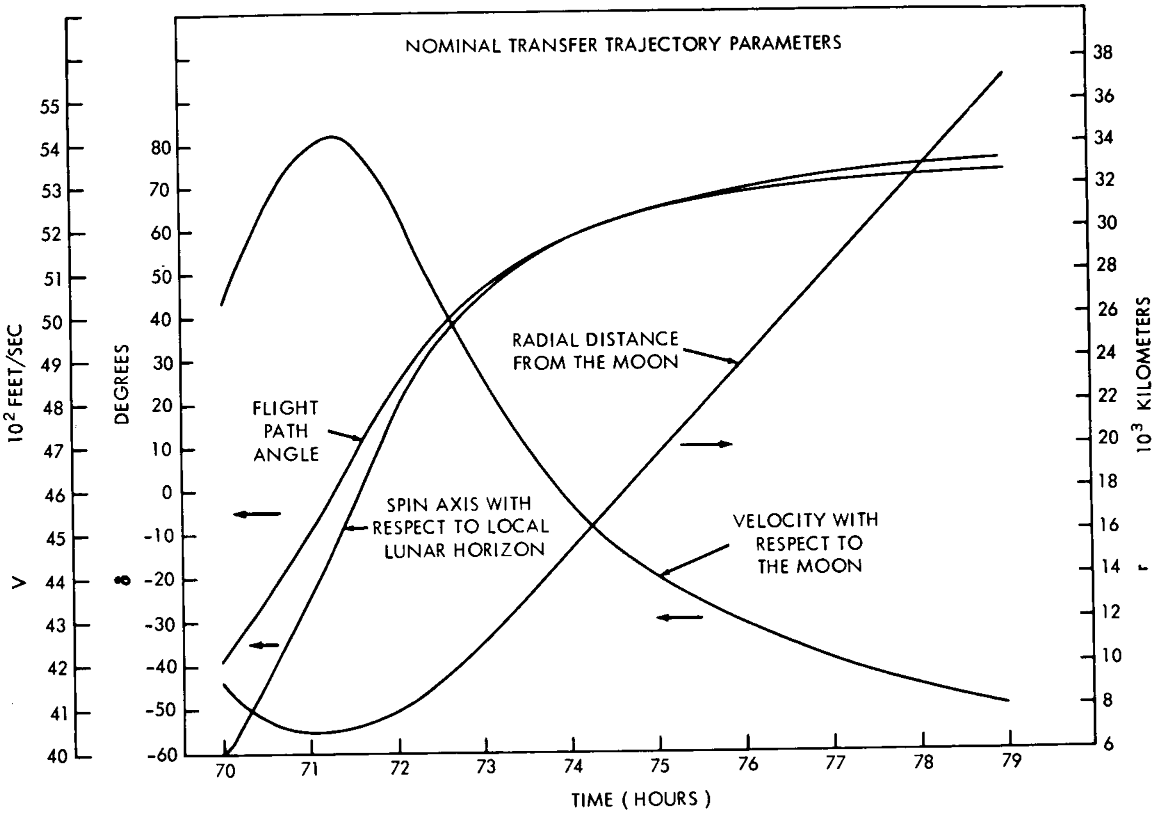

NOMINAL TRANSFER TRAJECTORY PARAMETERS
FLIGHT PATH ANGLE
SPIN AXIS WITH RESPECT TO LOCAL LUNAR HORIZON
RADIAL DISTANCE FROM THE MOON
VELOCITY WITH RESPECT TO THE MOON
V 10² FEET/SEC
δ DEGREES
r 10³ KILOMETERS
TIME ( HOURS )
40
41
42
43
44
45
46
47
48
49
50
51
52
53
54
55
-60
-50
-40
-30
-20
-10
0
10
20
30
40
50
60
70
80
6
8
10
12
14
16
18
20
22
24
26
28
30
32
34
36
38
70
71
72
73
74
75
76
77
78
79

COMPARISON OF PROBABILITIES

NOTE: 4TH STAGE FIRED AT POINT OF CLOSEST APPROACH

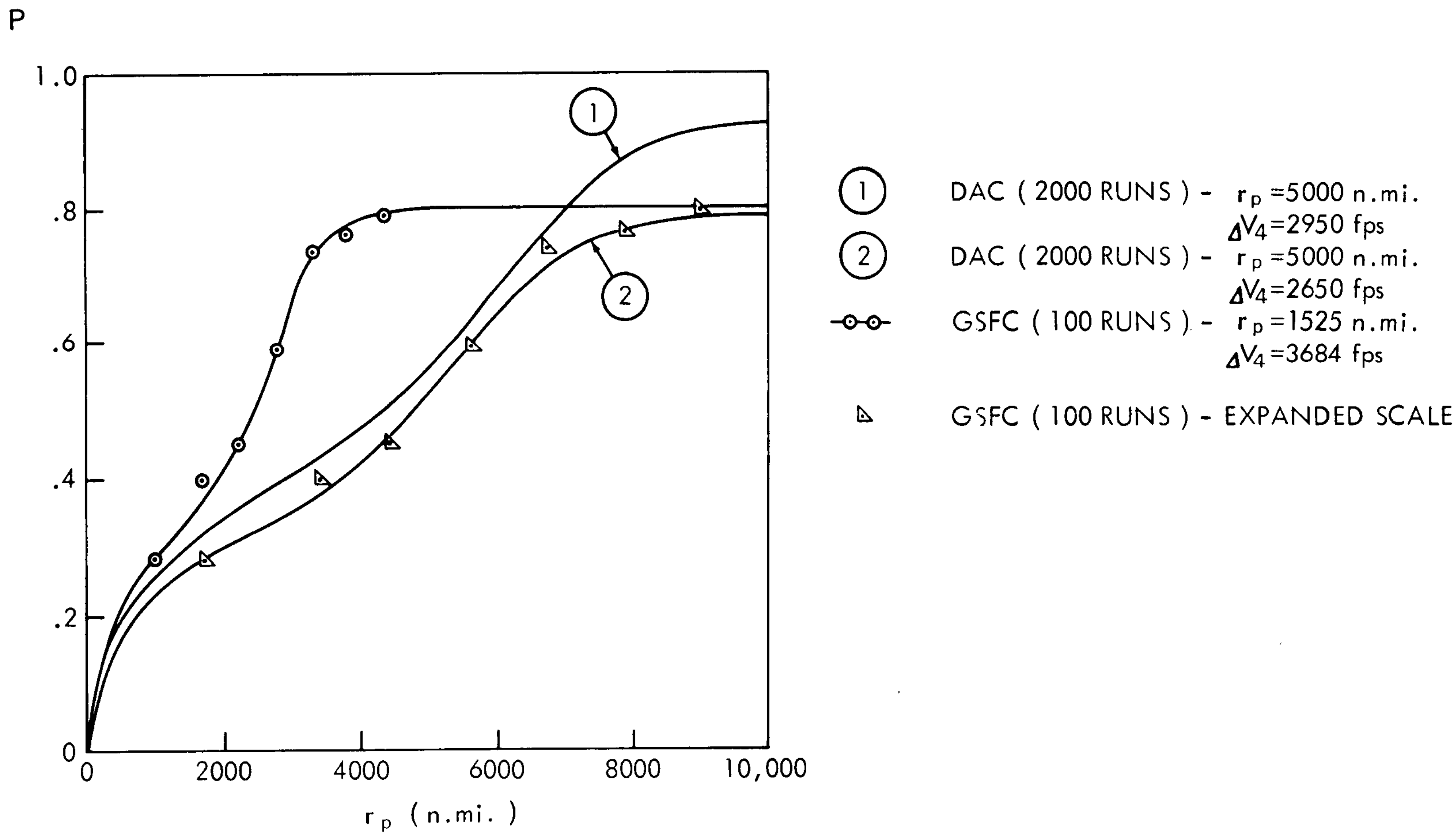

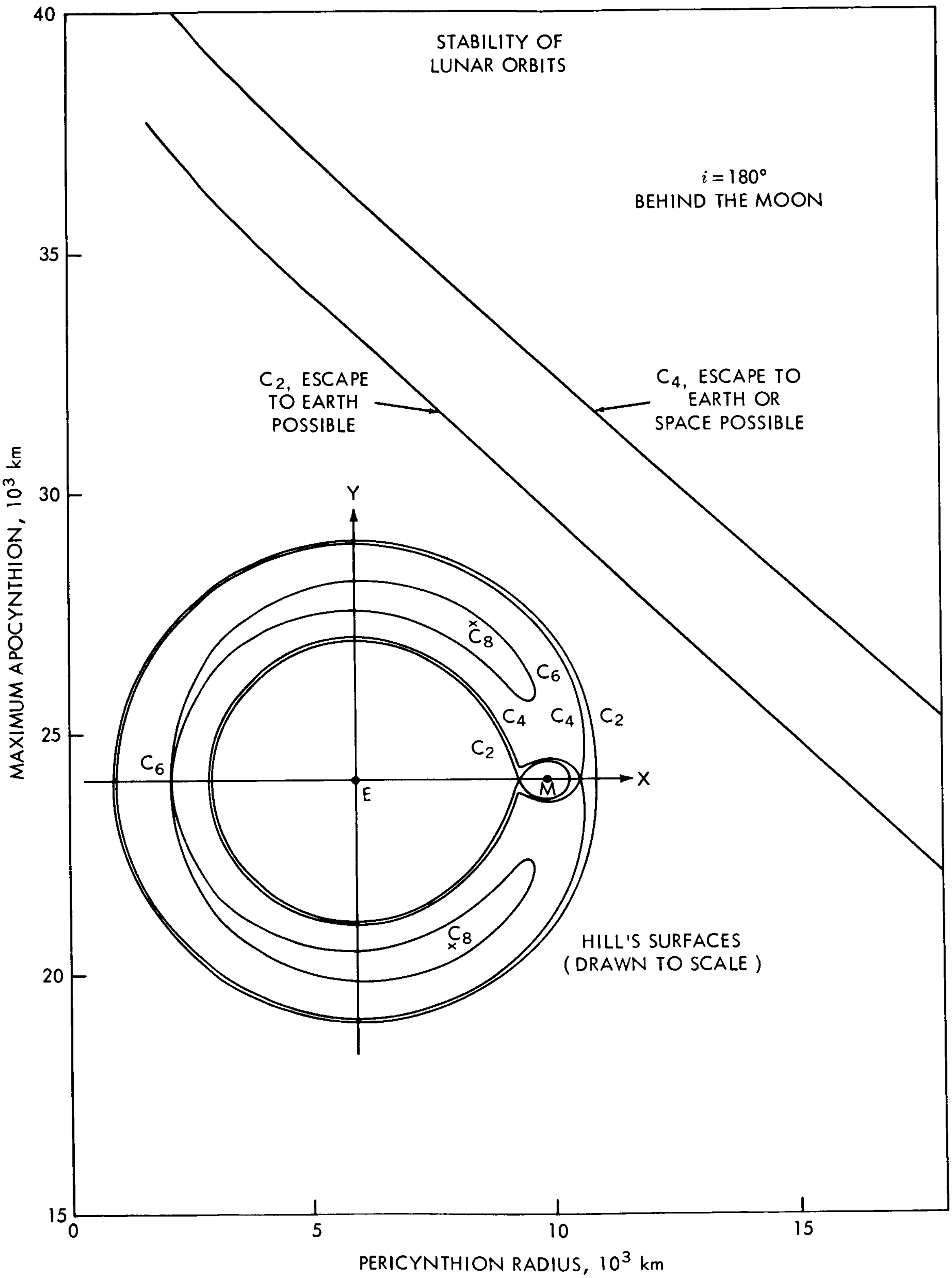

STABILITY OF LUNAR ORBITS
$i = 180°$
BEHIND THE MOON
$C_2$, ESCAPE TO EARTH POSSIBLE
$C_4$, ESCAPE TO EARTH OR SPACE POSSIBLE
HILL'S SURFACES (DRAWN TO SCALE)
Y
X
E
M
$C_2$
$C_4$
$C_6$
$C_8$
MAXIMUM APOCYNTHION, $10^3$ km
PERICYNTHION RADIUS, $10^3$ km
40
35
30
25
20
15
0
5
10
15

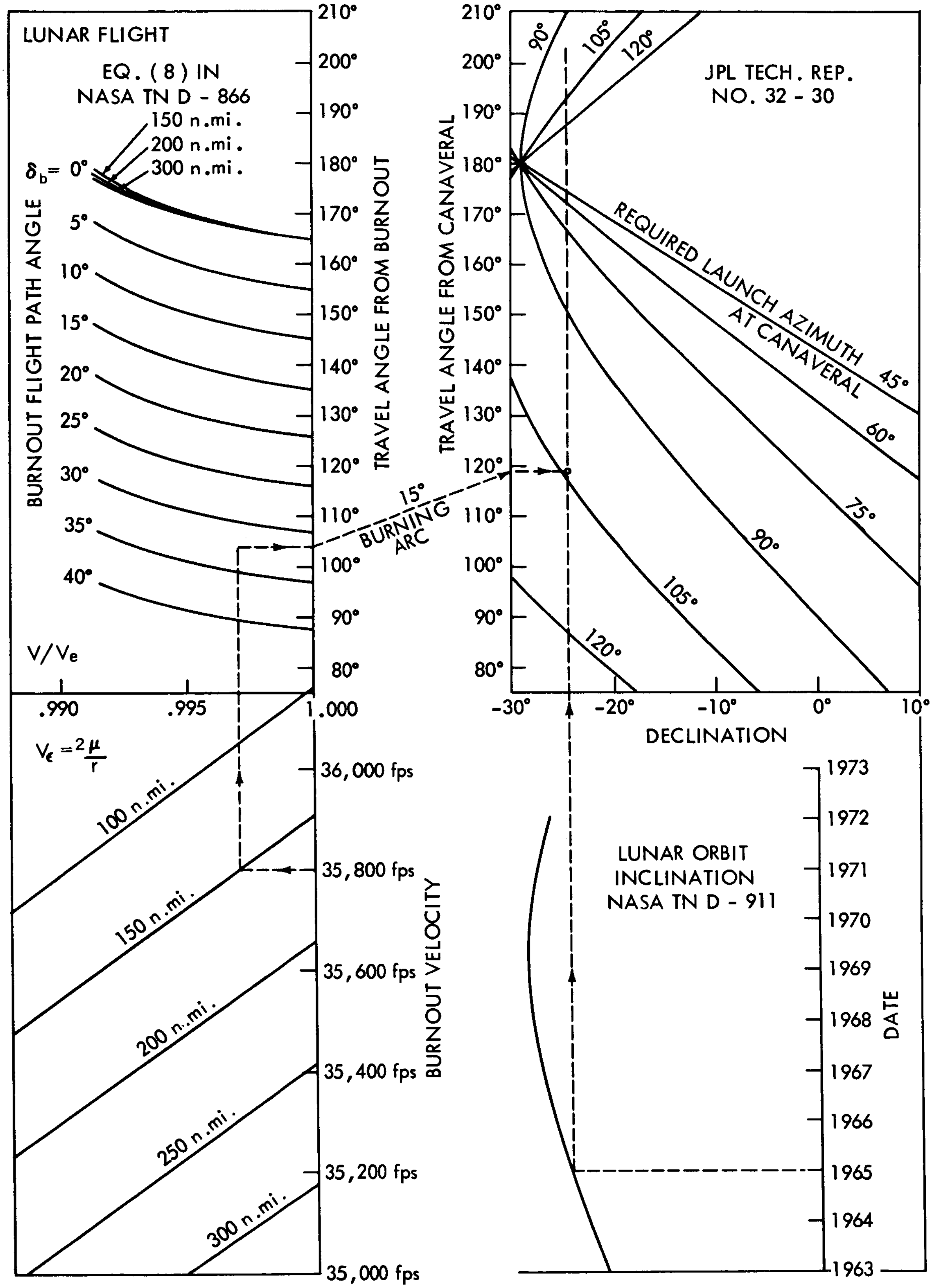
LUNAR FLIGHT
EQ. (8) IN NASA TN D - 866
150 n.mi.
200 n.mi.
300 n.mi.
$\delta_b$= 0°
5°
10°
15°
20°
25°
30°
35°
40°
BURNOUT FLIGHT PATH ANGLE
V/Ve
.990
.995
1.000
TRAVEL ANGLE FROM BURNOUT
15° BURNING ARC
JPL TECH. REP. NO. 32 - 30
TRAVEL ANGLE FROM CANAVERAL
REQUIRED LAUNCH AZIMUTH AT CANAVERAL
90°
105°
120°
45°
60°
75°
210°
200°
190°
180°
170°
160°
150°
140°
130°
120°
110°
100°
90°
80°
-30°
-20°
-10°
0°
10°
DECLINATION
$V_\epsilon = \frac{2\mu}{r}$
100 n.mi.
150 n.mi.
200 n.mi.
250 n.mi.
300 n.mi.
36,000 fps
35,800 fps
35,600 fps
35,400 fps
35,200 fps
35,000 fps
BURNOUT VELOCITY
LUNAR ORBIT INCLINATION NASA TN D - 911
1973
1972
1971
1970
1969
1968
1967
1966
1965
1964
1963
DATE

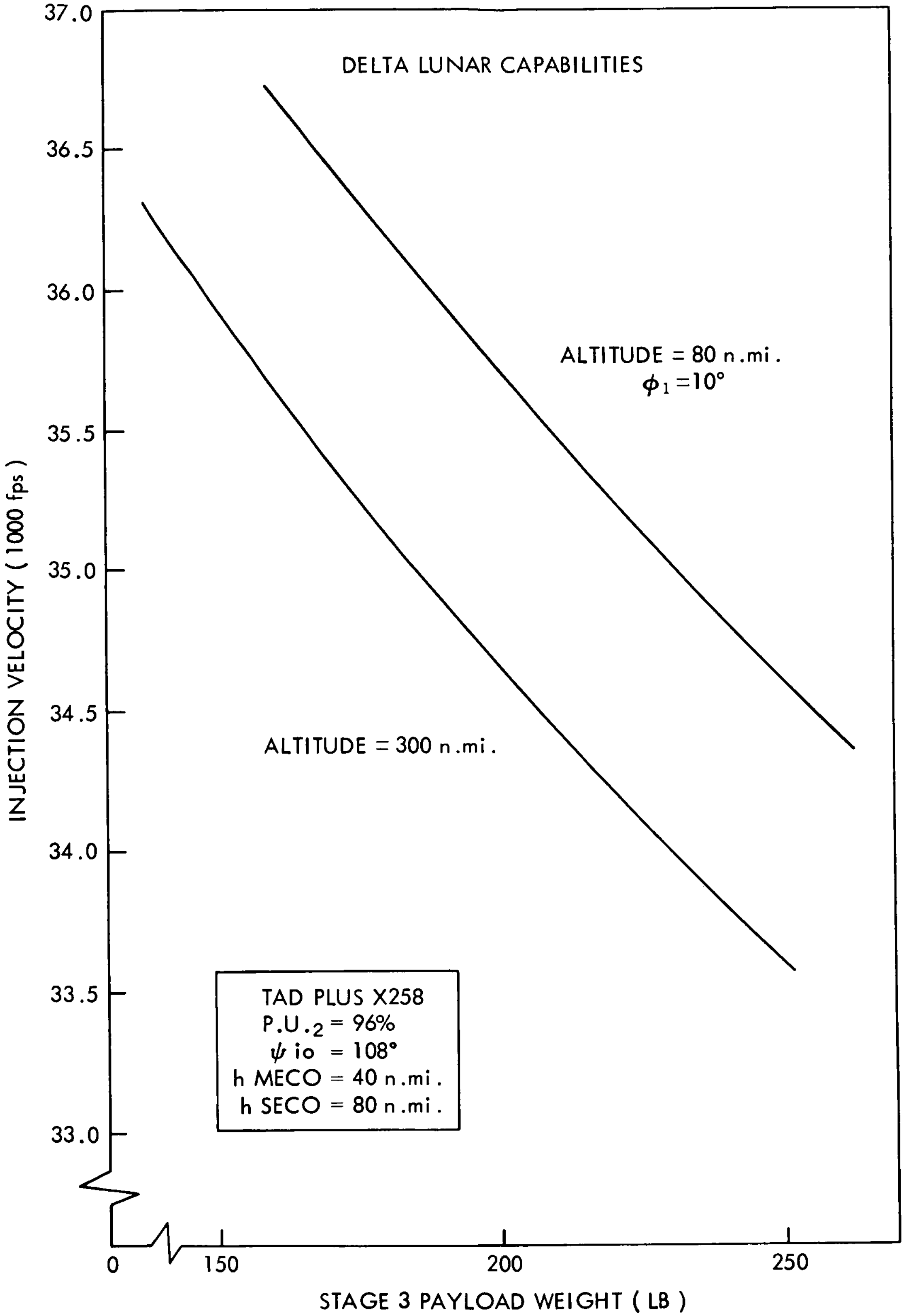

DELTA LUNAR CAPABILITIES
ALTITUDE = 80 n.mi.
$\phi_1$ = 10°
ALTITUDE = 300 n.mi.
TAD PLUS X258
P.U.$_2$ = 96%
$\psi$ io = 108°
h MECO = 40 n.mi.
h SECO = 80 n.mi.
INJECTION VELOCITY (1000 fps)
37.0
36.5
36.0
35.5
35.0
34.5
34.0
33.5
33.0
0
150
200
250
STAGE 3 PAYLOAD WEIGHT (LB)

# APPENDIX II

## IMP D & E ORBITAL STUDY

R. K. Squires and R. Kolenkiewicz

The Special Projects Branch in studying the IMP D&E mission set out to do two things: To verify the probability of success that Mr. Y. Kork obtained and to further improve the probability of success. Both objectives were met. The Monte Carlo procedure was mechanized such that the direction of tip-off was randomly distributed over 0-180 degrees, while the amount of tip-off and the transfer orbit injection velocity were normally distributed with 0.5 degrees and 41 fps 1-sigma errors, respectively. The spin-axis direction was assumed to have a 1-sigma error of 2.0 degrees for the purposes of the retro-maneuver. This maneuver was initiated every hour, on the hour, in moon reference. Any orbit which produced a lunar apocynthion less than 38,000 km and a pericynthion above the lunar surface was considered to be a successful orbit. This criterion is approximately equivalent to the Hill surface for stability. One hundred Monte Carlo cases were run to determine the probability of success. The following are the significant results of the study.

1. Y. Kork's run is verified.

2. It is possible to obtain a 92 percent success probability (but 1-2 percent is meaningless with a sample size of 100) providing one of the following is possible:

   a. Flight-path angles of 15 degrees are possible.

   b. Parking orbit coasts of 30 degrees are permitted.

   c. Or a compromise of a. and b. in the ratio of 1 to 2, respectively.

3. Verification of the stability criteria has been initiated by integrating three orbits for three months. Two that met the success criteria survived for three months, the other did not.

4. The optimum nominal essentially aims at the moon. Approximately half of the orbits are direct, the other half are retrograde. The inclinations of the orbits ranged from 41 to 165 degrees when the most stable orbits obtainable were examined.

5. The launch azimuth is 90 degrees. The major error contributing to the lack of mission success is the large speed uncertainty. Therefore, the optimum is found by minimizing the effects of speed errors. Maximum effectiveness of the retro kick motor is obtained when the spin axis is as close as possible to the moon's orbital plane, i.e., 90-degree launch azimuth. The spin axis is also aligned as closely as

possible to the vehicle velocity vector with respect to the moon. This is accomplished through the high flight-path angle or the parking orbit, or both. The flight time is such that plus and minus 3-sigma cases in transfer-orbit injection speed have equal probability of success. The characteristics of the nominal are given in Figures 1, 2, and 3 and Table I.

To insist on a low flight-path angle and no parking orbit reduces the success probability to about 50 percent.

The stability checks were made for the following orbits:

I. $r_p$ = 31,710 km

$r_a$ = 84,008 km

$\omega$ = -149° with respect to moon's orbit plane

Period = 347 hrs.

Stay time in moon reference = 67 hrs.

II. $r_p$ = 3091 km

$r_a$ = 3442 km

$\omega$ = 117.°

Period = 4.65 hrs.

Lifetime exceeds 3 months.

III. $r_p$ = 3994

$r_a$ = 11,763

$\omega$ = 2.6°

Period = 17.4 hrs.

Lifetime exceeds 3 months.

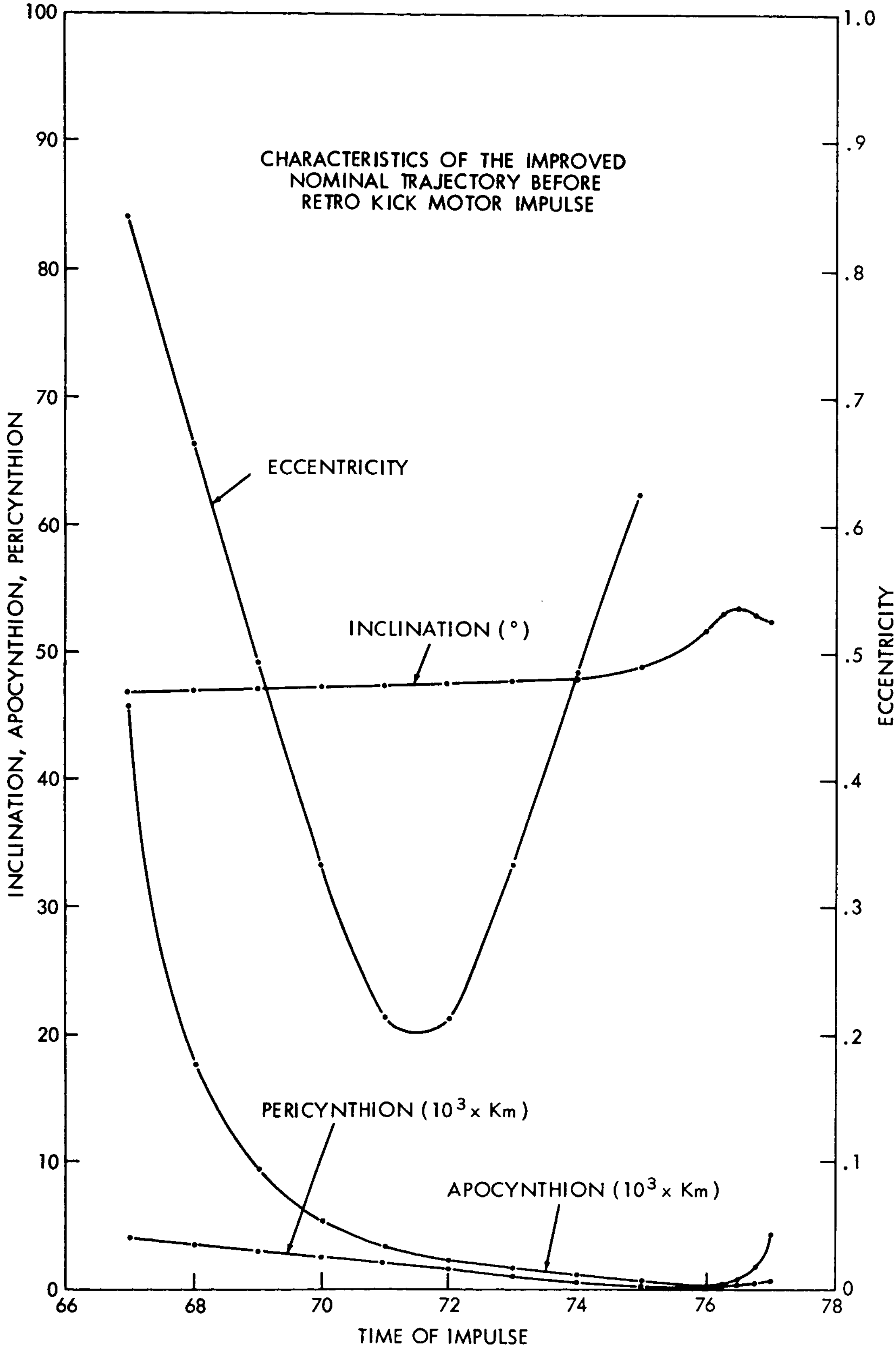
CHARACTERISTICS OF THE IMPROVED
NOMINAL TRAJECTORY BEFORE
RETRO KICK MOTOR IMPULSE
ECCENTRICITY
INCLINATION (°)
PERICYNTHION (10³ x Km)
APOCYNTHION (10³ x Km)
INCLINATION, APOCYNTHION, PERICYNTHION
ECCENTRICITY
TIME OF IMPULSE
100
90
80
70
60
50
40
30
20
10
0
1.0
.9
.8
.7
.6
.5
.4
.3
.2
.1
0
66
68
70
72
74
76
78

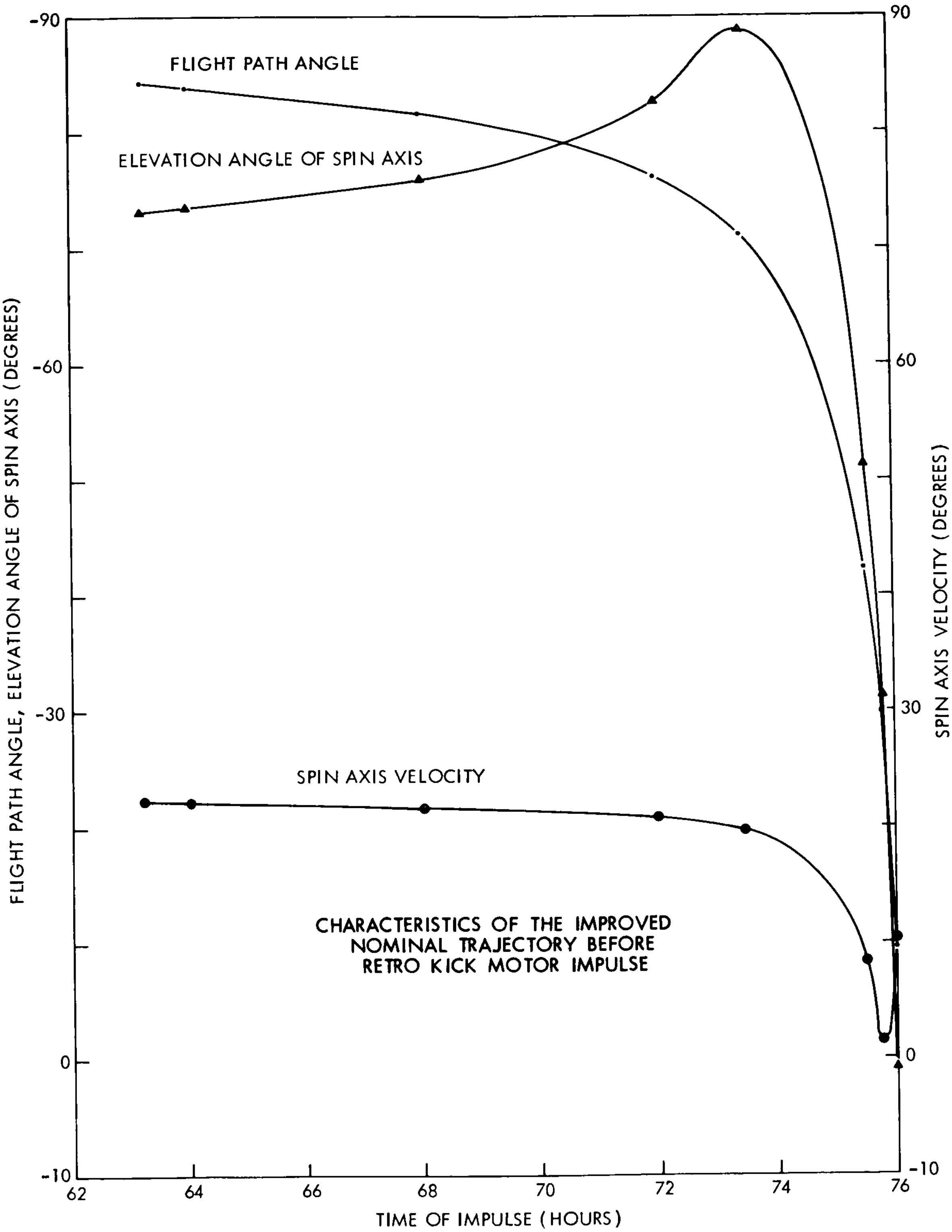

FLIGHT PATH ANGLE
ELEVATION ANGLE OF SPIN AXIS
SPIN AXIS VELOCITY
CHARACTERISTICS OF THE IMPROVED NOMINAL TRAJECTORY BEFORE RETRO KICK MOTOR IMPULSE
FLIGHT PATH ANGLE, ELEVATION ANGLE OF SPIN AXIS (DEGREES)
SPIN AXIS VELOCITY (DEGREES)
TIME OF IMPULSE (HOURS)
-90
-60
-30
0
-10
90
60
30
0
-10
62
64
66
68
70
72
74
76

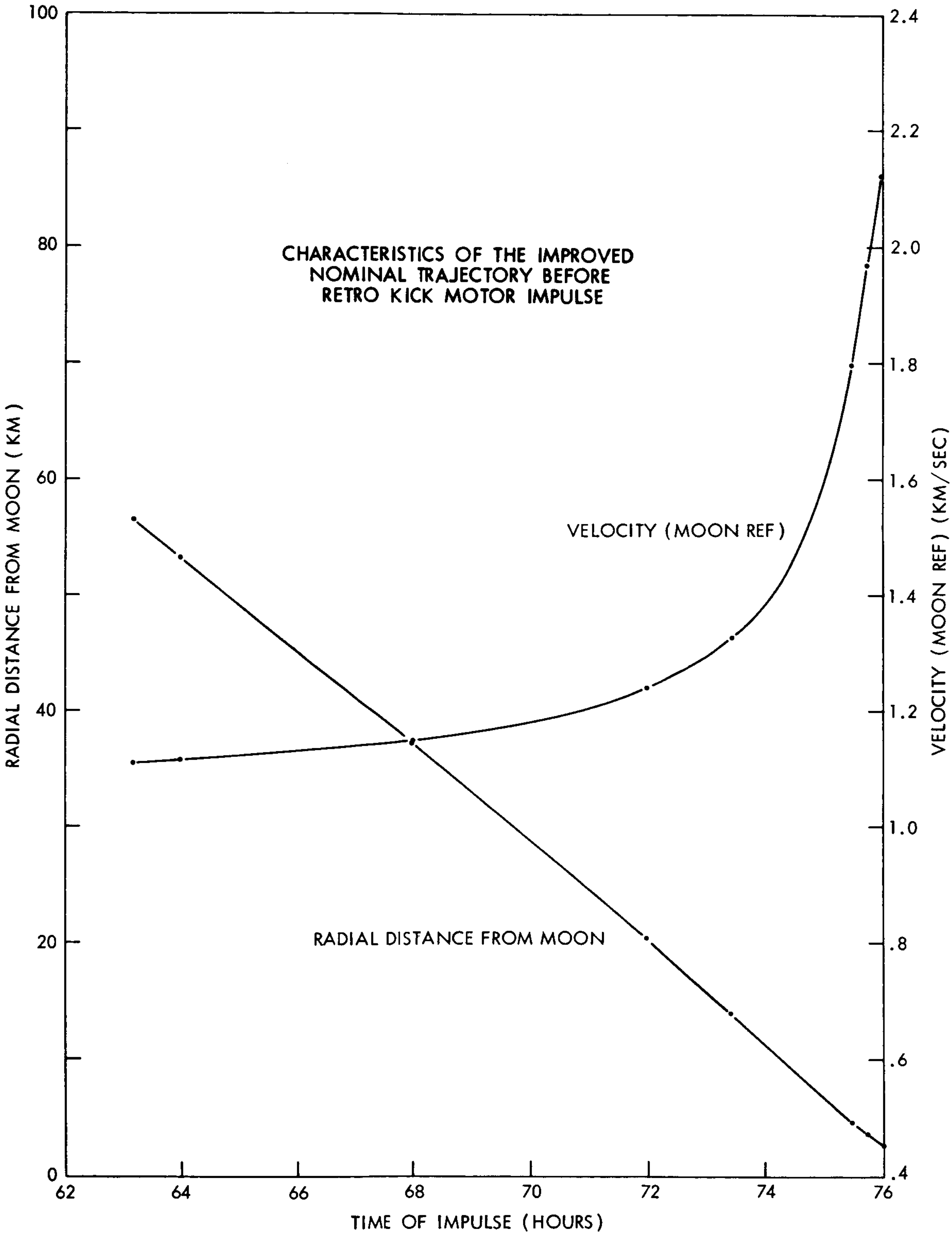
CHARACTERISTICS OF THE IMPROVED
NOMINAL TRAJECTORY BEFORE
RETRO KICK MOTOR IMPULSE
VELOCITY (MOON REF)
RADIAL DISTANCE FROM MOON
RADIAL DISTANCE FROM MOON (KM)
VELOCITY (MOON REF) (KM/SEC)
TIME OF IMPULSE (HOURS)
0
20
40
60
80
100
.4
.6
.8
1.0
1.2
1.4
1.6
1.8
2.0
2.2
2.4
62
64
66
68
70
72
74
76

Table I

CHARACTERISTICS OF ANCHORED IMP ORBITS FOR 100 MONTE CARLO CASES

| | Retro Time After Launch (hours) | Pericynthion (km) | Apocynthion (km) | Eccentricity | Inclination With Ref. to Moon Orbital Plane (degrees) | Period (hours) | Spin Axis Elevation Angle (degrees) |
|---|---|---|---|---|---|---|---|
| NOM | 74 | 4019 | 11597 | .4852 | 132.009 | 17.201 | -67.057 |
| RUN | $t_4$ | $V_p$ | $V_a$ | e | i | T | Spin Axis Position |
| 1 | 82 | 4155 | 17037 | .6079 | 80.712 | 27.193 | 11.576 |
| 2 | 68 | 6978 | 10615 | .2067 | 137.298 | 20.570 | 26.663 |
| 3 | 77.75 | 2415 | 4513 | .3028 | 56.821 | 5.084 | 62.404 |
| 4 | 80 | 3315 | 17647 | .6837 | 70.589 | 26.753 | 22.883 |
| 5 | 78 | 2119 | 8026 | .5822 | 47.305 | 9.007 | 27.671 |
| 6 | 81 | 2939 | 12609 | .6219 | 59.289 | 17.088 | 34.364 |
| 7 | 79 | 2035 | 10322 | .6706 | 69.771 | 12.108 | 29.520 |
| 8 | 82 | 4952 | 21278 | .6224 | 87.234 | 37.445 | 9.587 |
| 9 | 84 | 5099 | 21416 | .6154 | 76.401 | 38.058 | 20.747 |
| 10 | 77 | 3372 | 5538 | .2431 | 54.845 | 7.413 | 61.617 |

| RUN | $t_4$ | $V_p$ | $V_a$ | e | i | T | Spin Axis Position |
|---|---|---|---|---|---|---|---|
| 11 | 72 | 3344 | 9240 | .4686 | 144.634 | 12.442 | 26.522 |
| 12 | 70 | 6413 | 14938 | .3993 | 136.442 | 27.499 | 17.486 |
| 13 | 74 | 2052 | 8895 | .6252 | 140.886 | 10.096 | -31.767 |
| 14 | 70 | 8605 | 20166 | .4018 | 135.686 | 43.015 | 5.789 |
| 15 | 83 | 9544 | 30865 | .5276 | 95.373 | 71.601 | 4.971 |
| 16 | 69 | 9765 | 20340 | .3513 | 134.072 | 46.041 | 8.147 |
| 17 | 69 | 10821 | 33779 | .5147 | 128.667 | 83.024 | 13.088 |
| 18 | 74 | 2494 | 11162 | .6347 | 127.320 | 14.067 | -72.580 |
| 19 | 70 | 8012 | 16635 | .3498 | 136.855 | 34.108 | 5.619 |
| 20 | 67(?) | 15108 | 210752 | .866 | 125.311 | 946.146 | 12.376 |
| 21 | 86(?) | 35800 | 116597 | .5302 | 114.057 | 524.399 | 5.180 |
| 22 | 78 | 2559 | 5485 | .3637 | 58.261 | 6.360 | 70.302 |
| 23 | 73 | 2616 | 8808 | .5420 | 148.487 | 10.762 | 27.104 |
| 24 | 73 | 2242 | 6315 | .4760 | 149.980 | 6.977 | 9.630 |
| 25 | 84 | 11605 | 33534 | .4858 | 94.741 | 84.534 | 4.729 |
| 26 | 72 | 3027 | 12241 | .6035 | 133.194 | 16.628 | -78.920 |
| 27 | 66(?) | 15769 | 77776 | .6629 | 126.008 | 252.190 | 12.567 |

| RUN | $t_4$ | $V_p$ | $V_a$ | e | i | T | Spin Axis Position |
|---|---|---|---|---|---|---|---|
| 28 | 74 | 1843 | 6831 | .5751 | 160.122 | 7.120 | 54.594 |
| 29 | 77 | 1800 | 9801 | .6897 | 104.276 | 11.013 | -6.653 |
| 30 | 73.75 | 2231 | 6154 | .4678 | 153.642 | 6.768 | 22.259 |
| 31 | 71 | 3049 | 14808 | .6585 | 128.590 | 21.033 | -46.351 |
| 32 | 81 | 2977 | 13136 | .6305 | 62.805 | 18.029 | 30.422 |
| 33 | 80 | 3782 | 23131 | .7189 | 67.131 | 38.919 | 26.657 |
| 34 | 74 | 2036 | 9682 | .6525 | 126.207 | 11.180 | -42.647 |
| 35 | 72 | 2160 | 10929 | .6699 | 133.748 | 13.200 | -71.939 |
| 36 | 75.75 | 2254 | 3167 | .1685 | 130.565 | 3.518 | 71.983 |
| 37 | 75 | 1851 | 5452 | .4931 | 162.520 | 5.501 | 40.221 |
| 38 | 70 | 6677 | 12036 | .2864 | 132.581 | 22.564 | 23.150 |
| 39 | 69(?) | 11138 | 39727 | .5621 | 129.448 | 101.118 | 10.859 |
| 40 | 72 | 2193 | 8932 | .6057 | 150.123 | 10.343 | 32.493 |
| 41 | 74.75 | 1798 | 6035 | .5409 | 161.792 | 6.111 | 34.481 |
| 42 | 78 | 1732 | 9023 | .6779 | 71.815 | 9.831 | 33.046 |
| 43 | 77.5 | 1870 | 8153 | .6270 | 45.251 | 8.845 | 28.149 |
| 44 | 79 | 1912 | 8927 | .6473 | 66.596 | 9.946 | 36.529 |

| RUN | $t_4$ | $V_p$ | $V_a$ | e | i | T | Spin Axis Position |
|---|---|---|---|---|---|---|---|
| 45 | 76.5 | 2516 | 6512 | .4426 | 105.434 | 7.561 | 73.266 |
| 46 | 69 | 1702 | 10098 | .7114 | 141.126 | 11.299 | -69.730 |
| 47 | 74.5 | 2042 | 4908 | .4123 | 165.809 | 5.107 | 44.038 |
| 48 | 78 | 2253 | 4593 | .3418 | 54.201 | 4.992 | 65.487 |
| 49 | 75.25 | 3427 | 3883 | .6239 | 142.310 | 5.509 | 83.690 |
| 50 | 72 | 2151 | 16997 | .7753 | 125.132 | 23.356 | -29.909 |
| 51 | 74 | 2623 | 9933 | .5822 | 131.242 | 12.401 | -60.512 |
| 52 | 80 | 2736 | 13283 | .6584 | 68.199 | 17.871 | 25.376 |
| 53 | 85(?) | 15040 | 30503 | .3395 | 103.638 | 85.671 | -3.022 |
| 54 | 74 | 2070 | 7555 | .5698 | 138.590 | 8.324 | -30.166 |
| 55 | 71 | 2711 | 7243 | .4553 | 152.074 | 8.753 | 37.670 |
| 56 | 69 | 10366 | 22677 | .3726 | 136.124 | 52.945 | 2.487 |
| 57 | 72 | 2099 | 5408 | .4408 | 154.693 | 5.734 | 13.520 |
| 58 | 77.25 | 1922 | 3838 | .3326 | 70.701 | 3.854 | 71.818 |
| 59 | 73 | 2675 | 8463 | .5197 | 140.035 | 10.361 | 3.224 |
| 60 | 67 | 8335 | 11106 | .1425 | 131.796 | 23.894 | 19.186 |
| 61 | 77 | 2192 | 4447 | .3397 | 75.546 | 4.768 | 72.312 |

| RUN | $t_4$ | $V_p$ | $V_a$ | e | i | T | Spin Axis Position |
|---|---|---|---|---|---|---|---|
| 62 | 76 | 2645 | 5986 | .3871 | 91.373 | 7.068 | 72.853 |
| 63 | 84 | 8537 | 27967 | .5323 | 93.779 | 61.476 | 8.215 |
| 64 | 73 | 3113 | 13340 | .6216 | 128.497 | 18.602 | -58.308 |
| 65 | 68(?) | 12670 | 64683 | .6724 | 126.208 | 189.634 | 14.241 |
| 66 | 71 | 4299 | 9583 | .3806 | 141.103 | 14.418 | 16.969 |
| 67 | 86(?) | 38787 | 41445 | .3312 | 118.854 | 200.320 | -8.221 |
| 68 | 74 | 1841 | 6314 | .5486 | 158.701 | 6.491 | 22.008 |
| 69 | 72.25 | 2103 | 4876 | .3973 | 155.157 | 5.140 | 23.743 |
| 70 | 71 | 3759 | 8704 | .3968 | 143.382 | 12.265 | 25.690 |
| 71 | 85(?) | 28832 | 43243 | .1999 | 122.323 | 170.563 | -6.647 |
| 72 | 74 | 2951 | 11107 | .5802 | 129.331 | 14.692 | -80.339 |
| 73 | 79 | 1790 | 9391 | .6797 | 81.385 | 10.422 | 21.127 |
| 74 | 81 | 7393 | 34725 | .6489 | 89.954 | 76.190 | 8.946 |
| 75 | 67 | 10624 | 12339 | .7469 | 136.681 | 30.673 | 7.991 |
| 76 | 78.25 | 1780 | 6972 | .5932 | 53.925 | 7.218 | 21.930 |
| 77 | 69 | 5545 | 9517 | .2637 | 139.304 | 16.294 | 30.181 |
| 78 | 70 | 7664 | 19743 | .4407 | 134.882 | 39.994 | 11.851 |

| RUN | $t_4$ | $V_p$ | $V_a$ | e | i | T | Spin Axis Position |
|---|---|---|---|---|---|---|---|
| 79 | 73 | 2340 | 16362 | .7498 | 124.307 | 22.545 | -42.296 |
| 80 | 85 | 9944 | 27673 | .4713 | 95.429 | 64.311 | 5.970 |
| 81 | 74 | 2794 | 11258 | .6023 | 131.956 | 14.683 | -71.717 |
| 82 | 76.5 | 2426 | 3468 | .1767 | 117.943 | 3.989 | 84.914 |
| 83 | 69 | 10490 | 27053 | .4412 | 132.911 | 64.121 | 7.691 |
| 84 | 71 | 5608 | 12960 | .3960 | 141.673 | 22.302 | 3.841 |
| 85 | 77.5 | 1965 | 3966 | .3374 | 58.888 | 4.026 | 64.234 |
| 86 | 83 | 5443 | 20296 | .577 | 82.898 | 36.399 | 11.241 |
| 87 | 70 | 6262 | 16607 | .4524 | 137.923 | 30.483 | 15.179 |
| 88 | 75 | 2166 | 11396 | .6806 | 120.110 | 13.921 | -42.802 |
| 89 | 71 | 5580 | 13345 | .4103 | 133.775 | 22.949 | 27.132 |
| 90 | 78 | 2971 | 6181 | .3508 | 61.398 | 7.717 | 71.183 |
| 91 | 81 | 3653 | 17805 | .6595 | 75.566 | 27.708 | 17.384 |
| 92 | 84 | 9893 | 27883 | .4762 | 100.662 | 64.718 | 1.271 |
| 93 | 68(?) | 10603 | 29616 | .4727 | 132.962 | 71.094 | 10.968 |
| 94 | 80 | 3038 | 16022 | .6812 | 65.929 | 23.194 | 27.618 |
| 95 | 71.75 | 1783 | 4411 | .4244 | 154.335 | 4.296 | 21.565 |

| RUN | $t_4$ | $V_p$ | $V_a$ | e | i | T | Spin Axis Position |
|---|---|---|---|---|---|---|---|
| 96 | 67(?) | 14520 | 59155 | .6058 | 129.905 | 176.274 | 7.503 |
| 97 | 69 | 10514 | 28673 | .4634 | 132.764 | 68.379 | 7.868 |
| 98 | 74 | 3780 | 12897 | .5467 | 128.111 | 18.983 | -79.763 |
| 99 | 79.75 | 2708 | 8278 | .5070 | 41.272 | 10.150 | 34.999 |
| 100 | 76 | 2437 | 33331 | .1553 | 134.541 | 3.863 | 72.798 |

OPTIONAL FORM NO. 10
5010-104
UNITED STATES GOVERNMENT

# *Memorandum*

TO : FILE

DATE: December 13, 1963

FROM : W. M. Kaula

SUBJECT: Calculation of Perturbations of Lunar Orbiters

1. Summary. Three types of calculations were carried out. Their principal characteristics and results:

a. Lifetimes for IMPs D & E. Runge-Kutta integration of the Lagrangian planetary equations was carried out for the 100 orbits of a Monte Carlo study. For these orbits, the important part of the disturbing function is the earth effect which is long-periodic with respect to both the lunar satellite and the earth-moon orbit. 92 orbits survived 40 days; 75, 80 days; 67, 120 days; 61, 160 days; 56, 200 days; 48, 300 days; and 43, 400 days.

b. Lifetimes for Langley Lunar Orbiters. The same calculation was carried out for lunar satellites having a 20-n. mi. pericenter height and a 750-n. mi. apocenter height. For these orbits, the important part of the disturbing function is the $J_3$ term of the moon's gravity field, if it has a magnitude implying the same stresses in the moon as does the earth's $J_3$ in the earth. Of 12 orbits with varying inclination and pericenter argument, 11 survived 20 days; 7, 40 days; 5, 100 days; and 3, 400 days.

c. Perturbations by variations in the moon's gravitational field. Linear perturbations of the Lagrangian planetary equations were calculated for a typical variety of IMP D & E orbital specifications. The variations in the lunar field were assumed to be of an order-of-magnitude implying the same stresses in the moon as do terms of the same wave-length in the earth's field. Assuming as a criterion of success that the anticipated perturbations due to at least two tesseral harmonic terms exceed ±500 meters, the semi-major axis for retrograde orbits should be less than about 4 lunar radii, for direct orbits, 6 lunar radii. Lowering the criterion to ±100 meters, it becomes about 7 lunar radii for retrograde orbits and 10 lunar radii for direct orbits.

2. Lifetime Calculations. These calculations were carried out by standard Runge-Kutta numerical integration (see Appendix) of the standard Lagrangian planetary equations (see Appendix) with a disturbing function which can be summarized as:

$$R = \sum_{\ell} R_{EL\ell} + \sum_{\ell, j} R_{ES\ell_j} + R_{S20} + R_{M2010} + R_{M2210} + 2R_{M3021}$$

$R_E$ is the third-body disturbing function of the earth. $R_{EL}$ is the long-period part, and $R_{ES}$ is the short-period part: i.e., containing monthly, semi-monthly, etc., terms. The subscript $\ell$ pertains to the degree in the expansion of the disturbing function in Legendre polynomials; the subscript j, to the eccentricity function in the coefficient and the short-period part of the argument of each term of the development. $R_{S20}$ is the third-body disturbing function of the sun, which is carried only to include the second-degree Legendre polynomial and which neglects the effect of eccentricity of the earth's orbit around the sun. $R_{M2010}$ is the secular effect of the moon's oblateness, and $R_{M2210}$ is the semi-monthly effect of the moon's equatorial ellipticity. $2R_{M3021}$ is the long-period effect of a third zonal harmonic in the moon's gravitational field: the 2 appears because the one term $2R_{M3021}$ is used in place of the two equal terms $R_{M3021} + R_{M301(-1)}$. The mathematical definition of R is given in the Appendix, and the derivations in references (1) and (2).

All the parameters in R are known except $J_3$, the third-degree zonal harmonic coefficient, which is completely unknown. It is included because, if the $J_3$ of the moon is large enough to entail stresses in the moon comparable to those implied in the earth by its $J_3$, then the perigee heights will have perturbations large enough to greatly affect the lifetimes of closely approaching lunar orbiters. The $J_n$, or $C_{nm}$ and $S_{nm}$, coefficients are the same magnitude as potential term coefficients in a system of units where the gravitational constant k, the mass M, and the radius $a_e$ of the planet are all unity. Since k, dimension $L^3M^{-1}T^{-2}$, is the same everywhere, the time unit must scale as $L^{3/2} M^{-1/2}$. Hence stress, dimension $ML^{-1} T^{-2}$, must scale as $M^2 L^{-4}$, or coefficients $J_n$ must be $M^{-2} L^4$ times as great to imply comparable stresses. For the moon compared to the earth, the ratio $M^{-2} L^4$ is $.0123^{-2} \times .2725^4$ or about 36.3, so a reasonable order-of-magnitude for the lunar $J_3$ is $\pm 36.3 \times 2.58 \times 10^{-6} \approx \pm 9.3 \times 10^{-5}$.

Numerical values of other parameters used are given in Table III-1.

Options possible in each lifetime run are:

(1) The maximum degree $\ell$ of the Legendre polynomial for the earth's disturbing function, $R_{EL}$ or $(R_{EL} + R_{ES})$.

(2) Whether or not terms short-period with respect to the orbit of the earth around the moon, $R_{ES} + R_{M2210}$, are to be taken into account.

(3) If short-period terms are to be included, the maximum power of the eccentricity of the earth's orbit about the moon to be taken into account, which determines the range of subscript j.

(4) Whether or not solar perturbations, arising from $R_{S20}$, are to be taken into account.

(5) Whether or not a hypothetical $J_3$ effect, $2R_{M3021}$, is to be included.

(6) The integration interval.

(7) The printout interval.

(8) Whether longitudes are measured from the vernal equinox or the earth-moon line at a particular epoch.

(9) Whether inclinations are measured from the earth-moon orbit plane or the lunar equatorial plane. The corrections of $R_M$ in the former option or of $R_E$ in the latter option have not been made in the program, since the inclination is small and the choice of reference plane depends on which part of $R$ is more important.

The program was tested against the Pines-Wolf Encke integration system "ITEM" for an orbit with elements $a = 1.8795$ lunar radii; $e = .0537$ ; and $i = 127.2°$ . Results of the comparison are given in Table III-2.

The principal calculation made on the 100 Monte Carlo orbits generated by Special Projects Branch was of lifetimes up to 400 days with a disturbing function ($R_{EL_2} + R_{M2010}$) long-periodic with respect to the earth-moon orbit, and integration interval of 20 days. The results are given in Table III-3 and Figures III-1 and III-2. The following alternatives were tested on a few characteristic orbits:

(1) Shorter integration intervals with the same disturbing function gave the same results as the 20-day interval. An interval longer than 20 days was not tested, since it took only 11 minutes to compute all 100 lifetimes.

(2) Inclusion of terms short-periodic with respect to the earth-moon orbit, arising from $R_{ES_{20}} + R_{M2210}$, together with the necessary shortening of the integration interval, resulted in moderate shortening of some lifetimes less than 120 days, and extreme shortening in only one case, as given in the 7th column of Table III-3.

(3) Inclusion of $R_{M3021}$, $R_{S20}$, or $R_{EL3}$ perturbations had no effect on lifetimes.

(4) Varying of the time of injection into orbit around the moon by 1/2 hour had significant effect on the lifetime only for a few trajectories headed directly toward the moon, as given in the last two columns of Table III-3.

The lifetime calculation was also made for orbits with characteristics approximating those of the Langley lunar orbiter, using a long-periodic disturbing function $R_{EL2} + 2R_{M3021}$, incorporating the "equal-stress" $J_3$ coefficient of $-9.3 \times 10^{-5}$. It was also made for orbits of higher pericenter, as given in Table III-4.

For a zero $J_3$, all these orbits have indefinite lifetimes. For a $J_3$ of $+9.3 \times 10^{-5}$, the lifetime is that given in Table III-4 for a pericenter argument differing by 180°. Since the sign as well as the magnitude of $J_3$ is unknown at present, Table III-4 indicates that for a pericenter height of 20 nautical miles, even the optimum choice of pericenter argument at injection chances a lifetime less than 200 days. In the first approximation, the lifetime depends on how close is the orbiter at injection to the minimum of an oscillation of the pericenter height with the same period as the pericenter argument. The magnitude of the pericenter height oscillations is due not only to the large $J_3$, but also to the long period of the pericenter revolution: about 400 to 500 days.

3. Calculation of Perturbations by Variations of the Lunar Gravitational Field. If fully normalized spherical harmonics are used—i.e., functions such that the integral of the square over the unit sphere is $4\pi$—then the order of magnitude of potential coefficients $\overline{C}_{nm}$, $\overline{S}_{nm}$ of the earth's gravitational field follows roughly a rule of $\pm 6. \times 10^{-6}/n^2$.

If the "equal-stress" assumption is made, then the order-of-magnitude of potential coefficients of the moon's gravitational field will be roughly $\pm 36 \times 6 \times 10^{-6}/n^2 = 2 \times 10^{-4}/n^2$.

The perturbations caused by such coefficients were calculated by using the expression of the spherical harmonic potential in Keplerian elements (see Appendix) as a disturbing function in the Lagrangian planetary equations and integrating them, assuming that on the right-hand side of the equations the semi-major axis, eccentricity, and inclination remain constant, while the mean anomaly, argument of pericenter, longitude of the node, and lunar sidereal time have a constant rate of change with respect to time. The calculation was carried out for spherical harmonics up to $(n,m) = (4,4)$ for 10 orbits distributed over the variety of 100 orbits obtained in the IMP D & E Monte Carlo study.

The results are summarized in Table III-5. It appears that most IMP D & E orbits will be adequate to obtain some measure of the $J_3$ zonal harmonic coefficient, which would be of great value in planning subsequent closer orbits. To obtain a measure of the tesseral harmonics in the lunar field, which cause perturbations of monthly, semi-monthly, etc. period, is more difficult. If an amplitude of ±500 meters in these perturbations due to at least two coefficients is considered adequate for determination of these harmonics, then about 50 percent of the IMP orbits are successful. These orbits have semi-major axes which are roughly less than 4 lunar radii for retrograde orbits and 6 lunar radii for direct orbits. If an amplitude of ±100 meters is considered adequate, then about 75 percent are successful. These orbits have semi-major axes which are roughly less than 7 lunar radii for retrograde orbits and 10 lunar radii for direct orbits.

Hence IMP D & E will almost definitely be of value in determining the $J_3$ zonal harmonic, and will have a fair chance of determining tesseral harmonics which are of equally great geophysical interest.

## References

(1) Kaula, W. M. (1961) Geophys. J. 5, 104.

(2) Kaula, W. M. (1962) Astron. J. 67, 300.

(3) Kozai, Y. (1963) Publ. Astron. Soc. Japan 15, 301.

TABLE III-1

Numerical Values of Parameters Used in Lunar Orbiter Calculations

| Parameters | Value (All angles in radians) |
|---|---|
| Moon | |
| Radius | 1738.0 Km |
| Oblateness, $J_2$ | .000220 |
| Equatorial ellipticity, $J_{2_2}$ | .000024 |
| Earth's orbit with respect to moon | |
| Earth/moon mass ratio | 81.3 |
| Semi major axis in lunar radii | 221.17 |
| Eccentricity | .0549 |
| Mean inclination to lunar equator | .1164 |
| Longitude of node, 1959 Jan 0.0 | 0.31602 |
| Mean motion of node per day | -.0009242 |
| Argument of pericenter, 1959 Jan 0.0 | 0.2933968 |
| Mean motion of pericenter per day | +.0028676 |
| Mean anomaly, 1959 Jan 0.0 | 5.3599926 |
| Anomalistic mean motion per day | +.2280271 |
| Sun's orbit with respect to moon | |
| Sun/moon mass ratio | $2.7 \times 10^7$ |
| Semi-major axis in linar radii | $8.58 \times 10^4$ |
| Eccentricity | .000 |
| Inclination | .000 |
| Longitude, 1959 Jan 0.0 | 4.8767 |
| Mean motion per day | +.0172028 |

TABLE III-2

Comparison of Integrations for Eccentricity

Initial elements a = 1.8795, e = .0537, i = $127.2^0$

| Days | Runge-Kutta Integration of Lagrangian Equations | Pines-Wolf "ITEM" Program, Encke-type |
|---|---|---|
| 0 | .05370 | .05375 |
| 2 | .05368 | .05374 |
| 4 | .05385 | .05378 |
| 6 | .05401 | .05410 |
| 8 | .05396 | .05401 |
| 10 | .05361 | .05384 |
| 20 | .05297 | .05281 |
| 40 | .05071 | .05067 |
| 60 | .04961 | .04949 |
| 80 | .04778 | .04788 |
| 100 | .04665 | .04642 |

TABLE III-3

Lifetime Calculations for IMP D & E Orbits, 100 "Monte Carlo" Cases

Injection at 1965 June 12

| No. | Semi-Major Axis in Lunar Radii | Eccen-tricity | Inclination Resp. Earth-Moon Orbit | Argument of Peri-Center | Lifetimes in Days | | | |
|---|---|---|---|---|---|---|---|---|
| | | | | | Long-Period Var. Only | Short-Period Terms Incl. | Injection $\frac{1}{2}$ Hour Early | Injection $\frac{1}{2}$ Hour Late |
| 1 | 6.097 | .6079 | 1.409 | 6.197 | <80 | <60 | <80 | <80 |
| 2 | 5.061 | .2067 | 2.396 | 0.415 | >400 | | >400 | >400 |
| 3 | 1.993 | .3028 | 0.992 | 0.696 | <260 | <260 | | |
| 4 | 6.030 | .6837 | 1.232 | 6.008 | <100 | | <80 | <80 |
| 5 | 2.919 | .5822 | .8256 | .312 | <80 | | | |
| 6 | 4.473 | .6219 | 1.035 | .015 | <100 | | | |
| 7 | 3.555 | .671 | 1.218 | .228 | <40 | <27 | | |
| 8 | 7.346 | .622 | 1.522 | 6.247 | <60 | <60 | | |
| 9 | 7.628 | .615 | 1.333 | .025 | <60 | | | |
| 10 | 2.564 | .243 | .957 | .788 | <400 | | | |
| 11 | 3.620 | .469 | 2.524 | .260 | >400 | >400 | | |
| 12 | 6.142 | .399 | 2.381 | .681 | >400 | >400 | | |
| 13 | 3.149 | .625 | 2.459 | 6.126 | <140 | | | |
| 14 | 8.277 | .402 | 2.368 | .919 | >400 | | | |
| 15 | 11.625 | .528 | 1.664 | 5.706 | <80 | | | |

TABLE III-3 (Cont'd)

| No. | Semi-Major Axis in Lunar Radii | Eccentricity | Inclination Resp. Earth-Moon Orbit | Argument of Peri-Center | Lifetimes in Days: Long-Period Var. Only | Lifetimes in Days: Short-Period Terms Incl. | Lifetimes in Days: Injection ½ Hour Early | Lifetimes in Days: Injection ½ Hour Late |
|---|---|---|---|---|---|---|---|---|
| 16 | 8.661 | .351 | 2.340 | 1.002 | >400 | | | |
| 17 | 12.831 | .515 | 2.246 | 1.214 | >400 | >400 | | |
| 18 | 3.929 | .635 | 2.222 | 5.943 | <180 | | | |
| 19 | 7.091 | .350 | 2.388 | .723 | >400 | | | |
| 20 | 27.269 | .866 | 2.187 | 1.625 | >400 | | | |
| 21 | 43.843 | .530 | 1.991 | 4.360 | <20 | | | |
| 22 | 2.314 | .364 | 1.017 | .199 | <220 | | | |
| 23 | 3.287 | .542 | 2.591 | .519 | >400 | | | |
| 24 | 2.462 | .476 | 2.618 | 6.080 | >400 | >400 | | |
| 25 | 12.986 | .486 | 1.653 | 5.480 | <80 | | | |
| 26 | 4.392 | .603 | 2.325 | 5.656 | >400 | | | |
| 27 | 26.912 | .663 | 2.199 | 1.702 | <120 | <4 | | |
| 28 | 2.495 | .575 | 2.795 | 1.420 | >400 | | | |
| 29 | 3.337 | .690 | 1.820 | .0666 | <200 | | | |
| 30 | 2.412 | .468 | 2.681 | 6.281 | >400 | | | |
| 31 | 5.137 | .658 | 2.244 | 5.495 | <300 | | | |
| 32 | 4.636 | .630 | 1.096 | .010 | <80 | | | |
| 33 | 7.742 | 7.189 | 1.172 | 5.699 | <120 | | | |
| 34 | 3.371 | .652 | 2.203 | 6.245 | <80 | | | |
| 35 | 3.766 | .670 | 2.334 | 5.633 | <280 | | | |
| 36 | 1.560 | .168 | 2.279 | 2.222 | >400 | | | |
| 37 | 2.101 | .493 | 2.836 | 1.651 | >400 | | | |

TABLE III-3 (Cont'd)

| No. | Semi-Major Axis in Lunar Radii | Eccen-tricity | Inclination Resp. Earth-Moon Orbit | Argument of Peri-Center | Lifetimes in Days | | | |
|---|---|---|---|---|---|---|---|---|
| | | | | | Long-Period Var. Only | Short-Period Terms Incl. | Injection ½ Hour Early | Injection ½ Hour Late |
| 38 | 5.383 | .286 | 2.314 | .111 | >400 | | | |
| 39 | 14.633 | .562 | 2.259 | 1.292 | >400 | | | |
| 40 | 3.201 | .606 | 2.620 | 1.252 | >400 | | | |
| 41 | 2.253 | .541 | 2.824 | 1.457 | >400 | | | |
| 42 | 3.094 | .678 | 1.253 | .386 | <20 | | | |
| 43 | 2.883 | .627 | .790 | .102 | <60 | | | |
| 44 | 3.118 | .647 | 1.162 | .461 | <20 | | | |
| 45 | 2.597 | .443 | 1.840 | 6.200 | <220 | <220 | | |
| 46 | 3.395 | .711 | 2.463 | 5.395 | <360 | | | |
| 47 | 1.999 | .412 | 2.894 | 1.413 | >400 | | | |
| 48 | 1.970 | .342 | .946 | .475 | <220 | | | |
| 49 | 2.103 | .624 | 2.484 | 6.015 | <20 | | | |
| 50 | 5.510 | .775 | 2.184 | 5.636 | <180 | | >400 | 0 |
| 51 | 3.612 | .582 | 2.290 | 6.245 | <140 | | | |
| 52 | 4.608 | .658 | 1.190 | .135 | <60 | | | |
| 53 | 13.102 | .339 | 1.809 | 5.825 | <60 | | | |
| 54 | 2.769 | .570 | 2.419 | .288 | <100 | | | |
| 55 | 2.864 | .455 | 2.654 | .505 | >400 | | | |
| 56 | 9.506 | .373 | 2.725 | 1.170 | >400 | | | |
| 57 | 2.160 | .441 | 2.700 | 6.250 | >400 | | | |
| 58 | 1.657 | .333 | 1.234 | .260 | <160 | | | |

TABLE III-3 (Cont'd)

| No. | Semi-Major Axis in Lunar Radii | Eccentricity | Inclination Resp. Earth-Moon Orbit | Argument of Peri-Center | Lifetimes in Days | | | |
|---|---|---|---|---|---|---|---|---|
| | | | | | Long-Period Var. Only | Short-Period Terms Incl. | Injection ½ Hour Early | Injection ½ Hour Late |
| 59 | 3.204 | .520 | 2.444 | .917 | >400 | | | |
| 60 | 5.593 | .142 | 2.300 | 4.575 | >400 | | >400 | >400 |
| 61 | 1.910 | .340 | 1.318 | .127 | <280 | | | |
| 62 | 2.483 | .387 | 1.595 | 6.216 | <260 | | | |
| 63 | 10.502 | .532 | 1.637 | 5.978 | <60 | <48 | | |
| 64 | 4.733 | .622 | 2.243 | 5.920 | <160 | | | |
| 65 | 22.253 | .673 | 2.203 | 1.467 | <60 | | | |
| 66 | 3.994 | .381 | 2.463 | 6.197 | >400 | | | |
| 67 | 23.082 | .331 | 2.074 | 5.096 | <200 | | | |
| 68 | 2.346 | .549 | 2.770 | .899 | >400 | | | |
| 69 | 2.008 | .397 | 2.708 | 5.915 | >400 | | | |
| 70 | 3.585 | .397 | 2.502 | .031 | >400 | | | |
| 71 | 20.735 | .200 | 1.960 | 4.997 | <60 | | | |
| 72 | 4.044 | .580 | 2.257 | 5.976 | <200 | | | |
| 73 | 3.217 | .680 | 1.420 | .213 | <20 | | | |
| 74 | 12.117 | .649 | 1.570 | 5.522 | <80 | | | |
| 75 | 6.606 | .747 | 2.385 | .742 | >100 | | | |
| 76 | 2.518 | .593 | .941 | .456 | <20 | | | |
| 77 | 4.333 | .264 | 2.431 | .158 | >400 | | | |
| 78 | 7.885 | .441 | 2.354 | .919 | >400 | | | |
| 79 | 5.380 | .750 | 2.169 | 5.461 | <320 | | >400 | 0 |
| 80 | 10.822 | .471 | 1.665 | 5.974 | <60 | | | |

TABLE III-3 (Cont'd)

| No. | Semi-Major Axis in Lunar Radii | Eccen-tricity | Inclination Resp. Earth-Moon Orbit | Argument of Peri-Center | Lifetimes in Days | | | |
|---|---|---|---|---|---|---|---|---|
| | | | | | Long-Period Var. Only | Short-Period Terms Incl. | Injection ½ Hour Early | Injection ½ Hour Late |
| 81 | 4.043 | .602 | 2.303 | 6.025 | <180 | | | |
| 82 | 1.696 | .177 | 2.058 | .045 | >400 | | | |
| 83 | 10.801 | .441 | 2.320 | 1.189 | >400 | | | |
| 84 | 5.342 | .396 | 2.473 | .615 | >400 | | >400 | >400 |
| 85 | 1.706 | .337 | 1.028 | .658 | <120 | | <100 | <120 |
| 86 | 7.405 | .577 | 1.447 | 6.076 | <80 | | | |
| 87 | 6.579 | .452 | 2.407 | .888 | >400 | | | |
| 88 | 3.902 | .681 | 2.096 | 5.978 | <160 | | | |
| 89 | 5.444 | .410 | 2.335 | .394 | >400 | | | |
| 90 | 2.633 | .351 | 1.072 | .149 | <240 | | | |
| 91 | 6.173 | .660 | 1.319 | 5.890 | <120 | | | |
| 92 | 10.868 | .476 | 1.757 | 6.067 | <60 | | | |
| 93 | 11.570 | .473 | 2.321 | 1.376 | >400 | | | |
| 94 | 5.483 | .681 | 1.151 | 6.022 | <100 | | | |
| 95 | 1.782 | .424 | 2.694 | 5.568 | >400 | | | |
| 96 | 18.318 | .606 | 2.267 | 1.610 | >400 | | | |
| 97 | 11.274 | .463 | 2.317 | 1.223 | >400 | | | |
| 98 | 4.798 | .547 | 2.236 | 5.904 | <200 | | | |
| 99 | 3.161 | .507 | .720 | .293 | >400 | | | |
| 100 | 10.290 | .155 | 2.348 | 2.334 | >400 | | | |

TABLE III-4

Lifetime Calculations for Langley Lunar Orbiter and Modifications Thereof
Assuming Lunar $J_3 = -.000093$

Injection at 1965 June 12

| Pericenter Height n. mi. | Apocenter Height n. mi. | Semi-major Axis in Lunar Radii | Eccen-tricity | Inclination to Lunar Equator | Argument of Pericenter | Lifetime Days |
|---|---|---|---|---|---|---|
| 20 | 750 | 1.406 | .2734 | 20° | 0° | <40 |
| 20 | 750 | 1.406 | .2734 | 20° | 60° | >400 |
| 20 | 750 | 1.406 | .2734 | 20° | 120° | >400 |
| 20 | 750 | 1.406 | .2734 | 20° | 180° | <180 |
| 20 | 750 | 1.406 | .2734 | 20° | 240° | <80 |
| 20 | 750 | 1.406 | .2734 | 20° | 300° | <40 |
| 20 | 750 | 1.406 | .2734 | 30° | 0° | <20 |
| 20 | 750 | 1.406 | .2734 | 30° | 60° | <40 |
| 20 | 750 | 1.406 | .2734 | 30° | 120° | >400 |
| 20 | 750 | 1.406 | .2734 | 30° | 180° | <200 |
| 20 | 750 | 1.406 | .2734 | 30° | 240° | <80 |
| 20 | 750 | 1.406 | .2734 | 30° | 300° | <40 |
| 120 | 750 | 1.447 | .2367 | 20° | 0° | >400 |
| 120 | 750 | 1.447 | .2367 | 20° | 60° | >400 |
| 120 | 750 | 1.447 | .2367 | 20° | 120° | >400 |
| 120 | 750 | 1.447 | .2367 | 20° | 180° | >400 |
| 120 | 750 | 1.447 | .2367 | 20° | 240° | <180 |
| 120 | 750 | 1.447 | .2367 | 20° | 300° | <140 |
| 120 | 750 | 1.447 | .2367 | 30° | 0° | <120 |
| 120 | 750 | 1.447 | .2367 | 30° | 60° | >400 |
| 120 | 750 | 1.447 | .2367 | 30° | 120° | >400 |
| 120 | 750 | 1.447 | .2367 | 30° | 180° | <300 |
| 120 | 750 | 1.447 | .2367 | 30° | 240° | <180 |
| 120 | 750 | 1.447 | .2367 | 30° | 300° | <120 |
| 250 | 1000 | 1.659 | .2367 | 20° & 30° | All | >400 |

TABLE III-5

Amplitude of Periodic Perturbations Anticipated Due to Irregular Variations in Lunar Gravitational Field

Assuming normalized spherical harmonic coefficients $\{\bar{C}_{nm},\bar{S}_{nm}\} = \pm .35 \times 10^{-4}/n^2$

| Semi-Major Axis in Lunar Radii | Eccentricity | Inclination | Spherical harmonic indices nm for terms expected to cause perturbations of magnitude >1000 m. | 500 to 1000 m. | 100 to 500 m. |
|---|---|---|---|---|---|
| 1.993 | .3028 | 0.992 | 22,30,31,40 | 32,33,41,42,43 | 44 |
| 2.462 | .4760 | 2.617 | 22,30,31,32,40, 41 | 42 | 33,43 |
| 2.597 | .4426 | 1.840 | 22,30,31,40 | 32,33,41 | 42,43,44 |
| 2.691 | .6629 | 2.199 | 22,30,31,32,33, 40,41,42,43 | 44 | |
| 3.555 | .6706 | 1.218 | 22,30,31,32,33, 40,41 | 43,44 | 42 |
| 3.620 | .4686 | 2.524 | 22,30,40 | 31 | 32,33,41,42 |
| 6.097 | .6079 | 1.409 | 22,30,40 | | 31,32,33,41 |
| 6.142 | .3993 | 2.381 | 30 | 22 | 31 |
| 10.512 | .5323 | 1.6367 | 30 | 22 | |

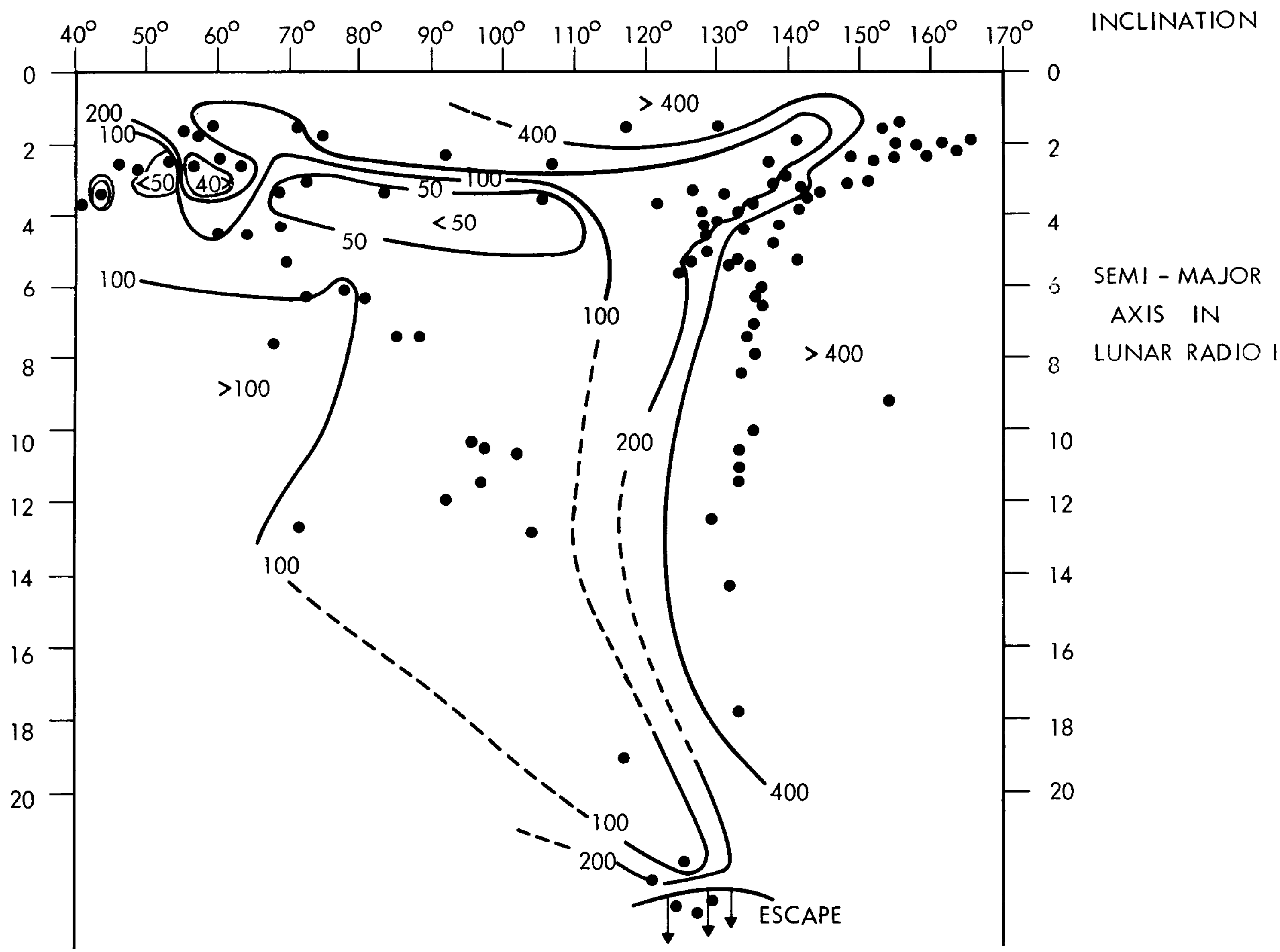


Figure III 1–Results of a Lifetime Study for a 100-Run Monte Carlo Analysis of an Improved Nominal Lunar Transfer Trajectory.

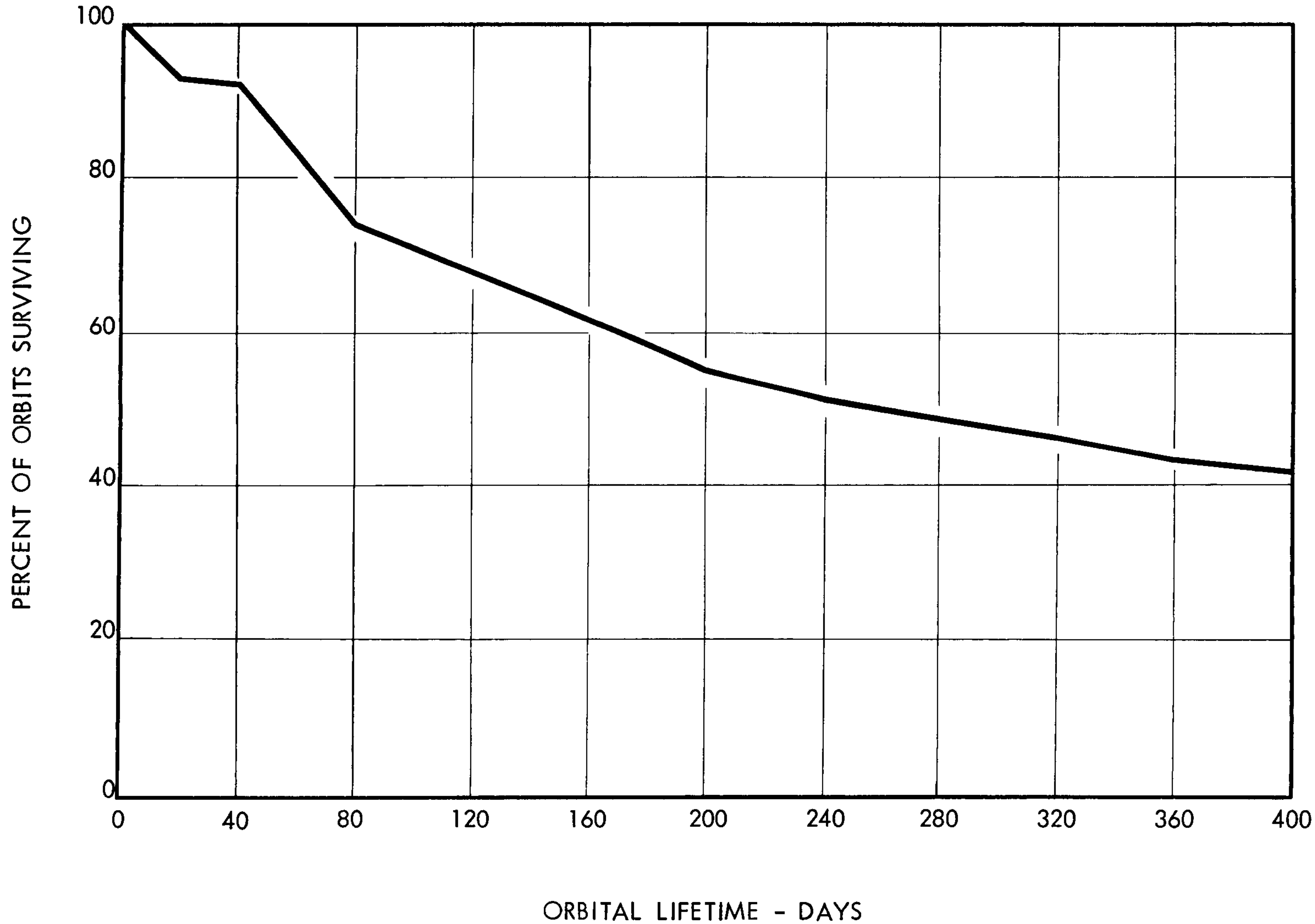


Figure III 2–Results of a Lifetime Study for a 100-Run Monte Carlo Analysis of an Improved Nominal Lunar Transfer Trajectory: Lifetimes in Days.

## APPENDIX

### 1. Lagrangian Equations of Motion

Osculating Keplerian elements

$S_1 \equiv M$: mean anomaly

$S_2 \equiv a$: semi-major axis

$S_3 \equiv e$: eccentricity

$S_4 \equiv i$: inclination

$S_5 \equiv \omega$: argument of perigee

$S_6 \equiv \Omega$: longitude of node

$n = S_2^{-3/2}$

$\eta = (1 - S_3^2)^{1/2}$

$$D = nS_2^2 \eta \sin S_4$$

$$\dot{S}_1 = n - \frac{\eta^2}{nS_2^2 S_3} \cdot \frac{\partial R}{\partial S_3} - \frac{2}{nS_2} \cdot \frac{\partial R}{\partial S_2}$$

$$\dot{S}_2 = \frac{2}{nS_2} \cdot \frac{\partial R}{\partial S_1}$$

$$\dot{S}_3 = \frac{\eta^2}{nS_2 S_3} \cdot \frac{\partial R}{\partial S_1} - \frac{\eta}{nS_2^2 S_3} \cdot \frac{\partial R}{\partial S_5}$$

$$\dot{S}_4 = \frac{\cos S_4}{D} \cdot \frac{\partial R}{\partial S_5} - \frac{1}{D} \cdot \frac{\partial R}{\partial S_6}$$

$$\dot{S}_5 = -\frac{\cos S_4}{D} \cdot \frac{\partial R}{\partial S_4} + \frac{\eta}{nS_2^2 S_3} \cdot \frac{\partial R}{\partial S_3}$$

$$\dot{S}_6 = \frac{1}{D} \cdot \frac{\partial R}{\partial S_4}$$

2. Disturbing Function:

$kM = 1$ for the moon, and the unit of length is the moon's radius thruout.

$$R_{EL\ell} = m_E \sum_{m,p,h} \frac{a^\ell}{a_E^{\ell+1}} [2-\delta_{om}] \frac{(\ell-m)!}{(\ell+m)!} F_{\ell mp}(i) F_{\ell mh}(i_E)$$

a.

$$\times H_{\ell p(2p-\ell)}(e)\, G_{\ell h(2h-\ell)}(e_E) \cos[(\ell-2p)\omega - (\ell-2h)\omega_E + m(\Omega-\Omega_E)],$$

where $m_E$ is the mass of the earth in lunar masses;

quantities subscripted by E pertain to the earth's orbit with respect to the moon;

$\delta_{om}$ is the Kronecker delta;

$m, p, h$ are all summed from 0 to $\ell$;

$F_{\ell mp}$, $F_{\ell mh}$, $H_{\ell p(2p-\ell)}$, $G_{\ell h(2h-\ell)}$ are all defined below.

$$R_{ES\ell j} = m_E \sum_{m,p,h} \frac{a^\ell}{a_E^{\ell+1}} [2-\delta_{om}] \frac{(\ell-m)!}{(\ell+m)!} F_{\ell mp}(i) F_{\ell mh}(i_E)$$

b.

$$\times H_{\ell p(2p-\ell)}(e) G_{\ell hj}(e_E) \cos[(\ell-2p)\omega - (\ell-2h)\omega_E - (\ell-2h+j)M_E + m(\Omega-\Omega_E)],$$

where $j \neq 2h - \ell$.

$$R_{S20} = m_S \sum_{m,p,h} \frac{a^2}{a_S^3} [2-\delta_{om}] \frac{(2-m)!}{(2+m)!} F_{2mp}(i) F_{2mh}(i_S)$$

c.

$$\times H_{\ell p(2p-\ell)}(e) \cos[(2-2p)\omega + m\Omega - (2-2h)\lambda_S],$$

where quantities subscripted by S pertain to the sun's orbit with respect to the moon;

m, p, h are all summed from 0 to 2.

$$R_{M2010} = -J_2 \frac{F_{201}(i)\,G_{210}(e)}{a^3}, \qquad \text{d.}$$

where $J_2$ is the oblateness coefficient of the moon's gravitational potential.

$$R_{M2210} = J_{22} \frac{F_{221}(i)\,G_{210}(e)}{a^3} \cos 2(\Omega - M_E - \omega_E - \Omega_E), \qquad \text{e.}$$

where $J_{22}$ is the equational ellipticity coefficient of the moon's gravitational potential.

$$R_{M3021} = -J_3 \frac{F_{302}(i)\,G_{321}(e)}{a^4} \sin\omega \qquad \text{f.}$$

where $J_3$ is the third degree zonal, or 'pear shape', coefficient of the moon's gravitational potential.

$$F_{\ell mp}(i) = \sum_t \frac{(2\ell-2t)!}{t!\,(\ell-t)!\,(\ell-m-2t)!\,2^{2\ell-2t}} \sin^{\ell-m-2t} i \sum_{s=0}^{m} \binom{m}{s} \cos^s i$$

$$\times \sum_c \binom{\ell-m-2t+s}{c} \binom{m-s}{p-t-c} (-1)^{c-k}, \qquad \text{g.}$$

where k is the integer part of $(\ell - m)/2$;

t is summed from 0 to the lesser of p or k; and

c is summed over all values making the binomial coefficients non-zero.

$$H_{\ell p(2p-1)}(e) = \frac{(-\beta)^{\ell-2p'}}{(1+\beta^2)^{\ell+1}} \binom{2\ell+1-2p'}{\ell-2p'} \sum_d \frac{\binom{\ell+1}{d}\binom{2p'+1}{d}}{\binom{\ell-2p'+d}{d}} \beta^{2d} \qquad \text{i.}$$

where $\beta = \dfrac{e}{1+(1-e^2)^{1/2}}$

$p' = p, \; p \leq \ell/2$

$p' = \ell - p, \; p \geq \ell/2$; and

d is summed over all values making the binomial coefficients non-zero.

$$G_{\ell h(2h-\ell)}(e) = \frac{1}{(1-e^2)^{\ell-1/2}} \sum_{d=0}^{h'-1} \binom{\ell-1}{2d+\ell-2h'} \binom{2d+\ell-2h'}{d} \left(\frac{e}{2}\right)^{2d+\ell-2h'} \qquad \text{j.}$$

where $h' = h, \; h \leq \ell/2$,

$h' = \ell - h, \; h \geq \ell/2$.

For $j \neq 2h - \ell$, k.

$$G_{\ell hj}(e) = (-1)^{|j|} (1+\beta^2)^{\ell} \beta^{|j|} \sum_{k=0}^{\infty} P_{\ell hjk} Q_{\ell hjk} \beta^{2k}$$

where $\beta$ is defined as in 2i above.

$$P_{\ell hjk} = \sum_{\nu=0}^{q} \binom{2h'-2\ell}{q-\nu} \frac{(-1)^{\nu}}{\nu!} \left[\frac{(\ell-2h'+j')e}{2\beta}\right]^{\nu}$$

$q = k + j', \; j' > 0, \; q = k, \; j' < 0$;

$$Q_{\ell hjk} = \sum_{\nu=0}^{q} \binom{-2h'}{q-\nu} \frac{1}{\nu!} \left[\frac{(\ell - 2h' + j')\, e}{2\beta}\right]^{\nu}$$

$$q = k,\ j' > 0;\ q = k - j',\ j' < 0;$$

h' is defined as in 2j above.

$$R = \sum_{\ell=0}^{\ell_{max}} \left[ R_{EL\ell} + \sum_{j=-j_{max}}^{j_{max}} R_{ES\ell j} \right] + R_{S20} + R_{M2010} + R_{M2210} + 2R_{M3021} \qquad \ell.$$

$$\frac{\partial R}{\partial S_1} = \frac{\partial R}{\partial M},\ \frac{\partial R}{\partial S_2} = \frac{\partial R}{\partial a},\ \frac{\partial R}{\partial S_3} = \frac{\partial R}{\partial e},$$

$$\frac{\partial R}{\partial S_4} = \frac{\partial R}{\partial i},\ \frac{\partial R}{\partial S_5} = \frac{\partial R}{\partial \omega},\ \frac{\partial R}{\partial S_6} = \frac{\partial R}{\partial \Omega}.$$

3. Runge-Kutta Integration

$\dot{S}_i\ [S_j,\ t] \equiv \dot{S}_i\ (S_1,\ S_2,\ S_3,\ S_4,\ S_5,\ S_6,\ t)$ , from the Lagrangian equations in Sec. 1.

$$w_i = \dot{S}_i\ [S_j(t),\ t]\ \Delta t$$

$$x_i = \dot{S}_i\ [S_j(t) + w_j/2,\ t + \Delta t/2]\ \Delta t$$

$$y_i = \dot{S}_i\ [S_j(t) + x_j/2,\ t + \Delta t/2]\ \Delta t$$

$$z_i = \dot{S}_i\ [S_j(t) + y_j,\ t + \Delta t]\ \Delta t$$

$$S_i(t + \Delta t) = S_i(t) + w_i/6 + x_i/3 + y_i/3 + z_i/6.$$

## 4. Expression of Spherical Harmonic Potential in Keplenian Elements.

$$V = \frac{kM}{\nu} \left[ 1 + \sum_{\ell=2}^{\infty} \left(\frac{a_e}{\nu}\right)^{\ell} \sum_{m=0}^{\ell} P_{\ell m} (\sin \phi) \{C_{nm} \cos m\lambda + S_{nm} \sin m\lambda\} \right],$$

where $a_e$ is equational radius; $\nu$, $\phi$, $\lambda$ are spherical polar coordinates; and $P_{\ell m}$ $(\sin \phi)$ is the Legendre Associated Polynomial; transforms to;

$$V = kM \left[ \frac{1}{\nu} + \sum_{\ell=2}^{\infty} \left(\frac{a_e}{a}\right)^{\ell} \sum_{m=0}^{\ell} \sum_{p=0}^{\ell} F_{\ell mp}(i) \sum_{q=-\infty}^{\infty} G_{\ell pq}(e) \right.$$

$$\times \left( \begin{Bmatrix} C_{\ell m} \\ -S_{\ell m} \end{Bmatrix}_{\ell-m \text{ odd}}^{\ell-m \text{ even}} \cos\{(\ell-2p)\,\omega + (\ell-2p+q)\,M + m\,(\Omega-\theta)\} \right.$$

$$\left.\left. + \begin{Bmatrix} S_{\ell m} \\ C_{\ell m} \end{Bmatrix}_{\ell-m \text{ odd}}^{\ell-m \text{ even}} \sin\{(\ell-2p)\,\omega + (\ell-2p+q)\,M + m\,(\Omega-\theta)\} \right) \right],$$

where $a, e, i, M, \omega, \Omega$ are the Keplerian elements, $\theta$ is the "lunar sidereal time", and $F_{\ell mp}$ $(i)$, $G_{\ell pq}$ $(e)$ are as defined in Secs. 2h, 2k of the Appendix. The lunar sidereal time $\theta$ is most conveniently taken as the mean longitude of the earth, which makes the reference meridian for lunar longitudes coincide with the mean direction of the earth.

APPENDIX IV
THE ANCHORED IMP SCIENTIFIC MISSION
Dr. N. Ness

ABSTRACT:

The primary goal of the anchored IMP satellite will be to investigate interplanetary magnetic fields, solar plasma fluxes, solar and galactic cosmic rays, and interplanetary dust distributions in the vicinity of the moon. A principal problem in cosmic electrodynamics is the interaction of a moving magnetized plasma and a solid object. This phenomenon can be definitively studied with an orbiting anchored IMP satellite whereby the interaction of the solar wind and the moon can be studied without the complicating effects of a planetary magnetic field. High energy particle detectors and ionization chambers are included in the instrument repertoire as well as a cosmic dust detector and a triaxial flux-gate magnetometer.

The possibility of performing simultaneous measurements in space with magnetometers, plasma and particle detectors on the anchored IMP and other spacecraft will provide invaluable data about the propagation of solar transient disturbances in interplanetary space. In addition, the anchoring of the satellite in the lunar gravitational field will allow the magneto-hydrodynamic wake of the earth in the interplanetary medium to be studied at lunar distances.

A second major objective of the anchored IMP mission will be a detailed analysis of its orbital dynamics. This will provide critical information on the lunar gravitational field and permit the investigation of the mass distribution in the moon. It will also improve the determination of the earth-moon mass ratio and the figure of the moon. Accurate knowledge of the lunar gravitational field is important in determining the bulk properties of the lunar body, and the development of more specific models of the lunar interior. Finally, detailed knowledge of the lunar gravitational field will be of importance in future lunar missions requiring accurate trajectory and orbital maneuvers.

## Introduction

Direct measurements of the physical properties and dynamical characteristics of the interplanetary medium have been performed in recent years through the utilization of deep space probes. The magnetic field of the earth has a strong effect on its immediate space environment and thereby drastically modifies certain of the characteristics of the interplanetary medium. Satellites which orbit the earth are in general thus unable to sample the undisturbed interplanetary medium.

The primary mission of the IMP (Interplanetary Monitoring Platform) program has been to develop an earth satellite with an orbital eccentricity sufficiently large so that detailed measurements of the interplanetary medium in the vicinity of the earth are possible. The IMP orbit as planned offers a unique opportunity to investigate the interplanetary medium and also the transition region between its unperturbed status and the magnetosphere of the earth. Many transient geophysical phenomena associated with solar activity are a direct result of the interaction of the earth's magnetic field, its atmosphere, and the solar corpuscular fluxes.

In continuing the exploration of the interplanetary medium and the interaction effects associated with solar particle fluxes and planetary objects, the next logical object for investigation is the closest neighbor of the earth, its own satellite, the moon. The possibility of utilizing the lunar gravitational field for "anchoring" an orbiting satellite in the interplanetary medium but yet in close proximity to the earth was recognized several years ago. The mission of the Able V program[1] was to place a 390-pound scientific satellite into a close orbit around the moon. The experiment repertoire was designed to investigate aspects of the lunar environment and included magnetometers, radiation sensors and micrometeorite detectors. Unfortunately this satellite program was not successful with all launches ending in destruction of the vehicle.

Since that time the investigation of the moon, its surface and its body properties, has become an increasingly important portion of the space research program. The investigation of the interplanetary medium in the vicinity of the moon remains to be explored and as yet there are insufficient plans for adequate investigation of these phenomena, particularly on a monitoring basis. The developments associated with the technical design of the IMP spacecraft have suggested that the basic spacecraft structure and telemetry system is appropriate for additional scientific missions. This led to a consideration of placing an IMP into a lunar orbit with the primary mission being the investigation of the particle and magnetic field environments in the vicinity of the moon, as was the original intent of the Able V program.

## Anchored IMP Mission

The technical capability of the IMP satellite and its associated launch vehicle is such that a relatively close lunar orbit is possible with the addition of a 4th stage injection motor. It is proposed that a slightly modified IMP satellite weighing approximately 110 pounds be placed into a lunar orbit during the time interval June to December, 1965 so as to coincide with the IQSY (International Year of the Quiet Sun).

The satellite will monitor the interplanetary medium and lunar environment throughout a major portion of its orbit, as in the case of the standard IMP. The transition region between the interplanetary medium undisturbed by the planetary object and that region of space in its immediate proximity where its presence dominates the physical phenomena will also be investigated.

A primary goal of the anchored IMP mission will be to investigate interplanetary magnetic fields, solar plasma fluxes, and solar and galactic cosmic rays in the vicinity of the moon. A principal problem in cosmic magneto-hydrodynamics is the interaction of a moving magnetized plasma such as the solar wind, and a solid object such as the moon. This phenomenon can be definitively studied with an anchored IMP spacecraft. High-energy particle detectors and ionization chambers are included in the instrument repertoire. The possibility of performing simultaneous measurements in space with magnetometers, plasma and cosmic ray detectors on the anchored IMP and other spacecraft, possibly a standard IMP, will provide invaluable data about the propagation of solar transient disturbances in interplanetary space.

The second major objective will be a detailed analysis of the orbital dynamics of the lunar orbiter. This will provide critical information on the lunar gravitational field and permit the investigation of the mass distribution in the moon. It will also improve the determination of the earth-moon mass ratio. The figure of the moon derived from perturbations of its own orbit suggest a concentration of mass outwards rather than into the moon's interior. Accurate knowledge of the lunar gravitational field is extremely important in determining the bulk properties of the lunar body, and development of more specific models of the lunar interior. In order to carry out the detailed studies of the orbital dynamics an appropriate range and range rate system is included in the experiment repretoire to provide sufficiently accurate data on the position of the spacecraft for such orbital analyses. Knowledge of the lunar gravitational field will be of great value in the future lunar missions requiring accurate trajectory maneuvers.

At the present time the nominal lunar orbit parameters corresponding to the primary constraints of the IMP spacecraft and launch vehicle are:

Pericynthion . . . . . . . . . . . 500 to 1500 kilometers
Apocynthion . . . . . . . . . . . 3000 to 10,000 kilometers
Inclination . . . . . . . . . . . . Highest possible up to 75°
Lifetime . . . . . . . . . . . . . . At least 6 months

Orbital characteristics of the anchored IMP are such that for most of each orbital period, data will be transmitted from the satellite which can be received by telemetry stations located on the earth. During the remainder of the time the satellite will be eclipsed by the moon with respect to radio reception by the earth. This eclipsing may yield additional information about the electron densities in the vicinity of the moon.

An important aspect of the anchored IMP will be the possibility of measuring simultaneously similar phenomena in space. The separation of spatial and temporal variations in the structure of the interplanetary medium and the detailed description of the propagation of solar transient phenomena require simultaneous measurements at points separated from each other in the vicinity of the earth. The anchored IMP provides for such measurements with identical instrumentation and hence provides a unique opportunity for such studies. The correlation of separate experiment's data on the same spacecraft as well as of similar or identical experiments on separate spacecraft allows for adequate experimental investigation of complex solar terrestrial relationships.

Detailed investigations of the interplanetary dust distribution in the vicinity of the earth have been handicapped by the lack of satellites sufficiently far removed from effects associated with the earth. The hypothesis that the moon's surface is covered with a thin layer of dust depends upon micrometeorite bombardment. Direct measurements of dust fluxes in the immediate vicinity of the moon will allow a critical evaluation of this hypothesis.

## Anchored IMP Experiments

Within the weight, volume, and power limitations of the anchored IMP spacecraft, it is anticipated that the complement of experiments will include the following:

(1) Magnetometer
(2) Plasma Probe
(3) Ionization Chamber
(4) Cosmic Ray Detector
(5) Micrometeorite Detector

Experiments similar to these have been flown on previous satellites and it is reasonably certain that the anchored IMP spacecraft will be capable of supporting all of these experiments if light-weight and low-power versions of them are selected. The following sections outline the scientific investigations that could be conducted with such a repertoire of experiments.

### 1. Magnetometer and Plasma Detectors

A lunar anchored spacecraft offers an opportunity to investigate a number of major magnetic field phenomena in space with a single experiment. The interpretation of the data in terms of the separate phenomena presents a distinct problem in interpretation and theoretical analysis. Sufficiently precise vector magnetic field and plasma measurements on the spacecraft will permit the partial solution to this problem as well as indicating the appropriate parameter ranges for more definitive measurements with future spacecraft.

### 1.1 Interplanetary Magnetic Field

The existence, general description, and temporal behavior of the interplanetary magnetic field have been deduced in the past from a variety of terrestrial observations. Recent direct measurements in space by Pioneer V[2] with a search coil magnetometer have been interpreted as consistent with a steady field component of 2.5 gammas normal to the ecliptic plane. In addition, it has also been reported that fluctuations as large as 50 gammas have been detected during times of magnetic disturbance.[3]

A steady field normal to the plane of the ecliptic is inconsistent with a number of models of the interplanetary magnetic field in which solar magnetic lines of force are stretched out away from the sun by the highly conducting streaming solar plasma. The low energy proton flux detected by Explorer X was directed at all times away from the sun, but fluctuated in magnitude and energy spectra as a function of time.[4] Measurements[5] by the Mariner spacecraft have indicated that the flux of low energy plasma from the sun presents a spectrum with considerable temporal and energy structure but in general is in agreement with the results from Explorer X.

Measurements of the interplanetary magnetic field[6] by Explorer X were distorted by a strong interaction between the streaming plasma and the magnetic field of the earth which led to the formation within the plasma stream of a cavity containing the geomagnetic field. The magnetometer measurements[7] on the Mariner spacecraft are incomplete for total vector information and thus do not provide definitive data on the interplanetary magnetic field. The data, however, is consistent with an interplanetary field in the plane of the ecliptic with a strength of approximately 5 gammas normal to a sun-satellite direction. The magnitude of this field component compares with Pioneer V but the direction is different by 90°. Recent data[8] on galactic fields indicate that they are on the order of 0.5 gammas and up to 2.5 gammas in interstellar space.

In general, the interplanetary magnetic field is considered to be approximately 5-10 gammas average value, although steady periods are possibly infrequent. The variability of the interplanetary magnetic field and the extreme limits expected during solar disturbances indicate that a wide dynamic range is required as well as precise vector measurements.

## 1.2 Lunar Magnetic Field

The direct measurement of the lunar magnetic field[9] and a precise determination of its geometrical properties is of vital importance in the study of the origin of the earth-moon system. The interpretation of terrestrial data suggests the nonexistence of a lunar magnetic field similar in origin to the earth in which a dynamo system of currents circulates in a fluid core. The presence of a lunar magnetic field may be indicative of a permanent state of magnetization which reflects an ancient field at the time of origin of the moon. It has been suggested by Gold[10] that the streaming solar plasma may provide a mechanism whereby the interplanetary magnetic field is captured by the finite electrical conductivity of the moon. This would then lead to a magnetic field configuration which could be interpreted as a lunar magnetic field.

Russian measurements of the lunar magnetic field on the second Cosmic rocket[11] indicate a surface field of less than 50 to 100 gammas corresponding to a magnetization intensity less than 0.25% of the earth's. The present experiment is designed to investigate magnetizations 50-100 times weaker than this figure. The streaming solar plasma is sufficiently strong that it will greatly distort[12] a lunar magnetic field regardless of its origin. It can reasonably be expected that a cavity and magnetic tail similar to that observed on Explorer X (in the anti-solar direction behind the earth) will also develop around on the moon.

The detailed measurement and accurate vector mapping of such a lunar magnetic field can only be accomplished with an orbiting spacecraft at low altitudes with a broad-band instrument. The IMP measurements will more clearly define the restraints to be placed on magnetic field experiments for a close lunar orbiting spacecraft. Measurements of the interplanetary field on the earth-moon trajectory will assist in the interpretation of the residual lunar magnetic field. It is important that these measurements of the lunar field be made at relatively quiet times when solar activity is low, so that the interpretations are as clear and unique as possible.

## 1.3 Interaction Effects Associated with the Streaming Solar Plasma and the Moon

The presense of an object such as the earth and its associated magnetic field in the solar stream leads to strong interactions between the solar particle flux and the geomagnetic lines of force. Since the moon possesses a much smaller magnetic field than the earth[11] and lacks an appreciable atmosphere,[13] a different class of interactions is expected. It has already been suggested in Section 2.2 that the solar stream will greatly distort any lunar magnetic field. In view of the differences existing between these two celestial bodies the structure of the magneto-hydrodynamic interactions in the vicinity of the moon will be determined primarily by the plasma dominated interactions.

This will be true unless the interplanetary magnetic field is compressed on the sun-lit hemisphere of the moon to a level equal to that corresponding to balance of magnetic energy and plasma kinetic energy. Typical figures for the expected plasma fluxes and the magnetic field strengths with equivalent energy densities are presented in Table I.

Table I

EQUIPARTITION OF PARTICLE KINETIC ENERGY AND MAGNETIC FIELD STRENGTH

| Proton Density (Number per $cm^3$) | Proton Bulk Velocity (Kilometers per sec.) | Magnetic Field Strength (Gammas) |
|---|---|---|
| 5 | 300 | 29 |
| 10 | 500 | 70 |
| 10 | 600 | 82 |

The moon thus offers the possibility of performing a simple experiment in magneto-hydrodynamics in which a streaming solar plasma containing a magnetic field is incident upon a solid spherical object possessing a small and thus effectively no magnetic field. The complete study of the interaction effects requires not only a magnetometer experiment, but also simultaneous plasma flux measurements. The classical problem of flow of a conducting fluid past various solid bodies under the influence of a magnetic field has been approached by a number of authors. (See Hasimoto (14, 15, 25), Imai (16, 25), Ludford (17, 18, 19, 25), McCune (20, 21, 25), Resler (21, 22, 25), Sears (22, 25), Stewartson (23, 24, 25), and others (25). Again, plasma and magnetic field measurements during quiet solar times such as the IQSY will permit straight-forward interpretations.

### 1.4 Energetic Particle Measurements

Terrestrial and recent satellite measurements of galactic and solar cosmic rays have indicated a direct dependency upon solar activity. The geomagnetic field strongly influences the particle dynamics and direct measurements in interplanetary space are required to understand the propagation of such particles in interplanetary space. An anchored IMP satellite can measure the spectral, directional, and temporal characteristics of both galactic and solar cosmic rays by using the moon's body as a shield for solar-particle fluxes without the complicating effects of an appreciable lunar magnetic field. Since the presently planned orbit is several lunar radii, it is expected that any direct lunar emission or albedo effects by secondary emission may be small since the moon subtends a small solid angle at the detector. The investigation of the spectral and directional characteristics and their time correlations with other satellites particle detectors will be especially revealing about the propagation of transient disturbances such as Forbush decreases in interplanetary space.

### 1.5 Dust Measurements

The moon, like the earth, is continually bombarded by meteoroids traveling with speeds of tens of kilometers per second. The effects of such impacts on the moon are, however, quite different from those on the earth. The major reason for these differences is that the moon lacks a protective atmosphere for decelerating or destructively ablating the incoming meteoroids.

All but the largest meteoroids which collide with the earth are decelerated or destroyed through ablation in the atmosphere. Meteoroids that are large enough to survive passage through the atmosphere appear as meteorites or, if their speeds at impact are sufficiently high, form hypervelocity craters on the surface of the earth. Not having been retarded by an atmosphere, meteoroids of all sizes impacting on the moon strike at speeds increased slightly from their initial values by the gravitational attraction of both the moon and the earth. At impact, the speeds range between about 3.8 km $sec^{-1}$ and 72 km $sec^{-1}$; thus, each collision occurs at hypervelocity. The mass of ejected material, its velocity and mass distributions, and the proportions of material in the form of particulate aggregates and plasma are presently unknown for the case of meteoroidal impacts on the moon.

The absence of an appreciable lunar atmosphere also makes negligible the atmospheric drag forces on any ejected dust particles. These ejected particles follow ballistic trajectories or orbital paths, depending on the speed and direction at ejection. Of particular interest are the smallest dust particles that have been ejected at sufficiently high speeds to escape from the gravitational field of the moon.

Measuring selected parameters of dust particles from a spacecraft situated in the vicinity of the lunar surface would yield much information about the frequency of impacts of dust particles and meteoroids on the moon. The large impact area provided by the lunar surface also makes possible a determination of the frequency and characteristics of impacts of meteoroids of much larger masses than can ever be observed directly with instruments on spacecraft.

A comprehensive investigation of the distributions of interplanetary dust particles in the vicinity of the moon and of small dust particles ejected from the moon by meteoroidal impacts would represent an effective means of evaluating the lunar impact hypothesis for the abundance of dust particles observed in the vicinity of the earth. Study of the structure of known meteoroid streams and sporadic showers is also possible since the measurement from the lunar orbiter will include the primary particles from the streams and lunar ejecta which may be identified with lunar impacts of stream particles.

## 2. Scientific Need for Selenodetic Satellite

As is well known, a knowledge of the state of the moon's interior is important to the problem of cosmogony and the development of the earth itself. Because of ignorance of the moon's interior, there are at present a wide variety of speculations as to the processes affecting the variations in the moon's mass distribution, and hence, the variations in its gravitational field: the moon may still be in a hetereogeneous state from the original collection of the bodies which formed it (Ref. 26); heating by radioactive matter may have caused irregularities by cracking due to thermal expansion (Ref. 27); or heating may lead to sufficient plasticity to permit isostatic compensation of the original irregularities (Ref. 28); or even to permit convection currents (Ref. 29). Furthermore, if the moon was ever much closer to the earth than it is now, as required by some theories of its origin (Refs. 30 and 31), there may be evidence thereof in its structure (Ref. 32). Better knowledge of the moon's gravitational field should therefore be of great value in reducing the present wide range of speculation.

In view of the variety of possibilities as to the state of the moon's interior, in planning a lunar orbiter it seems most prudent to take the earth as a standard. The simplest question which can be asked about the variations in the moon's gravitational field is whether they imply greater or smaller stress differences than variations of the same wave length in the earth's gravitational field. Scaling to allow for the moon-earth mass ratio of .0123 and radius ratio of .2725, the order of magnitude of the normalized spherical harmonic coefficients predicted on this equal-stress assumption is (Ref. 33):

$$\left\{ \overline{C}_{nm}, \overline{S}_{nm} \right\} = 2 \times 10^{-4} / n^2$$

The only harmonics of the moon's gravitational field now known are those for n = 2, owing to their effect on the physical libration. Their value is moderately smaller than predicted by the above rule:

$$\left\{ \overline{C}_{22}, \overline{S}_{22} \right\} = 2 \times 10^{-5}$$

### 2.1 Tracking Accuracy

The tracking presently planned for IMP series satellites is the range and range rate with a 136-Mc carrier. The accuracy anticipated at the distance of the moon is ± 200 meters in range and ±2 meters/sec in range rate. To utilize the more accurate range and range rate with a 2200-Mc carrier (± 10 meters range, ± 0.1 meters/sec range rate), either spacecraft power consumption must be increased to 60 or 70 watts and transponder weight to 15 pounds, or else probably expensive modifications must be made to use the 85-foot diameter antennas. The criterion used for orbit specification therefore was the number of harmonics of magnitude $\{C_{nm}, S_{nm}\}$ causing perturbations more than ± 500 meters in amplitude.

## 2.2 Orbit Specifications

In general, (1) sensitivity of orbits to a variety of perturbations increases with inclination to around 70°; (2) low inclination orbits are more sensitive to harmonics with large (n-m)/n; (3) high inclination orbits are more sensitive to harmonics with small (n-m)/n; and (4) the variety of perturbations will increase with eccentricity. However, perturbations by the earth, sun and radiation pressure will increase even more rapidly with eccentricity, so that it is desirable to keep the eccentricity less than 0.3 for accurate determination of perturbations by the lunar field as well as an adequate lifetime. This applies particularly to semimonthly perturbations caused by the earth, which will have the same period as some perturbations by the moon's field, and which therefore will distort determinations of variations in the moon's field if not carefully taken into account. Some anticipated orders of magnitude of perturbations which were calculated:

| Perigee Height | Apogee Height | Number of harmonics expected to cause perturbations larger than ± 500 meters | |
|---|---|---|---|
| (km) | (km) | At inclination 0° | At inclination 60° |
| 200 | 630 | 9 | 16 |
| 200 | 4100 | 9 | 16 |
| 500 | 544 | 5 | 16 |
| 500 | 996 | 9 | 16 |
| 500 | 5000 | 11 | 16 |
| 1000 | 1053 | 5 | 16 |
| 1000 | 1604 | 7 | 16 |
| 1000 | 6500 | 9 | 16 |
| 2500 | 2582 | 5 | 16 |
| 2500 | 3400 | 7 | 14 |
| 2500 | 11000 | 5 | 14 |

It is evident that as high an inclination as practicable is desired, even at the cost of a higher perigee height. If the inclination is to be nearly zero, then the perigee height should not be much more than 1000 km.

## References


1. Altshuler, et al., "The Scientific Objectives of the Able V Programs," Physics Today, Vol. 14, No. 1.

2. Coleman, P. J. Jr., L. Davis and C. P. Sonett, "Steady Component of the Interplanetary Magnetic Field: Pioneer V," Phys. Rev. Letters, 43-46 (1960).

3. Coleman, P. J. Jr., C. P. Sonett and L. Davis, Jr., "On the Interplanetary Magnetic Storm: Pioneer V", Journal Geophys. Res. 66-7, 2043-2046 (1961).

4. Bridge, H. S., C. Dilworth, A. J. Lazarus, E. F. Lyon, B. Rossi and F. Scherb, "Direct Observations of the Interplanetary Plasma", Journal of the Physical Society of Japan, Vol. 17, Supp. A-II, 533 (1962).

5. Snyder, C. and M. Naugebauer, "The Mission of Mariner II: Preliminary Observations", Science, 138, 1095-1100, (1962).

6. Heppner, J. P., N. F. Ness, T. L. Skillman and C. S. Scearce, "Magnetic Field Measurements with the Explorer X Satellite", Journal of the Physical Soc. of Japan, Vol. 17, Supp. A-II, 546, See also JGR 68, 1-46, (1963).

7. Coleman, P. J. Jr., L. Davis, Jr., E. J. Smith and C. P. Sonett, "The Mission of Mariner II: Preliminary Observations" Science 138, 1095-1100.

8. Davies, R. D., G. L. Verschuor and P. A. T. Wild, "Measurement of Magnetic Fields in Interstellar Clouds", Nature, 4854, 563, (1962).

9. Vestine, E. H., "Utilization of a Moon-Rocket System for Measurement of the Lunar Magnetic Field" Rand Corp., Report RM-1933, (1957).

10. Gold, T., "The Hydrogen Atmosphere of the Moon", 3rd Int. Space Sci. Symp., Wash., D. C. (1962).

11. Dolginov, S. H., E. G. Eroshenko, L. N. Zhugov, N. V. Pushkov and L. O. Tynrmina, "Magnetic Measurements on the Second Cosmic Rocket Artificial Earth Satellites-5, 16-23 (1960). (ARS Journal Supplement, 1640-1643 (1961).

12. Neugebauer, M., "Question of the Existence of a Lunar Magnetic Field," Phys. Rev. Letters 4-1, 6-8 (1960).

13. Herring, J. R. and A. L. Licht, "The Effect of the Solar Wind on the Lunar Atmosphere", Space Research I, 1132-1145 (1960).

14. Hasimoto, H., The Phy. of Fl., 2 (1959), 337-338.

15. Hasimoto, H., J. Fl. Mech., 8 (1960), 61-81.

16. Imai, I., Particl diff. equs. and continuum mech., Univ. of Wisconsin Press, Madison, Wis. (1961), 177-205.

17. Ludford, G. S. S., Arch, Rat. Mech. and Anal., 4 (1960), 405-411.

18. Ludford, G. S. S., J. Fl. Mech., 10, Part I (1960), 141-155.

19. Ludford, G. S. S. and Murray, J. D., J. Fl. Mech. 7 (1960), 516-528.

20. McCune, J. E., J. Fl. Mech. 7 (1960), 449-468.

21. McCune, J. E. and Resler, E. L., Stanford Univ. Press, 1960.

22. Resler, E. L. and Sears, W. R., J. Fl. Mech. 5 (1959), 257-273.

23. Stewartson, K., Proc. Camb. Phil. Soc. 52 (1956), 301-316.

24. Stewartson, K., J. Fl. Mech. 8 (1960), 82-96.

25. Proc of the International Symp. on Magneto-Fluid Dynamics, published in Rev. of Modern Physics, 32, (1960).

26. Urey, H. C., W. M. Elsasser and M. G. Rochester, Astrophys. J., 129, 842, (1959).

27. MacDonald, G. J. F., Science, 133, 1045, (1961).

28. O'Keefe, J. A. and W. S. Cameron, Icarus, 1, 271, (1962).

29. Kopal, Z., Planetary Space Sci., 9, 625, (1962).

30. Alfven, H., Icarus, 1, 357, (1963).

31. O'Keefe, J. A., Blacksburg Conf., Va., Aug. 12, (1963).

32. Kaula, W. M., J. Geophys. Res., 9, (17), (1963).

33. Kaula, W. M., Adv. in Sp. Sci. and Tech., 5, In Press, (1963).

September 27, 1963

APPENDIX V

DETAILED WEIGHT DISTRIBUTION FOR THE IMP D & E SPACECRAFT

| ITEM | SUBTOTALS | TOTALS |
|---|---|---|
| Experiments | | |
| Cosmic ray experiment | | |
| Telescope | 3.7 | |
| Elec. card No. 1 | 1.5 | |
| Elec. card No. 2 | 1.5 | 6.7 |
| Cosmic ray experiment | | |
| Ion chamber | 2.0 | 2.0 |
| Magnetic field experiment | | |
| Triazial fluxgate sensor | 1.5 | |
| Fluxgate accumulator | 1.3 | |
| Fluxgate electronics | 1.3 | |
| Fluxgate A/D electronics | 1.3 | 5.5 |
| Solar wind experiment | | |
| Plasma probe sensor (2) | 4.0 | |
| Electronics No. 1 | 1.5 | |
| Electronics No. 2 | 1.5 | 7.0 |
| Cosmic dust | 4.5 | 4.5 |
| Total Experiments: | | 25.7 |
| Total Allowable Experiments: | | 22.2 |
| Optical Aspect System | | |
| Optical aspect sensor | .8 | |
| Optical aspect sensor guide and converter | .4 | |
| Optical aspect sensor computer | .6 | 1.8 |
| Total Aspect: | | 1.8 |
| Power System | | |
| Solar conversion | | |
| Solar paddles (4) 3-mil glass | 22.6 | |

DETAILED WEIGHT DISTRIBUTION FOR THE IMP D & E SPACECRAFT (continued)

| ITEM | SUBTOTALS | TOTALS |
|---|---|---|
| Power System (Cont.) | | |
| Prime converter | 4.0 | |
| Battery | 6.9 | |
| Solar array regulator | .4 | |
| Encoder converter | .8 | |
| Multiconverter | 1.1 | 35.8 |
| Internal electrical | | |
| Harness | 4.5 | |
| Turn-on plug | .1 | |
| Separation switch | .1 | |
| Solar paddle erection switch | .1 | |
| RF filters | .1 | 4.9 |
| Total Power System: | | 40.7 |
| Telemetry Data System | | |
| Encoder | 2.1 | |
| DDP Mod C | 1.0 | |
| DDP Mod D | 1.2 | |
| Program 1 and undervoltage detector | .9 | |
| Program 2, and fluxgate Cal. | .9 | |
| Program 4 and apogee sequence timer | .9 | |
| Performance parameters | .9 | 7.9 |
| Total Data System: | | 7.9 |
| Telemetry Communications & Range Rate System | | |
| Transmitter | 1.4 | |
| Range rate No. 1 | 1.2 | |
| Range rate No. 2 | .7 | |
| Range rate No. 3 | 1.2 | |
| Command receiver No. 2 | 1.5 | |
| Antenna | .3 | |
| Antenna hybrid | .9 | 7.2 |
| Total Telemetry System: | | 7.2 |

DETAILED WEIGHT DISTRIBUTION FOR THE IMP D & E SPACECRAFT (continued)

| ITEM | SUBTOTALS | TOTALS |
|---|---|---|
| Spacecraft Structure | | |
| Platform | 3.9 | |
| Top cover | 3.0 | |
| Center tube | 2.4 | |
| Antenna supports | .9 | |
| Struts (8) | 1.5 | |
| Paddle arm bracket (4) | 3.1 | |
| Paddle arm and hinge (4) | 4.6 | |
| "D" frame (A-H) | 2.0 | |
| Fluxgate boom (2) | 1.0 | |
| Lower cone | .8 | |
| Active thermal control (converter) | 1.1 | |
| Passive thermal control coating | .9 | |
| Balance weight | 2.0 | |
| Apogee motor heat shield | 0.5 | |
| Apogee motor separation mechanism | 2.5 | 30.2 |
| Total Structure: | | 30.2 |
| Apogee Motor (4th stage) | 70.9 | 70.9 |
| Total Spacecraft Weight: | | 180.9 |

## APPENDIX VI

## IMP D & E TEMPERATURE CONTROL

S. Ollendorf

### I. Transfer Phase

a. Rocket Engine
The following is the result of a study made on the rocket engine during transfer to the moon.

1. Propellant

| Case Cover | Sun Looking Broadside T Initial | T Final | $\Delta$T Grain | Shade (70 hrs.) T Initial | T Final | $\Delta$T Grain |
|---|---|---|---|---|---|---|
| Vap. Dep. Alum. on Case | 20°C | 76°C | 4°C | 20°C | -1°C | 1.1°C |
| Super Insul. on Case | 20°C | 28°C | 1°C | 20°C | 11°C | 1°C |

Required--7°C → 60°C; $\Delta$T Grain < 22°C

Conclusion–Super insulation composed of 5 layers of aluminized mylar (.10" thick) with an outer layer of teflon-impregnated cloth (Amfab) is required. The latter is necessary to keep the mylar from overheating.

2. Nozzle

| Shade 70 hours | | | |
|---|---|---|---|
| Outside/Inside Cover / Cover | T Case | T Nozzle | T Case-Nozzle |
| Super/Super Insul./Insul. | 11°C (Super Insul. Case) | 3°C | 8°C |
| Super/Vap. Insul./Alum. | 11°C (Super Insul. Case) | -25°C | 35°C |
| Vap./Vap. Alum./Alum. | -1°C (Vap. Alum. Case) | -86°C | 87°C |

| Sun Looking Broadside - 70 hrs. | | | |
|---|---|---|---|
| Outside/Inside Cover / Cover | T Case | T Nozzle | T Case-Nozzle |
| Black/Black | 28°C (Super Insul.Case) | 1°C | 27°C |
| Black/Black | 76°C (Vap. Al. Case) | 1°C | 75°C |

Required–Temperature of nozzle should be as close to temperature of case as possible at time of firing and not be subjected to extreme low temperatures.

Conclusion–Applying super insulation to both sides of the nozzle is best but involves blowing off the shroud before firing or having the rocket exhaust take care of it. Another alternative, as shown above, is to restrict the launch window so that there is sufficient solar input to the nozzle during the transfer phase.

It might be noted that JPL has no low-temperature data on the nozzle material and further investigation may prove that a simpler method, such as vapor deposited aluminum, may suffice.

3. Retro Kick Motor Heat Shield Effects on Vehicle

Case I

Active control on five facets of spacecraft and on top and bottom, no heat input to top surface of spacecraft

Results–At zero degree sun angle, temperature can fall as low as -46°C in facets with minimal power dissipation and -35°C in the battery compartment. At 30° sun angle minimum facet temperature is -6°C with battery at -4°C.

Case II

Active control on top and bottom of spacecraft, passive coatings on facet sides, no heat input to top surface of spacecraft

Results–The results in this case were similar to those in Case I at 0° sun angle with minimum temperature reaching -48°C, and the battery falling to -45°C. At 30° sun angle, the minimum and battery temperatures were -3°C and -7°C respectively.

Solutions

(a) Remove Shield.

Consequence is that spacecraft temperature control surfaces might be contaminated by rocket exhaust.

(b) Use a solar transparent material (>10 mil thick) such as mylar for heat shield. This would allow spacecraft heating from sun during transfer and block out IR energy during engine firing (greenhouse effect).

(c) Restrict sun angle to 30° to 150°.

(d) Supply heaters to critical components.

## II. Retro Rocket Firing

Case I

Taking an average stainless steel case temperature during firing (165°C), the spacecraft skin temperature does not rise appreciably (< 5°C) above the point at which the skin normally runs during orbit (50°C).

Using the maximum case temperature of 345°C (for a titanium case), the spacecraft skin temperature rises 15°C above the orbital temperature. This causes only a 3°C rise in maximum component temperature.

The reason for this is that the increase in flux to the spacecraft from the hot engine is compensated for by a decrease in energy input from the sun due to blockage (17% blockage).

Conclusion–If blowback were not a cause for concern, the shield could be eliminated.

Case II

Again, using a maximum temperature of 345°C as a worst case, the temperature rise at the spacecraft skin to 110°C is encountered with a component increase of 10°C.

The increase in temperature over Case I is due to the higher emittance surface requirements to meet orbital conditions, resulting in much higher radiant interchange between the rocket and the vehicle during firing.

Conclusion–The increase in skin temperature as well as in the components themselves may affect the outside coatings and possibly cause a failure in critical electronics.

## III. Orbit Steady State

### Case I - Controlling sides, top and bottom

Assumptions

1. Shutters are on sides of facets B, C, E, F, G covering 90% of face. Shutters open in plane of rotation. Facet skin painted black beneath shutters as well as on facets containing no active control (A, D, H).

2. (a) Shutters are at minimum shutter angle when closed.
   (b) Shutters are at 90° angle when fully open.

3. No restriction as to sun angle exists.

4. The bottom surface is covered with blade type controllers which give an $\alpha_{max} = .22$, $\epsilon_{max} = .13$ when fully exposed to the sun and $\epsilon_{min} = .085$ in the shade. They are designed so that 50% of the control area is exposed at any one time.

The control areas (15% of spacecraft covers) are painted with black paint and evaporated aluminum with the uncontrolled surface (85%) covered with evaporated aluminum and black stripes.

For the top surface $\alpha_{max} = .135$, $\epsilon_{max} = .13$, $\epsilon_{min} = .085$, white paint instead of black is substituted on the control areas with approximately the same total coverage.

Results - Figures 1, 2, and 3 show the effects of opening and closing the shutters on maximum (facet C), minimum (facet E), and average spacecraft temperatures. Also shown is the modulated shutter position at a given sensor response. The minimum temperature at a zero-degree sun angle in facet A (not shown), containing the cosmic-ray experiment, with no active control, is -5°C with shutters on adjacent facets open and +10°C with shutters closed.

Actuation and Sensing

Actuation and sensing can both be attained through the use of bimetallic coils which view or are imbedded in the electronic packages. They should be thermally isolated from the skin so as not to be affected by the large temperature fluctuations found there.

### Transient Shadow Considerations

### Case I - Controlling sides, top and bottom

An important feature of the total active thermal control system is the ability of the spacecraft to recover after relatively long shadow periods, with power lockout, before entrance into a subsequent eclipse phase. This results in average orbital temperatures of +14°C for pericynthion shadows (Figure 4) and -1°C for apocynthion shadows (Figure 5) at extreme sun angles (0° and 180°), with minimum facet temperatures running +5°C and -18°C for each shadow orbit.

Taking the worst transient, 4 hours in the shade with a 7-hour power lockout, switching to the low $\epsilon$ surfaces and closing the shutters, the cooldown in Figure 6 shows a lower limit of -25°C after the shade period.

Case Ia = Controlling Sides only

If the controllers were removed from the top and bottom and replaced with passive coatings having a solar absorptance of $\alpha_{top}$ = .135 $\alpha_{bottom}$ = .22 with an emittance of $\epsilon$ = .13, the consequence would be a drop to approximately -30°C at the end of the shade period as opposed to -25°C for the case shown in Figure 6. Going to this limited system of control does not affect the orbital mean temperatures to a great degree during shade orbits. Results show average orbital temperatures of +12°c for pericynthion shadows and -5°C for apocynthion shadows. Typical coating distributions on top and bottom to achieve these properties would be:

| | |
|---|---|
| Top | 10% White<br>90% Vap. Dep. Al. |
| Bottom | 15% Black<br>85% Vap. Dep. Al. |

Prime Converter

In both cases the prime converter was assumed to be actively controlled with a perforated shroud over the "stovepipe" fin which exposes white paint during sun periods and evaporated aluminum during the shade. Through this method, the temperature was controlled to 50°C in the sun and held to -5°C or -15°C in the worst shade orbit depending on which active control system is chosen for the vehicle skin.

Transmitter

The transmitter usually ran about 10°C higher than the prime converter, or a maximum of 60°C at a 90°C sun angle. If this is overly critical, a stovepipe similar to the prime converter can be added, or the properties of the skin may be varied locally near the transmitter.

Case II - Control on Top and Bottom only

1. A case was run whereby the shutters were removed from the sides and blade type controllers were placed on top and bottom only. It was shown that effective control could be maintained keeping the solar absorptance constant and varying the emittance. The sides

of the spacecraft would have to be coated with polished gold or "alodyne" ($\alpha$ = 42, $\epsilon$ = .05).

The required emittance range $\epsilon_{min}$ = .32 to $\epsilon_{max}$ = .50, could be achieved with 40% of the top and bottom skins actively controlled with white paint and evaporated aluminum, with the uncontrolled portion made up of evaporated aluminum, black and white paint.

Results

Figures 7, 8, and 9 show the range of temperatures for the minimum, maximum, and average facets, while Figures 10, 11, and 12 show the transient responses of the spacecraft during a pericynthion and apocynthion type shadow for the nominal and worst case orbits.

These results (for extreme sun angles) show that lower mean orbital temperatures occur during apocynthion shadows for the average facet of the partially controlled spacecraft than of the fully controlled spacecraft (-17°C Case II vs. -1°C Case I). If the lunar mission were restricted so that only pericynthion shadows would exist, then either system would suffice (Figure 5 vs. Figure 11). For the worst transient, this system does not react very much differently than the fully active system (minimum temperature -28°C Case II vs. minimum temperature -25°C Case I).

An examination of Figures 7, 8, and 9 indicates that adequate control can be achieved using this method although the "fail safe" qualities of this system are not as good as Case I. That is, if a failure should occur in a facet or the blades should stick open or closed, greater temperature extremes will occur.

Prime Converter and Transmitter

The prime converter and transmitter reach approximately the same temperature levels as those indicated in Case I.

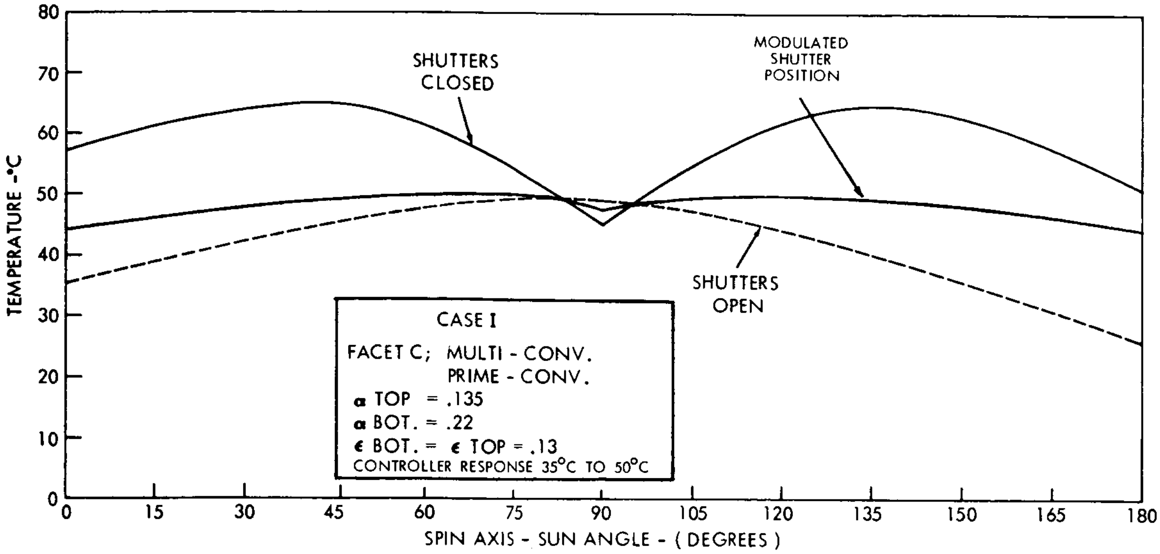


Figure 1

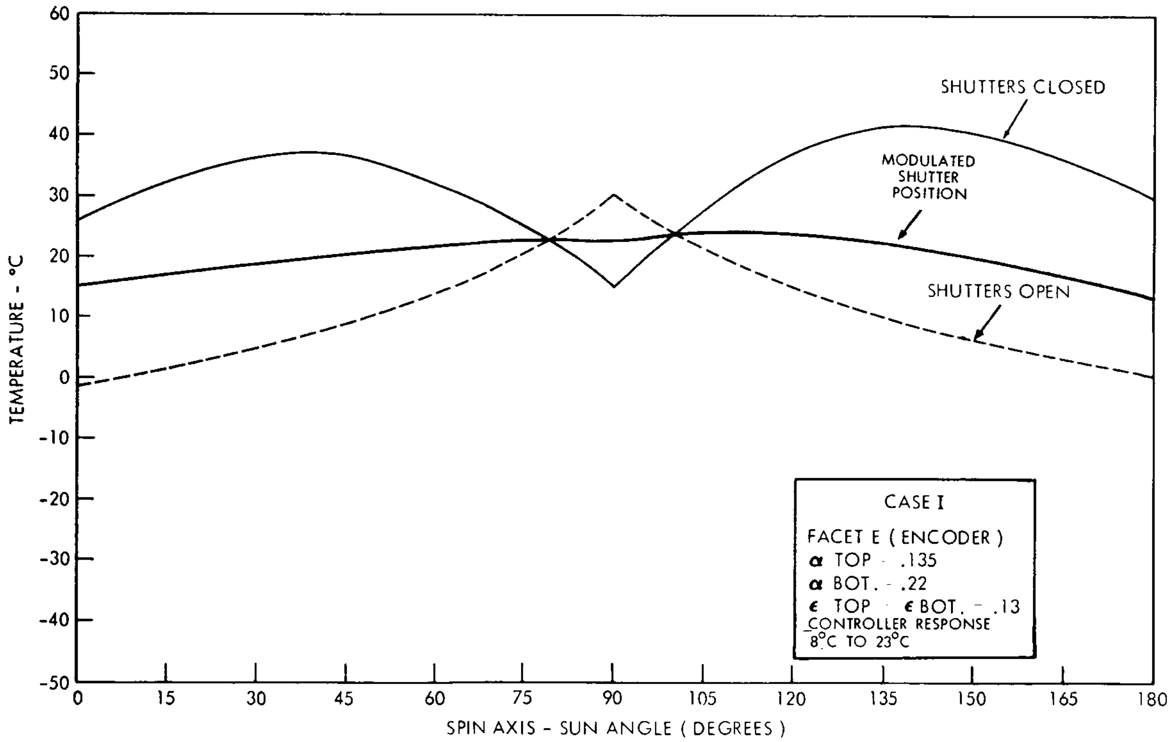


Figure 2

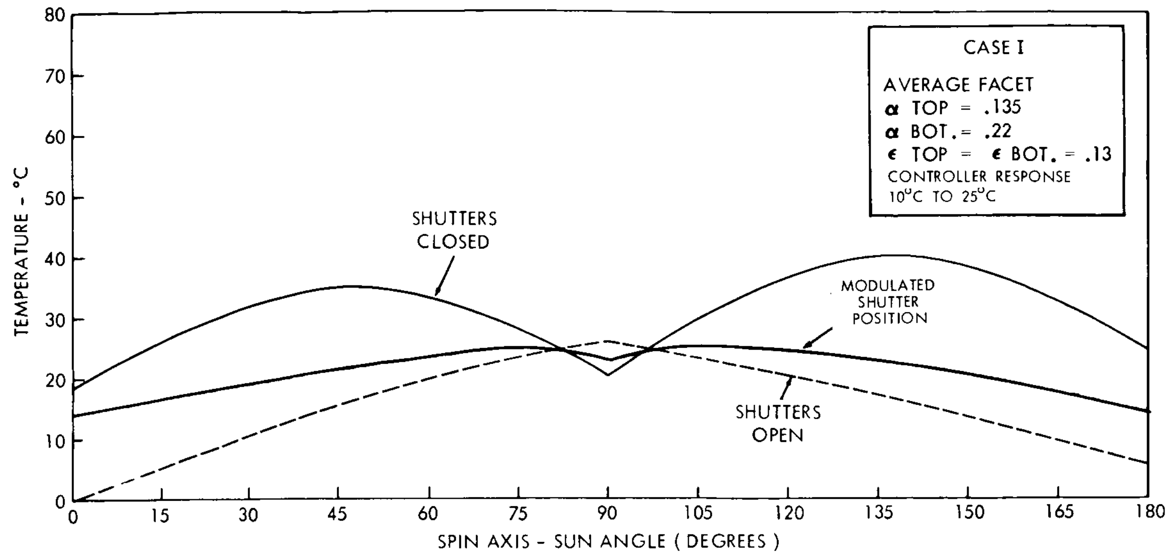


Figure 3

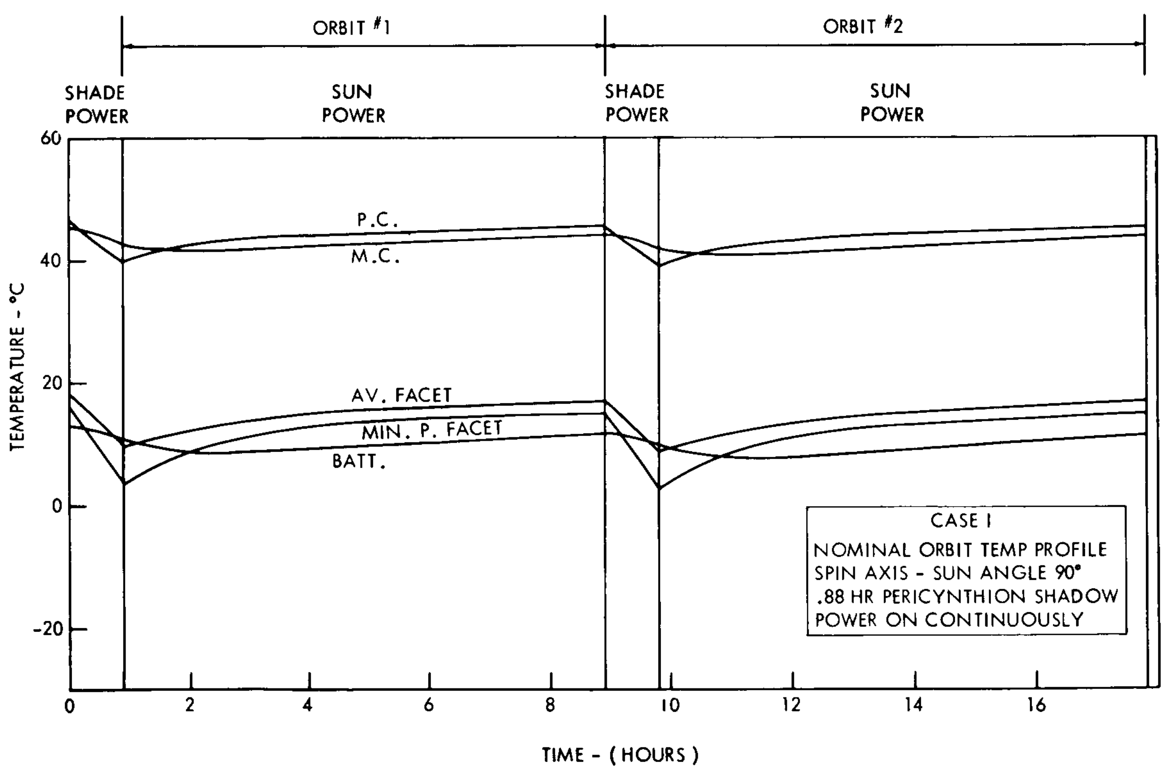


Figure 4

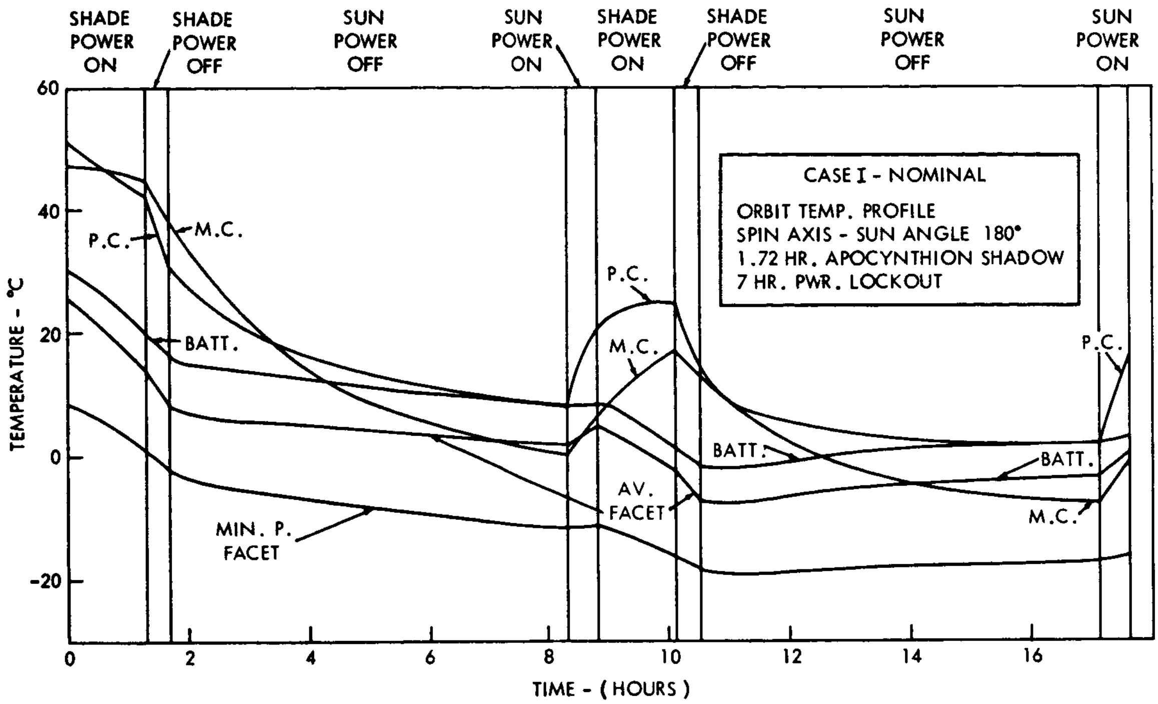


Figure 5

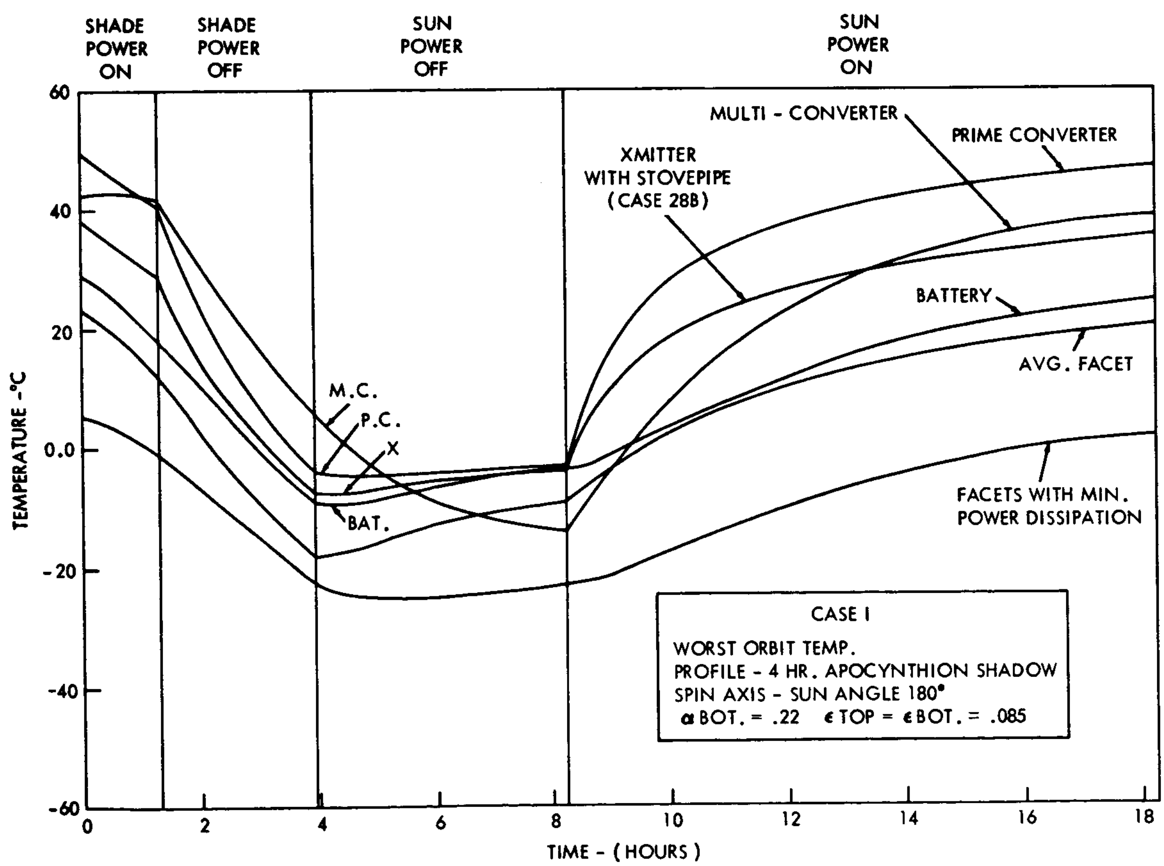


Figure 6

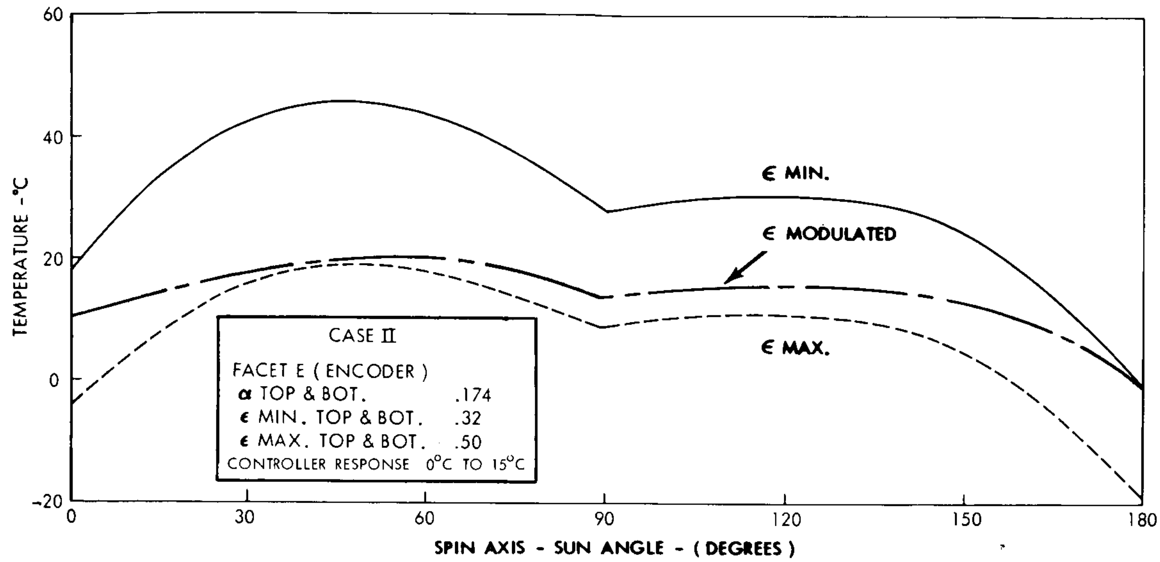


Figure 7

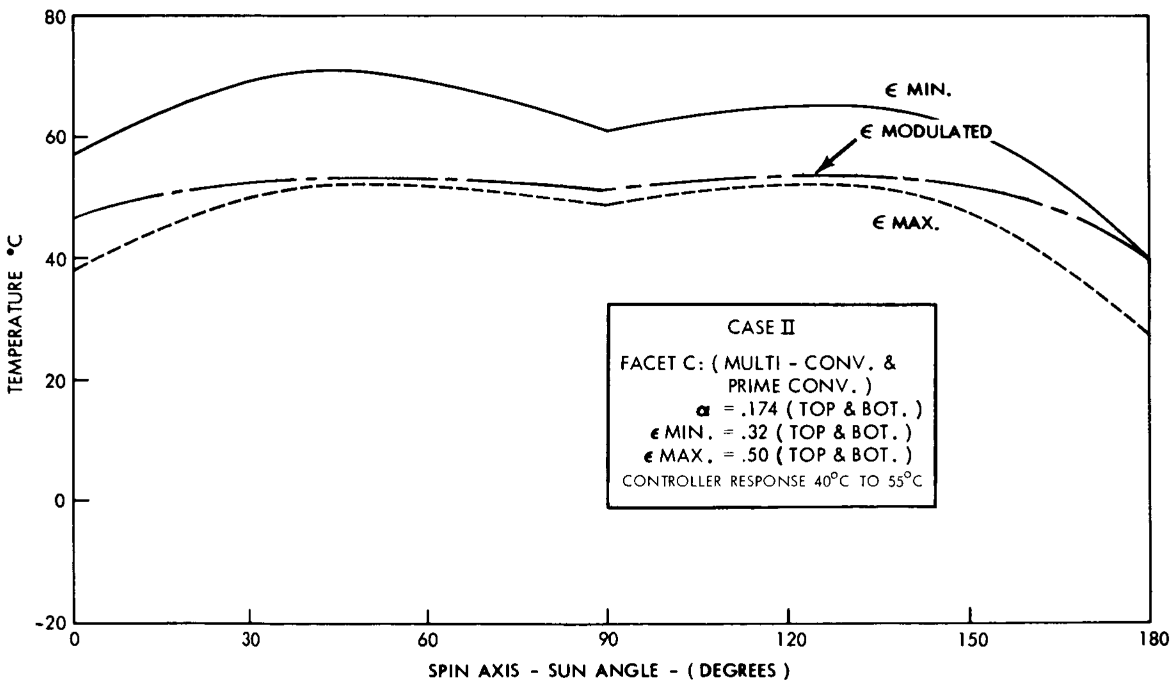


Figure 8

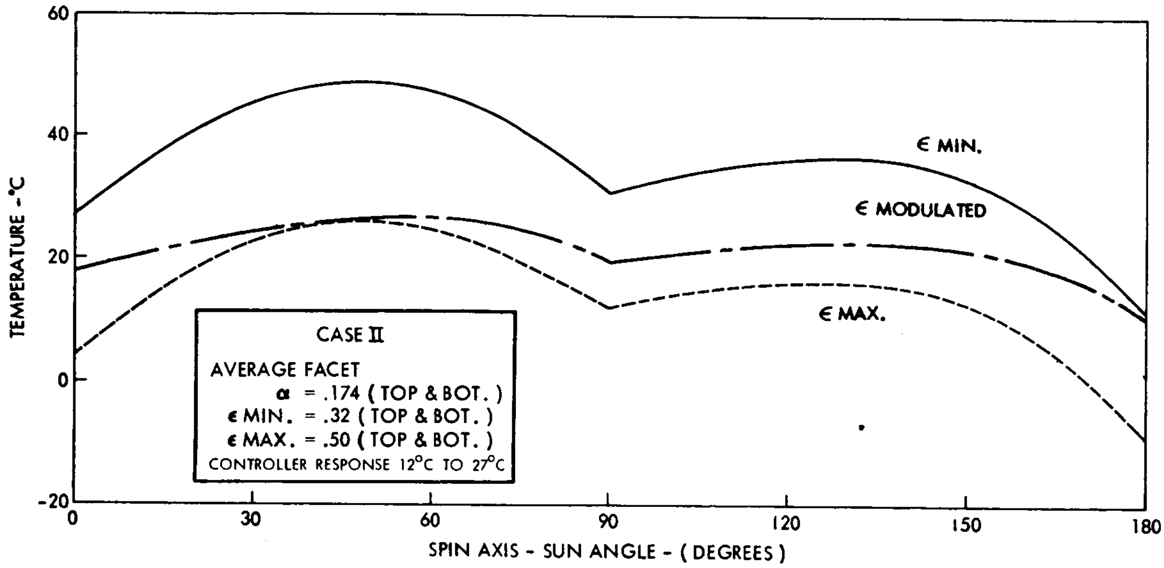


Figure 9

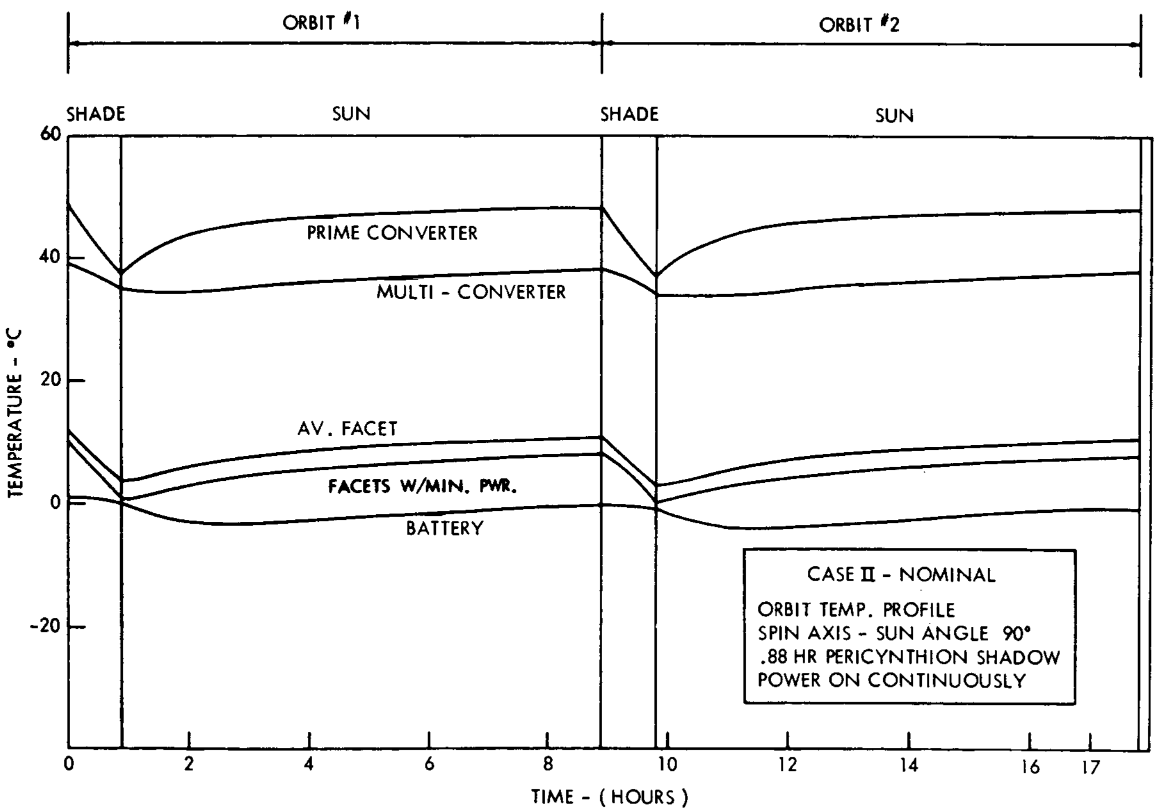


Figure 10

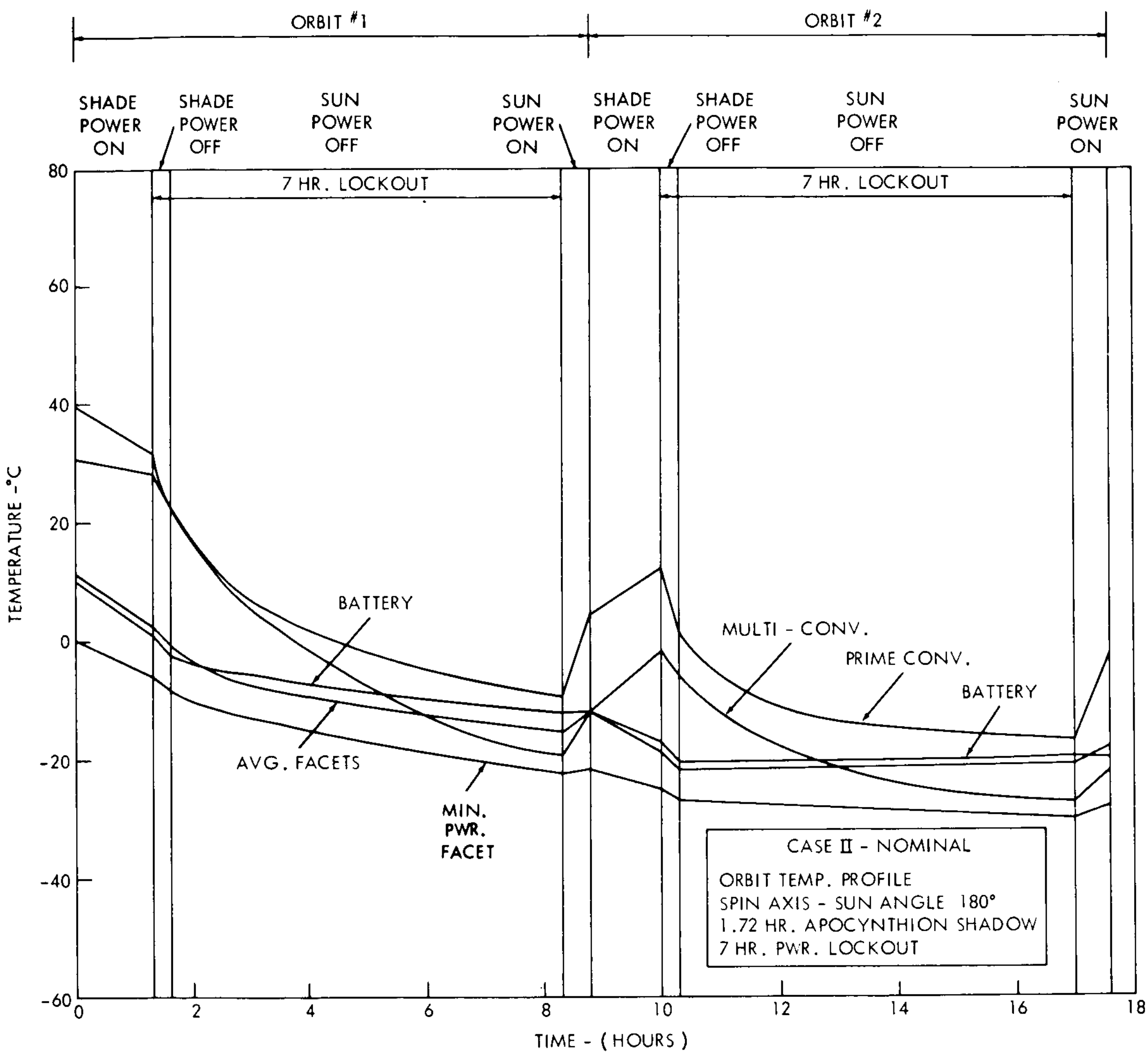
ORBIT #1
ORBIT #2
SHADE POWER ON
SHADE POWER OFF
SUN POWER OFF
SUN POWER ON
SHADE POWER ON
SHADE POWER OFF
SUN POWER OFF
SUN POWER ON
7 HR. LOCKOUT
7 HR. LOCKOUT
TEMPERATURE -°C
80
60
40
20
0
-20
-40
-60
BATTERY
AVG. FACETS
MIN. PWR. FACET
MULTI - CONV.
PRIME CONV.
BATTERY
CASE II - NOMINAL
ORBIT TEMP. PROFILE
SPIN AXIS - SUN ANGLE 180°
1.72 HR. APOCYNTHION SHADOW
7 HR. PWR. LOCKOUT
0
2
4
6
8
10
12
14
16
18
TIME - (HOURS)

Figure 11

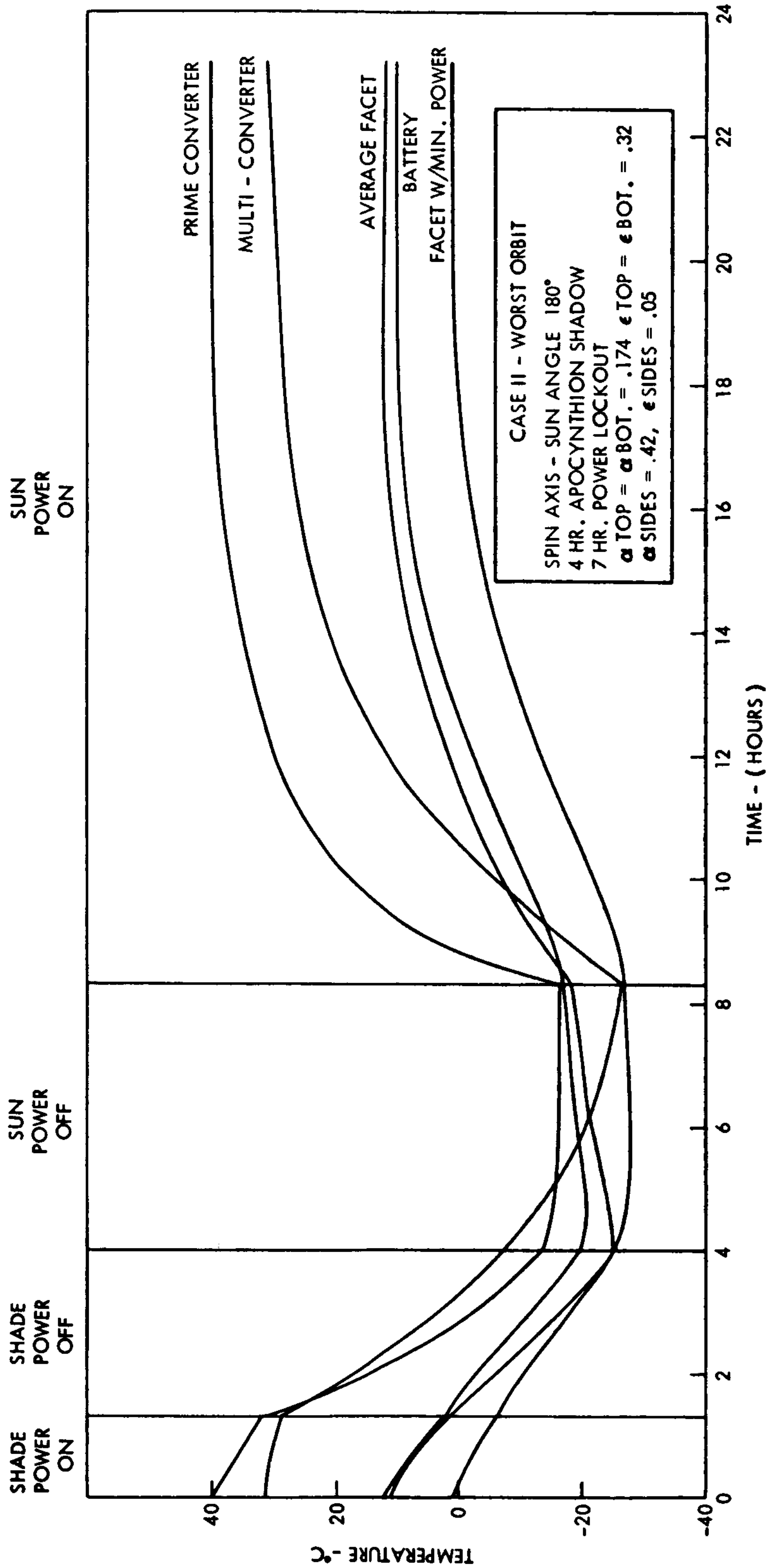
SHADE POWER ON
SHADE POWER OFF
SUN POWER OFF
SUN POWER ON
PRIME CONVERTER
MULTI - CONVERTER
AVERAGE FACET
BATTERY
FACET W/MIN. POWER
CASE II - WORST ORBIT
SPIN AXIS - SUN ANGLE 180°
4 HR. APOCYNTHION SHADOW
7 HR. POWER LOCKOUT
α TOP = α BOT. = .174 ε TOP = ε BOT. = .32
α SIDES = .42, ε SIDES = .05
TEMPERATURE -°C
40
20
0
-20
-40
0
2
4
6
8
10
12
14
16
18
20
22
24
TIME - (HOURS)

Figure 12

OPTIONAL FORM NO. 10
5010-104

UNITED STATES GOVERNMENT

# *Memorandum*

APPENDIX VII

TO : P.G. Marcotte - 672 DATE: 10/8/63

FROM : L.W. Slifer - 636.1
S.G. McCarron - 636.1

SUBJECT: Anchored IMP Solar Paddles

The expression for the normalized effective-paddle-area of the three-paddle IMP satellite as a function of paddle-spar angle, paddle-pitch angle, sun-line spin-axis angle, and angular rotation about the spin axis was programmed on the IBM 7090. The optimum average normalized effective-paddle-area for a complete range (0 to $\pi$) of sun-line spin-axis angle occurs at paddle-arm and paddle-pitch angles equal to $90^{o}$ and $35^{o}$, respectively. This on the average gives, with a slight margin, the power requirements for the proposed lunar IMP. (Figure 1)

Under these conditions, minima of the normalized effective-paddle-area versus sun-line spin-axis angle occur at sun-line spin-axis angles of $60^{o}$ and $120^{o}$. A plot of the normalized effective-paddle-area (where one paddle 20" x 27.6", weighing 6.6 lbs. (max.), gives 32 watts with normal incident sunlight) versus angular rotation about the spin axis for these conditions is shown in the Figure 2. The average power per revolution is 47 watts in both cases; however, a minimum of 36.2 watts occurs at $120^{o}$ rotation intervals.

Shadow effects have been considered from a qualitative standpoint only, but are not expected to present a problem for this configuration.

Since these results provide only a slight margin, several factors should still be considered:

1. Will voltage pulsing (3 per revolution) be tolerable, i.e., can this be adequately taken care of in the regulator design?

2. How serious are occasional undervoltage conditions?

3. Can additional solar cells (~10%) be used either by extension of the paddle width or by including body-mounted cells?

Luther W. Slifer Jr.
Luther W. Slifer, Jr.
Solar Power Sources Section
Space Power Technology Branch

S.G. McCarron
S.G. McCarron
Solar Power Sources Section
Space Power Technology Branch

Enc: Fig. 1 & 2

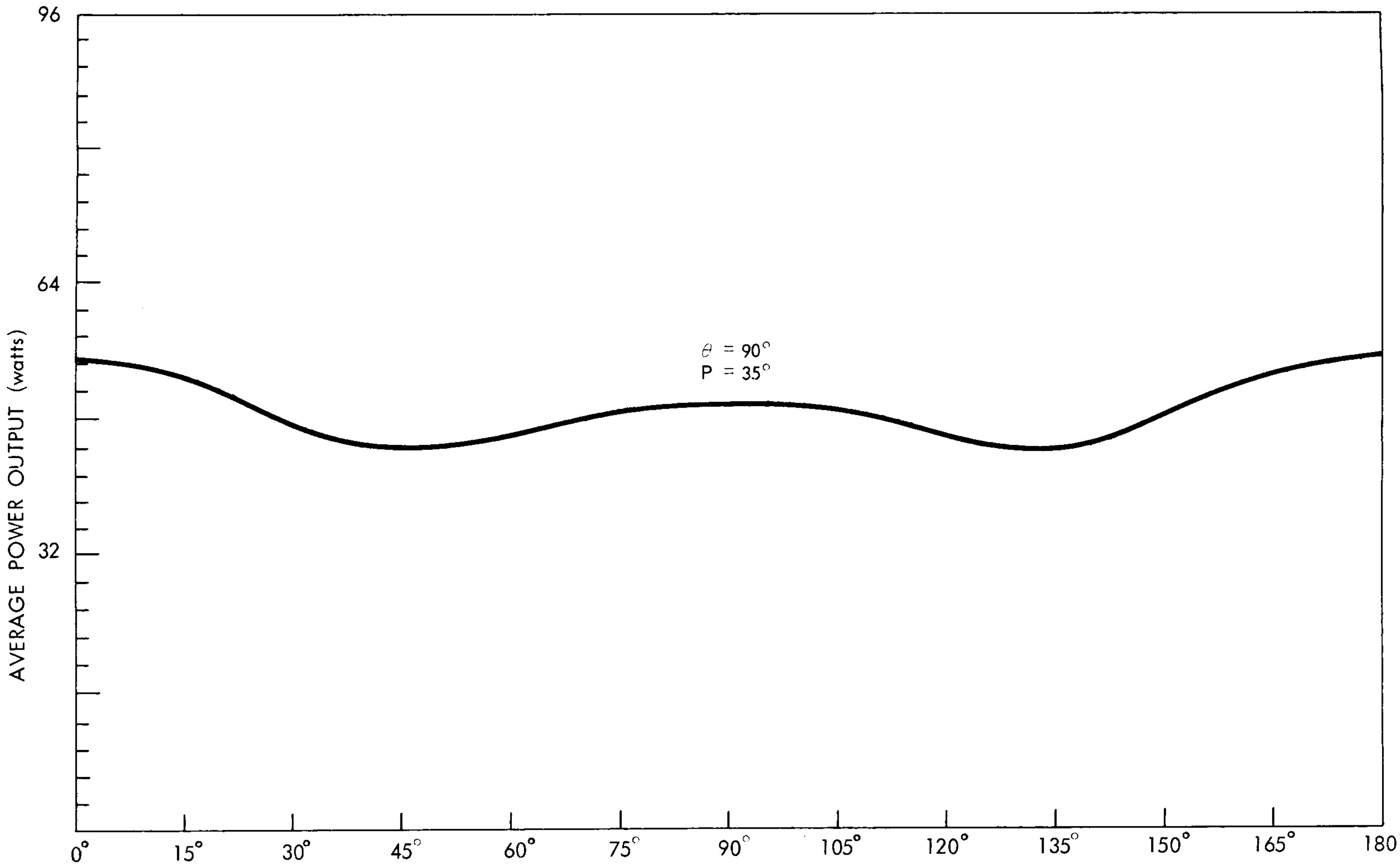


Figure 1--Sun-Line Spin-Axis Angle

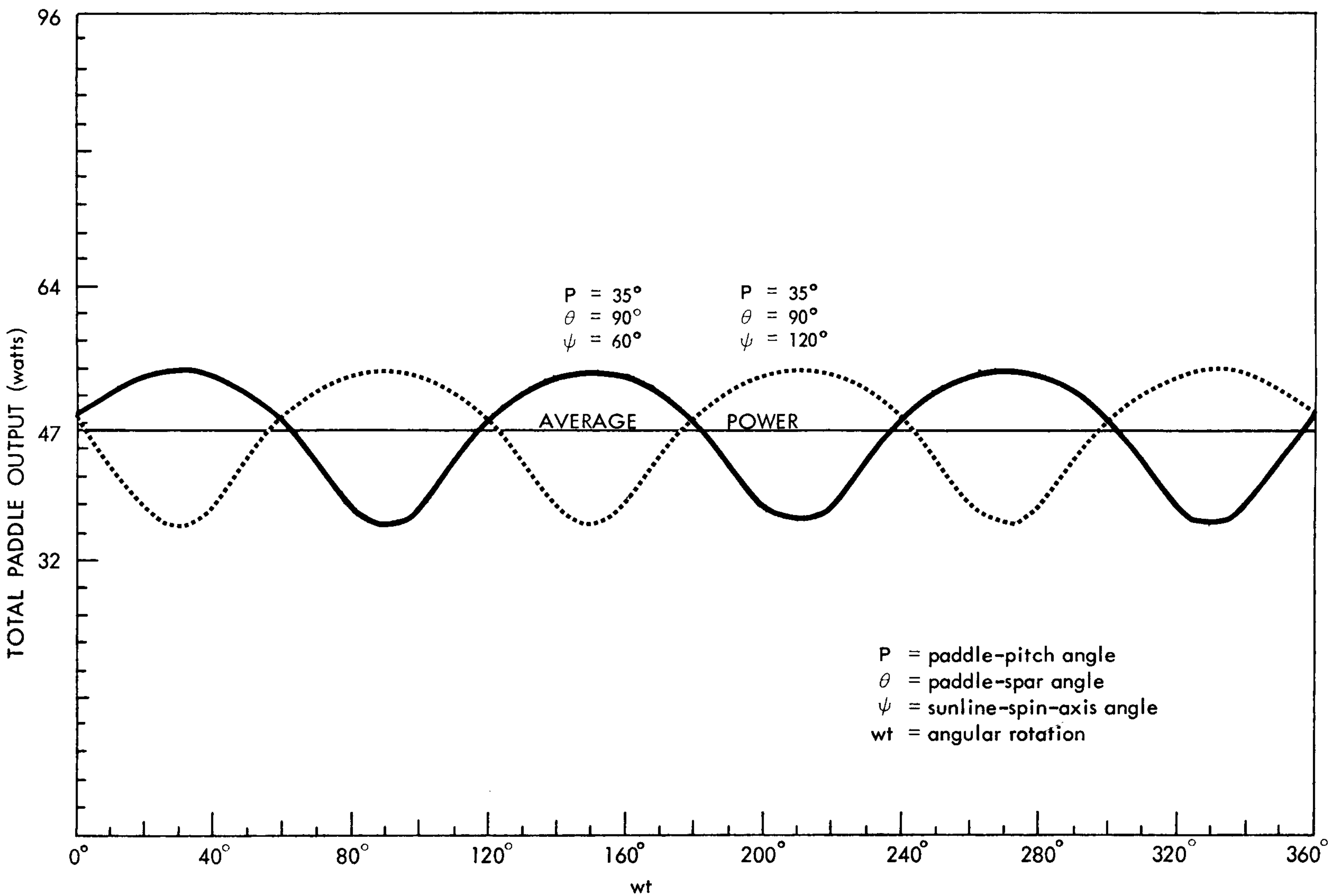
96
64
47
32
TOTAL PADDLE OUTPUT (watts)
P = 35°
θ = 90°
ψ = 60°
P = 35°
θ = 90°
ψ = 120°
AVERAGE POWER
P = paddle-pitch angle
θ = paddle-spar angle
ψ = sunline-spin-axis angle
wt = angular rotation
0°
40°
80°
120°
160°
200°
240°
280°
320°
360°
wt

Figure 2

OPTIONAL FORM NO. 10
5010-104
UNITED STATES GOVERNMENT

# *Memorandum*

APPENDIX VIII

TO : Mr. J. J. Madden
Project Resources Office

DATE: August 13, 1963

FROM : Mr. G. C. Kronmiller, Jr.
Project Manager, Goddard Range and Range Rate System

SUBJECT: Transponder Power Required to Track IMP D&E at Lunar Distances

The following is a calculation of the power in the down-link:

| | |
|---|---|
| Distance | 250,000 nm |
| Transmit Frequency | 136 mcs |
| Antenna Gain (Transmit) | 0 db |
| Antenna Gain (Receive) | +19 db |
| Losses (Polarization, Line, Misc.) | - 6 db |
| Space Loss | 188 db |
| Total Loss --- | -175 db |

Receiver N.F. + 3 db; 10 cps BW = + 10 db
Receiver 0 db S/N level = 174 dbm + 13 db = -161 dbm
Threshold for + 20 db S/N = 141 dbm

Carrier Power Transmitted = X dbm
Carrier Power Transmitted = -141 dbm +175 db
Carrier Power Transmitted = +34 dbm
Carrier Power Transmitted = 2.5 Watts
Sidetone Power = +3 db = +2.5 Watts

Total Power Required---5 Watts

Therefore, to insure adequate performance at least 6 watts of transmitted power should be provided for the ranging function.

G. C. Kronmiller, Jr.
Project Manager
Goddard Range and Range Rate System

531-1GCK:dkd

OPTIONAL FORM NO. 10
5010-104

UNITED STATES GOVERNMENT

# *Memorandum*

APPENDIX IX

TO : Paul Marcotte
Systems Integration Branch

DATE: September 25, 1963

FROM : William R. Schindler
Delta Project Manager

SUBJECT: Planning Information on an IMP D & E Mission and S-64 on Delta

REFERENCE: (a) Memo from P. Marcotte to W. R. Schindler dtd. 21 Aug. 63
(b) Memo from P. Marcotte to W. R. Schindler dtd. 11 Sept. 63
(c) Memo from J. Kork to W. R. Schindler dtd. 24 June 63
(d) Memo from W. R. Schindler to P. Marcotte dtd. 3 Sept. 63

The following information is in response to the reference (a) and (b) memoranda.

Ideally, a lunar orbiter should be launched so as to intercept the moon at maximum negative declination. Such launch times will occur on 4 December 1964, 14 June 1965, and approximate six-month multiples of these dates. Spacecraft orientation can be controlled so that spin axis-sun angle variations would be 30° to 150° or 150° to 30° during the initial four months of satellite lifetime.

The 180-pound payload weight used in the reference (c) study was the anticipated maximum for the TAD-X258 combination. Until actual TAD flight performance data is evaluated, the nominal 180-pound figure can be used for planning purposes. When such data is available, and spacecraft weight, orbit parameters and launch time are firmly established, an exact flight sequence and associated success probabilities for desirable orbits can be prepared. In the meantime, it is reasonable to use the information previously furnished in reference (c) and (d) for planning purposes. Elaboration or refinement of the calculations cited therein would be quite extensive and costly, and would provide little or no additional data which might influence a "feasibility" decision.

Enclosure 1 is a summary of orbit parameters for the 100 runs of the reference (c) study. The last column, $\phi$, is the angle between the pericynthian direction (line of apsides) and the sun, for the initial orbit only. The resulting trajectory will be a retrograde orbit, with the pericynthian point rotating in the direction of the sun. Rate of change of sun angle cannot, however, be readily established. This would require a determination of the rate of change of the orbital plane-ecliptic angle and the rotational rate of the intersection of these planes, all of which would require an unwarranted level of effort at this time.

The reference (c) study included the 71-pound JPL "Syncom" fourth stage motor with a velocity increment of 3684 fps for a 180-pound spacecraft. It was learned that JPL has developed a titanium case for this motor which will be approximately four pounds lighter. The only other "on shelf" motor which is applicable to the IMP D&E mission is the modified Thiokol TE-375 which weighs 85 pounds and has a velocity increment of 4830 fps for a 174-pound spacecraft.

To clarify a reference (d) statement concerning S-64, a TAD X-258 combination is capable of placing a payload of approximately 268 pounds into a 200-mile-perigee transfer orbit. It is estimated that a 125-pound engine would be required to "kick" the spacecraft into a 24-hour orbit thus permitting a payload weight (exclusive of engine) of approximately 143 pounds. We are not aware of an "on shelf" motor which meets this requirement. Aerojet is developing a 15-inch spherical motor (signus 15) which weighs 110 pounds, with a velocity increment of approximately 4800 fps for a 106-pound spacecraft. Scaling-up an existing motor appears to be straightforward but involves the necessary development and qualification of a new engine.

William R. Schindler
Delta Project Manager

Enclosure
IMP D & E Orbit Results

## IMP D & E ORBIT RESULTS

| RUN | $t_4$ | $r_p$ | $r_a$ | e | i | T | $r_r$ | $V_i$ | $\alpha_i$ | $\Delta t_4$ | $\lambda_i^*$ | $\phi$ |
|---|---|---|---|---|---|---|---|---|---|---|---|---|
| | Hrs | Km | Km | | Deg | Hrs | Km | Ft/Sec | Deg | Hrs | Deg | Deg |
| 1 | 78.0 | 2728 | 8,165 | .499 | 157.87 | 10.02 | 6,250 | 5239 | 6.39 | 3 | 53.84 | 23.2 |
| 2 | 68.0 | 4629 | 104,589 | .915 | 106.37 | 318.15 | 16,843 | 4859 | 21.62 | 3 | -161.58 | 129.6 |
| 3 | 68.0 | 3245 | 8,492 | .447 | 126.89 | 11.21 | 6,776 | 5609 | 8.30 | 10 | -161.68 | 146.3 |
| 4 | 72.0 | 3220 | 177,989 | .964 | 118.88 | 679.94 | 20,343 | 4536 | 25.57 | 4 | 140.83 | 134.2 |
| 5 | 73.0 | 1761 | 15,413 | .795 | 114.81 | 19.84 | 12,337 | 4772 | 8.55 | 13 | 125.00 | 156.3 |
| 6 | 75.5 | 1954 | 33,183 | .889 | 155.84 | 58.03 | 9,442 | 4761 | 36.72 | 3 | 89.87 | 67.4 |
| 7 | 73.5 | 2697 | 4,988 | .298 | 164.21 | 5.94 | 4,638 | 6080 | 13.72 | 5 | 118.81 | 142.7 |
| 8 | 72.5 | 2256 | 15,168 | .741 | 131.66 | 20.26 | 11,100 | 4868 | 15.27 | 14 | 133.07 | 144.2 |
| 9 | 67.0 | 5196 | 107,960 | .908 | 116.43 | 335.52 | 15,476 | 4947 | 22.33 | 3 | -146.76 | 132.6 |
| 10 | - | - | - | - | - | - | - | - | - | - | - | - |
| 11 | 67.0 | 4460 | 8,244 | .298 | 116.02 | 12.62 | 6,205 | 5777 | 4.61 | 5 | -147.19 | 135.8 |
| 12 | 72.25 | 2235 | 38,768 | .891 | 169.07 | 73.15 | 9,161 | 4949 | 37.72 | 2 | 137.16 | 69.8 |
| 13 | 73.0 | 4081 | 13,820 | .544 | 168.53 | 21.11 | 7,615 | 5102 | 6.18 | 3 | 126.68 | 56.6 |
| 14 | 74.5 | 1977 | 29,064 | .873 | 130.37 | 48.18 | 15,637 | 4525 | 21.08 | 12 | 104.31 | 139.9 |
| 15 | - | - | - | - | - | - | - | - | - | - | - | - |

$*L_i$ = =-23°

| RUN | $t_4$ | $r_p$ | $r_a$ | e | i | T | $r_r$ | $V_i$ | $\alpha_i$ | $\Delta t_4$ | $\lambda_i$* | $\phi$ |
|---|---|---|---|---|---|---|---|---|---|---|---|---|
| | Hrs | Km | Km | | Deg | Hrs | Km | Ft/Sec | Deg | Hrs | Deg | Deg |
| 16 | 74.75 | 2420 | 10,189 | .616 | 155.59 | 12.47 | 8,710 | 4984 | 16.00 | 9 | 100.76 | 129.8 |
| 17 | - | - | - | - | - | - | - | - | - | - | - | - |
| 18 | - | - | - | - | - | - | - | - | - | - | - | - |
| 19 | 71.0 | 2847 | 9,620 | .543 | 119.94 | 12.27 | 8,180 | 5243 | 1.00 | 13 | 154.18 | 156.00 |
| 20 | 71.0 | 2818 | 15,892 | .699 | 108.80 | 22.56 | 11,686 | 4911 | 8.82 | 11 | 154.14 | 150.4 |
| 21 | 72.0 | 2111 | 4,051 | .315 | 155.12 | 4.26 | 4,050 | 6275 | 10.18 | 7 | 140.53 | 120.5 |
| 22 | 73.75 | 2252 | 8,544 | .583 | 151.44 | 9.88 | 7,638 | 5185 | 12.51 | 12 | 115.08 | 136.2 |
| 23 | 65.0 | 5655 | 732,844 | .985 | 107.39 | 5594.04 | 15,788 | 5087 | 21.72 | 1 | -117.99 | 124.4 |
| 24 | 75.75 | 1880 | 5,323 | .478 | 172,29 | 5.39 | 4,807 | 5866 | 6.78 | 5 | 85.96 | 57.9 |
| 25 | 70.0 | 2807 | 19,792 | .752 | 111.88 | 29.94 | 12,335 | 4921 | 13.86 | 13 | 168.99 | 145.6 |
| 26 | 68.0 | 3483 | 14,388 | .610 | 113.68 | 21.06 | 9,561 | 5236 | 9.84 | 9 | -161.96 | 145.1 |
| 27 | - | - | - | - | - | - | - | - | - | - | - | - |
| 28 | 70.0 | 3665 | 17,327 | .651 | 106.19 | 26.81 | 11,461 | 4976 | 10.30 | 11 | 168.85 | 143.3 |
| 29 | 69.5 | 2270 | 213,920 | .979 | 165.16 | 885.93 | 10,716 | 4843 | 38.30 | 1 | 173.23 | 77.1 |
| 30 | - | - | - | - | - | - | - | - | - | - | - | - |
| 31 | 71.0 | 2487 | 15,910 | .730 | 115.39 | 21.99 | 11,366 | 4929 | 11.64 | 13 | 154.43 | 149.5 |

*$L_i$ = -23°

| RUN | $t_4$ | $r_p$ | $r_a$ | e | i | T | $r_r$ | $V_i$ | $\alpha_i$ | $\Delta t_4$ | $\lambda_i$* | $\phi$ |
|---|---|---|---|---|---|---|---|---|---|---|---|---|
| | Hrs | Km | Km | | Deg | Hrs | Km | Ft/Sec | Deg | Hrs | Deg | Deg |
| 32 | 71.0 | 3044 | 37,795 | .851 | 115.15 | 72.75 | 15,620 | 4713 | 20.41 | 11 | 154.92 | 138.4 |
| 33 | 76.0 | 1981 | 38,948 | .903 | 153.24 | 72.99 | 10,741 | 4518 | 35.37 | 3 | 82.56 | 70.7 |
| 34 | 71.0 | 2263 | 9,278 | .608 | 127.73 | 10.93 | 7,894 | 5282 | 5.41 | 14 | 154.46 | 156.7 |
| 35 | 77.75 | 2440 | 36,996 | .876 | 156.04 | 69.02 | 11,050 | 4447 | 33.75 | 3 | 57.12 | 73.6 |
| 36 | 69.0 | 3507 | 10,615 | .503 | 113.85 | 14.79 | 8,240 | 5333 | 1.44 | 9 | 176.82 | 164.6 |
| 37 | 67.75 | 1763 | 50,166 | .9321 | 142.08 | 104.25 | 6,990 | 5543 | 33.99 | 1 | -157.66 | 64.00 |
| 38 | 73.0 | 1875 | 21,547 | .840 | 110.83 | 31.60 | 14,234 | 4672 | 15.08 | 13 | 125.37 | 145.8 |
| 39 | 74.0 | 1755 | 24,084 | .864 | 133.91 | 36.61 | 14,301 | 4603 | 19.85 | 12 | 111.49 | 139.8 |
| 40 | 72.0 | 1923 | 16,159 | .782 | 114.77 | 21.43 | 12,165 | 4830 | 10.57 | 14 | 139.69 | 153.1 |
| 41 | 70.0 | 2440 | 20,094 | .783 | 115.77 | 29.82 | 12,435 | 4914 | 14.86 | 13 | 169.05 | 146.8 |
| 42 | 76.25 | 2416 | 14,688 | .718 | 156.94 | 19.71 | 7,049 | 5423 | 30.43 | 3 | 79.17 | 53.0 |
| 43 | - | - | - | - | - | - | - | - | - | - | - | - |
| 44 | 73.75 | 2108 | 4,143 | .326 | 162.82 | 4.35 | 3,682 | 6684 | 7.21 | 4 | 115.05 | 96.6 |
| 45 | 70.0 | 3146 | 20,342 | .732 | 105.55 | 31.73 | 12,728 | 4902 | 12.38 | 12 | 168.80 | 144.4 |
| 46 | 73.5 | 2466 | 38,294 | .879 | 162.11 | 72.50 | 8,995 | 4922 | 36.46 | 2 | 119.02 | 68.8 |
| 47 | 70.0 | 3808 | 2,990,177 | .998 | 101.92 | 45,664.1 | 21,102 | 4663 | 24.80 | 1 | 169.45 | 127.5 |

*$L_i$ = -23°

| RUN | $t_4$ | $r_p$ | $r_a$ | e | i | T | $r_r$ | $V_i$ | $\alpha_i$ | $\Delta t_4$ | $\lambda_i$* | $\phi$ |
|---|---|---|---|---|---|---|---|---|---|---|---|---|
| | Hrs | Km | Km | | Deg | Hrs | Km | Ft/Sec | Deg | Hrs | Deg | Deg |
| 48 | 76.0 | 2178 | 7,536 | .552 | 163.20 | 8.44 | 7,053 | 5195 | 15.91 | 10 | 82.65 | 116.8 |
| 49 | 74.0 | 1910 | 14,287 | .764 | 149.39 | 18.17 | 10,696 | 4816 | 17.57 | 10 | 111.58 | 138.5 |
| 50 | 69.0 | 3563 | 26,737 | .765 | 100.63 | 46.49 | 13,914 | 4905 | 14.12 | 10 | -176.73 | 138.9 |
| 51 | 71.75 | 1979 | 13,727 | .748 | 168.38 | 17.34 | 5,173 | 6032 | 16.93 | 2 | 144.42 | 47.2 |
| 52 | 73.0 | 2542 | 23,449 | .804 | 140.49 | 36.93 | 13,389 | 4681 | 20.97 | 11 | 126.27 | 140.1 |
| 53 | 69.0 | 3563 | 10,431 | .491 | 113.41 | 14.59 | 8,081 | 5355 | 1.94 | 9 | -176.75 | 144.8 |
| 54 | 74.0 | 2578 | 26,181 | .821 | 145.92 | 42.99 | 14,228 | 4586 | 22.33 | 9 | 111.91 | 138.4 |
| 55 | 78.0 | 3757 | 70,613 | .899 | 147.93 | 178.77 | 15,154 | 4080 | 32.93 | 3 | 53.53 | 82.5 |
| 56 | - | - | - | - | - | - | - | - | - | - | - | - |
| 57 | 67.0 | 5662 | 115,138 | .908 | 118.75 | 369.63 | 15,330 | 4946 | 22.58 | 3 | -146.66 | 132.9 |
| 58 | 74.0 | 2282 | 5,064 | .379 | 165.42 | 5.55 | 5,049 | 5780 | 15.71 | 6 | 111.67 | 93.2 |
| 59 | 71.0 | 2315 | 25,059 | .831 | 124.44 | 39.92 | 13,633 | 4790 | 8.88 | 13 | 154.88 | 143.3 |
| 60 | 65.0 | 6007 | 19,514 | .529 | 112.59 | 35.94 | 8,592 | 5450 | 11.23 | 4 | -117.99 | 120.7 |
| 61 | 82.5 | 1825 | 35,006 | .901 | 109.8 | 62.27 | 10,860 | 4336 | 33.49 | 5 | -12.35 | 65.1 |
| 62 | - | - | - | - | - | - | - | - | - | - | - | - |
| 63 | 68.0 | 2658 | 7,839 | .493 | 142.21 | 9.48 | 4,492 | 6196 | 1.19 | 2 | -161.19 | 42.0 |

*$L_i$ = -23°

| RUN | $t_4$ | $r_p$ | $r_a$ | e | i | T | $r_r$ | $V_i$ | $\alpha_i$ | $\Delta t_4$ | $\lambda_i$* | $\phi$ |
|---|---|---|---|---|---|---|---|---|---|---|---|---|
| | Hrs | Km | Km | | Deg | Hrs | Km | Ft/Sec | Deg | Hrs | Deg | Deg |
| 64 | 78.0 | 1979 | 12,307 | .723 | 168.58 | 15.05 | 10,199 | 4686 | 19.09 | 5 | 53.78 | 123.5 |
| 65 | 73.0 | 2027 | 70,095 | .944 | 103.60 | 170.73 | 20,039 | 4507 | 23.00 | 8 | 125.75 | 133.4 |
| 66 | 69.0 | 3916 | 10,701 | .464 | 111.05 | 15.58 | 8,127 | 5348 | 1.06 | 8 | -176.80 | 139.3 |
| 67 | 70.0 | 3255 | 16,991 | .678 | 114.92 | 25.39 | 11,086 | 4997 | 13.05 | 13 | 169.15 | 145.1 |
| 68 | 71.0 | 2599 | 17,230 | .738 | 107.69 | 24.61 | 12,422 | 4867 | 9.67 | 14 | 154.08 | 150.8 |
| 69 | 71.75 | 2601 | 8,327 | .524 | 163.5 | 10.07 | 4,780 | 6216 | 10.54 | 2 | 144.47 | 40.4 |
| 70 | 68.0 | 2825 | 4,784 | .258 | 119.71 | 5.85 | 3,418 | 6787 | 3.98 | 3 | -161.55 | 32.5 |
| 71 | 74.75 | 2797 | 25,131 | .800 | 107.8 | 41.12 | 8,519 | 4921 | 33.55 | 2 | 101.00 | 64.0 |
| 72 | 69.0 | 4190 | 117,750 | .931 | 114.84 | 375.34 | 17,503 | 4772 | 23.48 | 4 | -175.83 | 133.9 |
| 73 | 77.0 | 1891 | 3,645 | .317 | 170.80 | 3.63 | 3,605 | 6387 | 20.19 | 5 | 67.22 | 167.6 |
| 74 | 69.0 | 3394 | 13,335 | .594 | 118.59 | 19.07 | 9,315 | 5201 | 11.05 | 11 | -176.29 | 147.1 |
| 75 | 71.75 | 2428 | 4,740 | .323 | 151.51 | 5.35 | 3,754 | 6754 | 3.29 | 2 | 144.16 | 81.3 |
| 76 | 77.0 | 1932 | 7,623 | .596 | 169.96 | 8.23 | 7,151 | 5141 | 16.24 | 7 | 68.14 | 115.1 |
| 77 | 74.0 | 1885 | 14,506 | .770 | 167.74 | 18.50 | 6,681 | 5241 | 34.77 | 2 | 111.82 | 53.2 |
| 78 | - | - | - | - | - | - | - | - | - | - | - | - |
| 79 | 71.0 | 3374 | 66,002 | .903 | 109.14 | 161.07 | 17,880 | 4653 | 22.19 | 6 | 154.94 | 133.9 |

*$L_i$ = -23°

| RUN | $t_4$ | $r_p$ | $r_a$ | e | i | T | $r_r$ | $V_i$ | $\alpha_i$ | $\Delta t_4$ | $\lambda_i^*$ | $\phi$ |
|---|---|---|---|---|---|---|---|---|---|---|---|---|
| | Hrs | Km | Km | | Deg | Hrs | Km | Ft/Sec | Deg | Hrs | Deg | Deg |
| 80 | 69.75 | 2020 | 15,268 | .766 | 153.9 | 20.03 | 5,140 | 6121 | 17.45 | 1 | 173.42 | 55.8 |
| 81 | 72.0 | 3068 | 14,222 | .645 | 169.30 | 20.04 | 6,971 | 5261 | 16.38 | 1 | 141.04 | 55.9 |
| 82 | 75.0 | 2047 | 173,573 | .977 | 102.16 | 648.73 | 23,303 | 4354 | 25.40 | 5 | 96.98 | 128.1 |
| 83 | 74.0 | 2427 | 9,879 | .606 | 157.49 | 12.03 | 8,377 | 5055 | 17.24 | 10 | 111.73 | 130.0 |
| 84 | 70.0 | 3105 | 10,708 | .550 | 116.33 | 14.31 | 8,672 | 5229 | 7.80 | 11 | 168.63 | 151.4 |
| 85 | 78.25 | 1832 | 28,956 | .881 | 134.9 | 47.59 | 9,621 | 4627 | 34.50 | 4 | 49.76 | 60.5 |
| 86 | 70.0 | 3155 | 65,828 | .908 | 97.37 | 159.70 | 18,306 | 4716 | 20.80 | 7 | 169.01 | 132.8 |
| 87 | 75.75 | 2266 | 7,475 | .535 | 167.3 | 8.47 | 4,924 | 6013 | 19.87 | 3 | 86.40 | 31.8 |
| 88 | 70.0 | 2707 | 4,203 | .217 | 142.13 | 5.06 | 4,198 | 6280 | 7.25 | 6 | 169.51 | 108.5 |
| 89 | 71.0 | 1947 | 29,215 | .875 | 117.52 | 4.99 | 14,933 | 4743 | 19.04 | 12 | 154.68 | 143.0 |
| 90 | 77.0 | 2039 | 35,049 | .890 | 149.19 | 62.96 | 10,641 | 4495 | 34.45 | 3 | 68.02 | 69.5 |
| 91 | 70.75 | 2479 | 6,284 | .434 | 152.40 | 7.23 | 3,978 | 6728 | 5.77 | 2 | 158.82 | 130.9 |
| 92 | 66.0 | 5909 | 9,649 | .240 | 118.73 | 17.11 | 6,266 | 5799 | 6.67 | 4 | -132.37 | 108.1 |
| 93 | 74.75 | 2445 | 78,115 | .939 | 154.86 | 201.52 | 12,422 | 4415 | 36.14 | 2 | 100.69 | 76.5 |
| 94 | 66.0 | 5353 | 27,954 | .679 | 107.79 | 53.58 | 11,057 | 5228 | 14.08 | 5 | -132.70 | 127.3 |
| 95 | 71.0 | 2105 | 4,089 | .320 | 147.00 | 4.30 | 3,525 | 6597 | 6.27 | 2 | 155.11 | 37.2 |

*$L_i$ = -23°

| RUN | $t_4$ | $r_p$ | $r_a$ | e | i | T | $r_r$ | $V_i$ | $\alpha_i$ | $\Delta t_4$ | $\lambda_i^*$ | $\phi$ |
|---|---|---|---|---|---|---|---|---|---|---|---|---|
| | Hrs | Km | Km | | Deg | Hrs | Km | Ft/Sec | Deg | Hrs | Deg | Deg |
| 96 | 72.75 | 2460 | 4,777 | .320 | 157.8 | 5.42 | 4,603 | 6069 | 6.86 | 7 | 129.57 | 106.7 |
| 97 | 72.0 | 2228 | 23,124 | .824 | 120.94 | 35.58 | 13,658 | 4739 | 17.74 | 13 | 140.28 | 143.0 |
| 98 | 70.0 | 3231 | 13,594 | .616 | 119.94 | 19.23 | 9,688 | 5111 | 11.79 | 14 | 169.24 | 147.2 |
| 99 | 68.0 | 4045 | 15,346 | .583 | 109.36 | 23.80 | 9,759 | 5217 | 9.37 | 8 | -161.98 | 139.9 |
| 100 | 67.0 | 4529 | 75,520 | .887 | 114.38 | 199.63 | 15,159 | 4964 | 21.52 | 5 | -146.93 | 134.0 |

$^*L_i = -23°$

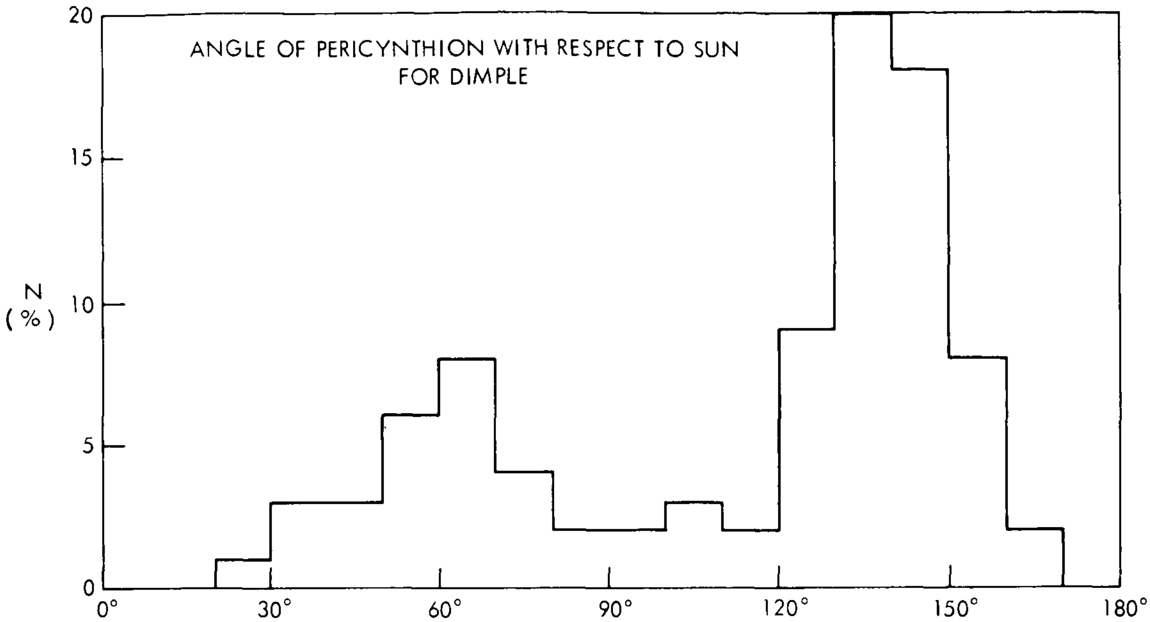


## SYMBOLS

$t_4$ - Lunar injection time (Hrs)

$r_p$ - Pericynthion radius (Km)

$r_a$ - Apocynthion radius (Km)

e - Orbital eccentricity

i - Orbital inclination with respect ecliptic plane (Deg)

T - Orbital period (Hrs)

$r_r$ - Radial distance from the center of moon at retro-firing (Km)

$V_i$ - Velocity before retro-firing (fps)

$\alpha_i$ - Angle between the spin axis and velocity vector at retro (Deg)

$\Delta t_4$ - Retro-window (Hrs)

$\lambda_i$ - Longitude of subsatellite point at the time of retro-firing (degrees; negative west, positive east)

Li = -23° (i.e., approx. const. = 23°S)

$\phi$ - Angle between the pericynthion direction and the sun (Deg)